COMPUTATIONAL STUDY OF HIGH ORDER NUMERICAL SCHEMES FOR FLUID-STRUCTURE INTERACTION IN GAS DYNAMICS

A Thesis submitted in partial fulfillment of the requirements for the degree of Doctor of Philosophy in the School of Mathematics, Statistics and Computer Science.

University of Kwazulu-Natal

By

José Caluyna Pedro

Pietermaritzburg July 2013

Dedication

To my wife:

Isabel Maria Joaquim Borges Pedro,

To my daughters:

Lianete Adneris Borges Caluyna Pedro,

Leonora Weya Borges Caluyna Pedro and

Luana Essanju Borges Caluyna Pedro,

for their moral support, patience and understanding, qualities which enabled me to successfully complete this work.

Declaration

I declare that this work is a result of my own research, except where specifically indicated to the contrary, and has not been submitted for any other degree or examination of this or any other university.

José Caluyna Pedro

Signed: Date:

I hereby certify that the statement above is true.

Precious Sibanda

Supervisor

Signed: Date:

ACKNOWLEDGMENTS

I would like to express my most grateful acknowledgement to the Instituto Nacional de Bolsas de Estudo (INABE) in Angola for fully funding this research.

Thanks also to the College of Agriculture, Engineering and Science of the University of Kwazulu-Natal, Pietermaritzburg Campus, for facilities to work in and for funding my attendance at conferences.

I would like to express my gratitude to Prof. Mapundi K. Banda, for his support in very different ways. The friendship he showed along the time we worked together was very important for the success of the project. Thanks also to Prof. Precious Sibanda for his advice and support.

I would like to thank Prof. Michael Dumbser, from the University of Trento in Italy, for his assistance with programming matters. This gratitude also extends to Prof. Emmanuel Lefrançois, from Université de Technologie de Compiègne, in France, and also to Montecinos Diego, Ph. D. student under Prof. E. F. Toro, at University of Trento, in Italy.

I would also like to acknowledge Prof. S. S. Motsa for his valuable assistance concerning programming using MatLab.

I would like to thank my family for their encouragement during my studies.

Special acknowledgements to:

- Prof. Reinaldo Rodrigues Ramos, Facultad de Matemática y Computacion, at Universidad de la Habana, Cuba, for inspiring me to complete the Ph. D. project.

- Prof. Bernardo Gabriel Rodrigues, who, for a long time was as a friend, an adviser, and a family.

- Mrs Marion Jordan, who for a long time acted as our guardian, mainly for my daughters.

- the Emaphethelweni Dominican brethren community, especially Father Martin, and the Dominican Angolan community, for their support.

My extensive acknowledgements are due to colleagues: Zodwa Makukula, Ahmed, Faiz, Ayube and Faustin, and to Ms Faith Nzimande.

ABSTRACT

Solving the fluid-structure interaction (FSI) problems is particularly challenging. This is because the coupling of the fluid and structure may require different solvers in different points of the solution domain, and with different mesh requirements.

In this thesis, a partitioned approach is considered. Two solvers are employed to deal with each part of the problem (fluid and structure), where the interaction process is realized via exchanging information from the fluid-structure interface in a staggered fashion.

One of the advantages of this approach is that we can take advantage of the existing algorithms that have been used for solving fluid or structural problems, which leads a reduction in the code development time, Hou (2012). However, it requires careful implementation so that spurious results in terms of stability and accuracy can be avoided.

We found that most fluid-structure interaction computations through a staggered approach are based on at most second order time integration methods.

In this thesis we studied the performance of some high order fluid and structure dynamic methods, when applied in a staggered approach to an FSI problem in a structure prediction way by combining predictors with time integration schemes to obtain stable schemes.

Nonlinear Euler equations for gas dynamics were investigated and the analysis was realized through the piston problem.

An adapted one-dimensional high order finite volume WENO_3 scheme for non-linear hyperbolic conservation laws-Dumbser (2007a), Dumbser et al. (2007b)-was considered and a numerical flux was proposed. The numerical results of the proposed method show the non-oscillatory property when compared with traditional numerical methods such as the Local Lax-Friedrichs.

So far to our knowledge, the WENO_3- as proposed in this work- has not been applied to FSI problems. Thus, it was proposed to discretize the fluid domain in space, and in order to adapt it to a moving mesh was reformulated to couple with an Arbitrary Lagrangian Eulerian (ALE) approach.

To integrate in time the structure we started by using Newmark_β schemes as well as the trapezoidal-rule backward differentiation formulae of order 2 ($TR - BDF2$). Two study cases were carried out by taking into account the transient effects on the fluid behaviour. In the first case, we only consider the structural mass in the dynamic coupled system and in the second case, a quasi-steady fluid was considered.

In order to test the performance of the structural solvers, simulations were carried out, firstly, without the contribution of fluid mass, and then a comparative study of the performance of various structure solvers in a staggered approach framework were realized in order to study the temporal accuracy for the partitioned fluid-structure

interaction coupling.

For a quasi-steady fluid case, the oscillation frequency of the coupled system was successfully estimated using the TR-BDF2 scheme, and the coupled system was solved for various Courant numbers in a structural predictor fashion. The results showed better performance of the TR-BDF2 scheme.

Newmark's schemes as well as the TR-BDF2 are only second order accuracy. However, the Newmark (average acceleration) is traditionally preferred by researchers as a structure solver in a staggered approach for FSI problems, although higher order schemes do exist. van Zuijlen (2004), in his partitioned algorithm proposed the explicit singly diagonal implicit Runge-Kutta (ESDIRK) family of schemes of order 3 to 5 to integrate both fluid and structure. Therefore in this work, these schemes were considered and applied as structural solvers. Their performance was studied through numerical experiments, and comparisons were realized with the performance of the traditional Newmark's schemes. The results show that although their computational cost is high, they present a high order of accuracy.

TABLE OF CONTENTS

LIST OF FIGURES

Chapter 1

INTRODUCTION

Fluid-structure interaction (FSI) problems arise in multi-physics, where one or more solid structures interact with an internal or surrounding fluid flow. FSI problems are crucial in the efficient and safe design of many science and engineering systems, e.g. blood flow through flexible arteries, aircrafts, and bridges, van Zuijlen (2004), Zill (1989).

Ignoring the effects of oscillatory interactions can often be fatal. For instance, in mechanical engineering, aircraft wings and turbine blades can brake due to FSI oscillations, van Zuijlen (2004). In building engineering the effects of oscillatory interactions have to be taken into account mainly in structures comprising materials susceptible to fatigue, such as bridges, Zill (1989).

A comprehensive study of FSI numerical simulations is essential since for most FSI problems analytical solutions to the model equations are impossible to obtain, Hou (2012). In this thesis we present a computational study of high order numerical schemes for FSI in gas dynamics.

In this Chapter we introduce the reader to the historical background of the different disciplines involved in the FSI problems that are discussed in this thesis and formulate

our objectives.

1.1 Historical Background

1.1.1 Structural Mechanics

Structural mechanics or the mechanics of structures defines the computation of deformations, deflections and internal forces or stresses within structures either to obtain designs with higher efficiency or to perform an evaluation of existing structures, van Zuijlen (2004). Structural mechanics applies to several engineering applications as part of applied mechanics. In structural mechanics one investigates the behaviour of vibratory mechanical systems such as machines, vehicles, industrial equipment, and civil engineering (e. g. the vibration of a bridge, deflection of a thin shell, bending of a beam, buckling of a column, or the torsion of a shaft) when subjected to either sustained or impulsive external loads or excitations, van Zuijlen (2004), Zill (1989), Auweraer (2001). Vibrations are defined as oscillations around the equilibrium position of the system, and they arise from a continuous exchange between kinetic and potential energy. It is important to highlight the fact that kinetic energy pertains to mass or inertia, while potential energy is concerned with the flexibility of a system. Structural analysis as it is known today developed over centuries. Even before the required methods for analyzing structures were developed, many types of structures, such as beams, arches, trusses, and frames, were used in construction for hundreds

of years. The successful construction of bridges, cathedrals, etc by ancient engineers (builders) showed that they had some understanding of structural features. It is known that Egyptian ancient builders formulated empirical rules that helped them to determine the size of structures and to plan a new structure, even though there is no evidence that they developed any theory of structural analysis. For example, the Egyptian Pharaoh Imhotep built the great pyramid of Saqqara around 2630 B. C. This pyramid is considered as the world's first structural engineering and master building, Heyman (1998), Becchi et al. (2001), Addis (2007).

The evolution of the theory of structural analysis started in, circa, 200 years ago. The fundamental principles of structural analysis appeared in the seventeenth century with Isaac Newton $(1642-1727)$. Newton formulated the laws of motion and the universal law of gravitation. As an outcome of his theory of gravitation the science of forces and motion, or mechanics, was developed. However, it was necessary to develop the science of mechanics of materials to make possible real and substantial advances with structural analysis, Heyman (1998).

Next, we highlight the main periods that saw the origin and development of structural analysis, see Maney (1915), Heyman (1998), Becchi et al. (2001), and Fernandez (2005).

(i) The period $(1825-1850)$, was considered as the constitution period of structural theory, Heyman (1998),

(ii) The establishment period of structural theory dated from $1850 - 1875$. It is in this period that the essential properties of technical artefacts were classified, Becchi et al. (2001), Fernandez (2005),

(iii) the period for the formation of the discipline of structural theory started with the establishment period up to 1900. One of the characteristics of this period was the constitution of the discipline's own conception of its epistemology, Heyman (1998).

(iv) the consolidation period of the structural theory was considered to be between 1900 and 1950. This period was characterized by the emerging of specialists and literature on constitution theory, Heyman (1998), Fernandez (2005).

Below we briefly describe some contributions that characterized the periods mentioned above.

In the middle of the 19^{th} century, Coulomb $(1736 - 1806)$ and Navier $(1785 - 1836)$ founded the science of the mechanics of materials (elastic theory). Navier's mathematical elastic theory was published in 1820. This motivated other researchers, among them Cauchy, who made contributions to the establishment of the structure of elastic theory in a scientific way.

In 1847 Squire Whipple $(1804 - 1888)$ introduced the first rational method of analyzing jointed trusses. This was followed by the publication of several excellent methods

for calculating deflections in the 1860's and 1870's. This resulted in a further acceleration of the rate of structural analysis development. Maney (1915) introduced the slope deflection method, the popular method used for the analysis of continuous beams and frames in USA, Maney (1915).

In the first half of the 20^{th} century several complex structural problems were formulated mathematically, but the lack of computing power made it difficult to solve the resulting equations and/or formulas. Up to 1940's much work was done with matrices in order to analyze aircraft structures. It was the development of digital computers that made practical the use of the equations and formulas for many types of structures, Heyman (1998), Addis (2007).

The complex cases in which a structure interacts with a fluid resulted in the challenging problems known as fluid-structure interaction problems. These are the subject of our study in this work.

1.1.2 Overview of theoretical concepts in structural dynamics

Throughout this thesis we are concerned with multi-physics problems, which involve two or more different interacting physical phenomena, Soulaïmani (2005). In this Section we present an overview of the theoretical concepts of structural dynamics.

In this thesis a structure is coupled to other fields, either a solid structure and a fluid or fluids. For this reason partitioned procedures are considered. The coupling

between the structure and the fluid is realized through a staggered approach, Felipa (1988), Piperno (1997).

A staggered approach can be derived from a second - order differential system in time, thus here we present an overview of the governing equations, Zill (1989).
From Newton's second law, or alternatively from Lagrange's equations, we can obtain the governing set of coupled second-order differential equations of motion, representing the behavioural dynamics of a viscously damped N degrees of freedom (N *d.o.f.*) mechanical system, as:

$$\mathbf{M}\ddot{\mathbf{q}}(t) + \mathbf{C}\dot{\mathbf{q}}(t) + \mathbf{K}\mathbf{q}(t) = \mathbf{f}(t), \tag{1.1}$$

where

$\mathbf{q}(t) = \left(\begin{array}{cccc} \mathbf{q}_1(t), & \mathbf{q}_2(t), & \ldots, & \mathbf{q}_n(t) \end{array} \right)^T \in R^n$ is the vector of time responses;

$\mathbf{f}(t) = \left(\begin{array}{cccc} \mathbf{f}_1(t), & \mathbf{f}_2(t), & \ldots, & \mathbf{f}_n(t) \end{array} \right)^T \in R^n$ is the vector of the excitation forces;

$\mathbf{M}$, $\mathbf{C}$, and $\mathbf{K}$ are the mass, damping and stiffness matrices, respectively. The matrix $\mathbf{M}$ is assumed to be positively defined, unless the contrary is stated, so that $\mathbf{M}^{-1}$ exists. In this thesis, structural dynamics are assumed under linear behaviour. Linear behaviour means that resilient elements (the springs) establish proportionality

between displacements and restoring forces, that is $f_e = -kq$; and the viscous dashpots (dampers) establish proportionality between velocities and damping forces, that is $f_d = -c\dot{q}$, Felipa (1978), Felipa (1979). The positive constant of proportionality k is called the stiffness constant and the positive constant c is the damping constant.

Depending on the existence or otherwise of excitation forces in the system, there are different vibratory models, Zill (1989), Edwards (2004).

Undamped free motion

In the absence of any damping ($\mathbf{C} = 0$) and excitation forces ($\mathbf{f}(t) = 0$), the system is called undamped and is given by

$$\mathbf{M}\ddot{\mathbf{q}}(t) + \mathbf{K}\mathbf{q}(t) = 0. \tag{1.2}$$

Damped free motion

In the absence of any excitation forces ($\mathbf{f}(t) = 0$), the system is called damped free and is given by

$$\mathbf{M}\ddot{\mathbf{q}}(t) + \mathbf{C}\dot{\mathbf{q}}(t) + \mathbf{K}\mathbf{q}(t) = 0. \tag{1.3}$$

Undamped motion with periodic forcing

For the equation of motion (1.1) without damping forces, the system is called undamped with periodic forcing and becomes

$$\mathbf{M}\ddot{\mathbf{q}}(t) + \mathbf{K}\mathbf{q}(t) = \mathbf{f}(t). \tag{1.4}$$

Time Integration Numerical Schemes for Structural Dynamics

The main focus of computational structural mechanics researchers is to introduce new and innovative approaches for the analysis of structural mechanics, see for instance, Butcher (1987), Sundnes (2001), Bardella (2003), van Zuijlen (2004), Bathe (2005), Bardella (2005), Bathe (2007), Bathe (2012). In general, the most used approach for the solution of the dynamic response of structural systems is the direct numerical integration of dynamic equilibrium equations, Newmark (1959), Wilson (1962), Wilson (1973), Thomas (1987), Chung (1993). Approaches can be classified either as explicit or implicit integration schemes. Explicit schemes basically calculate the state of a system at a later time $t + \Delta t$ given the state of the system at the current time t. Regarding solving actual structures that contain stiff elements, if we employ explicit schemes, very small time steps will be required in order to obtain a stable solution. Therefore, explicit schemes are conditionally stable with respect to the size of the time step. Implicit schemes find a solution by solving an equation involving both the current state of the system and the later one, which requires the solution of a

set of linear equations at each time step. However, larger time steps may be used. Therefore these schemes can be conditionally or unconditionally stable. For more details about explicit and implicit schemes for structure dynamics, see Hairer (1991) and Hairer (1993). In this thesis we are particularly interested in implicit time integration schemes for structures. These schemes are widely investigated and have been used by several researchers. For instance, one of the schemes that has been applied to structural dynamics on many practical engineering structures during the past four decades, is the implicit finite difference Newmark's scheme, Newmark (1959), Blom (1998), Lefrançois (2010). This scheme was presented by Newmark (1959) as a family of single-step integration methods for solving the structural dynamic problems for both blast and seismic loading. Additionally, this scheme has been modified by several other researchers. Wilson (1962) reformulated Newmark's scheme by introducing the matrix notation, by adding both stiffness and mass proportional damping, and by eliminating the need for iteration by the introduction of the direct solution of the equations at each time step. In 1973, the general Newmark scheme was modified by the introduction of the so-called Wilson θ factor. This was motivated by the observation that an unstable solution tends to oscillate around the exact solution. This modification made the scheme unconditionally stable, Wilson (1973). A further modification of the general Newmark scheme was through the use of the average acceleration method. The outcome was the so-called constant average acceleration

scheme, Blom (1998). This is also referred to by some authors as the Newmark-Wilson scheme, Spiegel (1999), Lefrançois (2010). This scheme has no numerical damping and is unconditionally stable, and is the most robust form of the Newmark method, Blom (1998). In 1973, the α method was introduced, motivated by the solution of the modified equation of motion, Wilson (1973):

$$\mathbf{M}\ddot{\mathbf{q}}^{t+\Delta t} + (1+\alpha)\mathbf{C}\dot{q}^{t+\Delta t} + (1+\alpha)\mathbf{K}\mathbf{q}^{t+\Delta t} = (1+\alpha)\mathbf{F}^{t+\Delta t} - \alpha\mathbf{F}^{t+\Delta t} + \alpha\mathbf{C}\dot{\mathbf{q}}^{t} + \alpha\mathbf{K}\mathbf{q}^{t}.$$

The performance of this scheme is similar to the use of stiffness damping. In 1993 a new family of one-step three-stage, numerically dissipative time integration schemes, called the generalized -α methods was presented. In the design of the α-methods an attempt was made to introduce some damping into a time integration scheme by using adjustable parameters, Chung (1993).

One of the properties of these direct numerical integration schemes is that they need specific integration parameters. A disadvantage is then that the parameters have to be selected, depending on the characteristics of the problem to be solved. If the parameters are set up incorrectly, huge solution errors may result, Bathe (2012). In order to correct this disadvantage of direct numerical integration schemes, Bathe (2012) recently proposed an implicit time integration scheme which does not involve the setting of any parameters but merely the selection of an appropriate time step size. This method combines the use of the trapezoidal rule and the Euler backward schemes.

Another well-known family of numerical schemes are the Runge-Kutta methods that have been the subject of many systematic studies. A Runge-Kutta scheme to be A-stable and perform well when applied to stiff systems must be implicit, see Alexander (1977).

We define the initial value problem for a system of first order ordinary differential equations by

$$\dot{q} = F(q,t), \qquad q(t=a) = q^0, \qquad t \in [a,b].$$

The general s-stage Runge-Kutta scheme is defined by

$$q^{n+1} = q^n + \sum_{i=1}^{s} b_i k_i,$$

where

$$k_i = \Delta t F\Big(t^n + c_i \Delta t, q^n + \sum_{j=1}^{s} a_{ij} k_j\Big), \quad i = 1, \ldots, s.$$

Such formulae can be represented conveniently by the Butcher Table:

c	A
	b^T

.

If the matrix A is strictly lower triangular, the scheme is explicit, otherwise the internal stages depend on both the current and later stages, which results in an implicit method. The Radau family of methods are an example of implicit Runge-Kutta schemes, see Butcher (2003). However there is an excessive cost in evaluating the stages in fully implicit Runge-Kutta schemes. Therefore many researchers have

opted for the diagonally Implicit Runge-Kutta (DIRK) schemes. Alexander (1977) derived new strongly s-stable diagonally implicit Runge-Kutta (DIRK) of order 2 in 2 stages, and of order 3 in 3 stages. van Zuijlen (2004) applied the explicit singly diagonally implicit Runge-Kutta (ESDIRK) family to structural dynamics. While an s-stage DIRK scheme uses s implicit stages, an s-stage ESDIRK scheme uses $s-1$ implicit stages once the first stage is explicit. Throughout this thesis we apply implicit schemes in order to integrate structural dynamics.

1.1.3 Fluid Dynamics

In this thesis we are concerned with partitioned procedures that couple a structure to fluids. In this Section we present an overview of fluid mechanics, emphasizing fluid dynamics - a sub-discipline of fluid mechanics that is concerned with fluid flow. Fluid dynamics has various engineering applications, such as

(i) calculating forces and momentum on aircraft,

(ii) determining the mass flow-rate of petroleum through pipelines, and

(iii) in weather prediction.

Fluid dynamics has sub-disciplines such as aerodynamics, which is concerned with studying the motion of air around objects, and hydrodynamics, which is concerned with the study of liquids in motion. It must be noted however that before the twenti-

eth century, hydrodynamics was considered to be synonymous with fluid dynamics, a fact that is still reflected in some fluid dynamics topics, see Acheson (1990), Batchelor (1967), Chanson (2009), and the references therein.

Hyperbolic conservation laws and differential equations

A wide range of subjects in which wave motion or advection is essential, are governed by hyperbolic partial differential equations. Among those subjects are gas dynamics, acoustics, elastodynamics, optics, geophysics, and biomechanics, Leveque (2002). In this thesis we deal with gas dynamics. In order to provide an overview of the governing equations pertaining to gas dynamics, some physical principles used to derive conservation laws, are introduced.

Conservation laws arise from physical principles. To see how this works, let us consider the simplest possible fluid dynamics problem in which a gas or liquid is flowing through a one-dimensional pipe with some known velocity $u(x,t)$. Let $q(x,t)$ be the unknown concentration or density of a chemical tracer. Then

$$\int_{x_1}^{x_2} q(x,t)dx \tag{1.5}$$

represents the total mass of the tracer in the section of a pipe between x_1 and x_2 at a particular time t. If the quantity q is conserved, then its total mass within $[x_1, x_2]$ can change only due to the flux or flow of q across the two endpoints x_1 and x_2, Leveque (2002). Let $F_i(t)$ be the rate at which the tracer flows past the fixed point x_i for

$i = 1, 2$. Therefore:

$$\frac{d}{dt}\int_{x_1}^{x_2} q(x,t)dx = F_1(t) - F_2(t) = [\text{inflow at } x_1] - [\text{outflow at } x_2]. \tag{1.6}$$

Equation (1.6) represents the basic integral form of the conservation law, which can be written as:

$$\frac{d}{dt}\int_{x_1}^{x_2} q(x,t)dx = f(q(x_1,t)) - f(q(x_2,t)). \tag{1.7}$$

By using standard notation from calculus we can rewrite equation (1.7) as

$$\frac{d}{dt}\int_{x_1}^{x_2} q(x,t)dx = -f(q(x,t))\Big|_{x_1}^{x_2}. \tag{1.8}$$

Now, assuming that the functions $q(x,t)$ and $f(q(x,t))$ are sufficiently smooth, we have

$$\frac{d}{dt}\int_{x_1}^{x_2} q(x,t)dx = -\int_{x_1}^{x_2} \frac{\partial}{\partial x} f(q(x,t))dx. \tag{1.9}$$

After some further modification, equation (1.9) becomes

$$\int_{x_1}^{x_2} \Big[\frac{\partial}{\partial t} q(x,t) + \frac{\partial}{\partial x} f(q(x,t))\Big] dx = 0. \tag{1.10}$$

Since this integral has to be zero for all values of x_1 and x_2, it follows that the integrand has to be identically zero, which gives a differential equation

$$\frac{\partial}{\partial t} q(x,t) + \frac{\partial}{\partial x} f(q(x,t)) = 0, \tag{1.11}$$

or:

$$q_t + f(q)_x = 0. \tag{1.12}$$

Equation (1.12) is the differential form of the conservation law, see Bressan (2000), Leveque (2002), Toro (1999).

In the introduction above we considered the function $q(x,t)$ as the density of some chemical tracer carried along with the fluid, but in such small quantities that the distribution of q does not affect the fluid velocity. Instead, if we consider the density of the fluid itself, particularly if we consider the fluid as compressible (a gas), then from physical principles it is possible to derive the conservation laws for gas dynamics, see Toro (1999), Bressan (2000), Leveque (2002) for more detailed considerations. For instance, a compressible gas in Lagrangian coordinates is modeled by the Euler equations given by a system of three conservation laws, Leveque (2002), Bressan (2000), Toro (1999)

$$\begin{cases} \rho_t + (\rho u)_x = 0 & \text{(conservation of mass)} \\ (\rho u)_t + (\rho u^2 + p)_x = 0 & \text{(conservation of momentum)} \\ E_t + ((E+p)u)_x = 0 & \text{(conservation of energy).} \end{cases}$$

Here ρ is the density, u the velocity, E the energy and p the pressure. The system is closed by an additional equation called the equation of state for the gas. In particular, if we consider an ideal polytropic gas, sometimes also called a gamma-law gas, the equation of state takes the form, Leveque (2002):

$$E = \frac{p}{\gamma - 1} + \frac{1}{2}\rho u^2.$$

Under ordinary conditions $\gamma = 1.4$.

Throughout this thesis we consider the nonlinear Euler equations to model the fluid. The Euler equations represent a simplified version of the more realistic Navier-Stokes equations. The latter equations additionally include the effects of fluid viscosity and heat conduction, Leveque (2002).

Numerical Methods for Hyperbolic Conservation Laws: Finite Volume Method and Higher Order WENO schemes

In this section, we give a brief review of the numerical methods used to solve partial differential equations (PDEs). Numerical methods replace the continuous problem given by the PDEs with a finite set of discrete counterparts. The domain of the PDEs has to be discretised into a finite set of points or values via a grid mesh. The outcome of the discretization of the PDEs on the grids are discrete values, Hoffmann (1993), Hirsch (1990). Philosophically, there are two different approaches: the finite difference method; and the finite volume method. The first approach uses the strong differential form of the PDE and approximates derivatives at discrete points, defined as grid points. The second approach concerns discretising the weak integral form of the PDE at discrete values defined as averages over finite volumes, Toro (1999), Leveque (2002). In this thesis we are mostly interested in the finite volume approaches, higher-order essentially non-oscillatory (ENO), and weighted essentially

non-oscillatory (WENO) schemes. Background information regarding these schemes can be found in Chapter 5 of the book by Toro (1999). Details of the finite volume schemes and WENO schemes will be given in Chapter 2. For finite volume schemes it is required to compute fluxes across the element interfaces, Leveque (2002). For these numerical flux functions, two point values of the numerical solution at the element interface are required, one extrapolated to the interface from the left, and another from the right, Jiang (1996). The finite volume scheme provides the integral average over the control volume rather than the discrete value at the spatial point, as is the case with the finite difference scheme. However to compute the flux at the element interfaces, the value at the interface needs to be defined. This process is known as the reconstruction step, Dumbser (2011).

The construction of higher order accurate numerical schemes can be realized through the use of essentially non-oscillatory (ENO) and weighted essentially non-oscillatory (WENO) interpolation, Harten et al. (1987), Jiang (1996). Consequently the WENO scheme produces a high order accurate point-wise reconstruction of the solution at the element interface. WENO schemes are based on essentially non-oscillatory (ENO) schemes. The ENO schemes were introduced in the form of cell averages by Harten et al. (1987). In their work, Harten et al. (1987) presented a hierarchy of uniformly high order accurate schemes. They generalized Gudonov's schemes as second order accurate Monotone Upstream-centered Schemes for Conservation Laws (MUSCL) ex-

tension to an arbitrary order of accuracy. The design includes an ENO piecewise polynomial reconstruction of the solution from its cell averages, time evolution via an approximate solution of the resulting initial value problem, and obtaining an average of this approximate solution over each cell. A new interpolation technique was applied in order to derive a reconstruction algorithm which, when used on piecewise smooth data, results in high-order accuracy whenever the function is smooth, avoiding the Gibbs phenomenon at discontinuities. The procedure uses an adaptive stencil of grid points and, as a result, the outcomes are highly nonlinear schemes.

Shu (1988) presented improvements to ENO schemes introduced by Harten et al. (1987) as well as to the total-variation-diminishing (TVD) and total-variation-bounded (TVB) schemes. These improvements consisted, respectively, of an ENO reconstruction procedure on the basis of fluxes instead of cell averages, and on TVD Runge-Kutta-type time discretization. As a result, the schemes became more simplified, mainly for multi-dimensional problems or problems with forcing terms. The work of Shu (1988) was later extended to the efficient implementation of ENO shock-capturing schemes, by providing a new simplified ENO construction procedure on the basis of numerical fluxes instead of cell-averages, Shu (1988). This improved work contained two other improvements, ENO-LLF (local Lax Friedrichs) and ENO-Roe, both of which give sharper shock transitions and improved overall accuracy for less computation cost. The subcell resolution idea of Harten et al. (1987), and the artificial

compression idea of Jiang (1996) used for the cell-average fashion, were applied to the ENO schemes based on fluxes and TVD Runge-Kutta time discretizations.

Liu et al. (1994) introduced a new version of ENO shock-capturing schemes, called weighted-ENO, or simply (WENO). The main idea was that instead of using the smoothest stencil to pick one interpolation polynomial for the ENO reconstruction, it used a convex combination of all candidates to achieve the ENO property. In addition, it improved accuracy by one order. The WENO scheme obtained is based on cell-averages and TVD Runge-Kutta time discretization.

Later, Jiang (1996) modified and improved the high order weighted essentially non-oscillatory (WENO) finite difference scheme of Liu et al. (1994), by proposing a new form of measuring the smoothness of a numerical solution, emulating the idea of minimizing the total variation (TV) of the approximation. It led to a fifth-order WENO scheme instead of the fourth-order that used the original smoothness measurement of Liu et al. (1994).

In order to make the point-wise WENO reconstruction of Jiang (1996) easily generalizable to unstructured grids, Dumbser (2007a) introduced a non-oscillatory finite volume scheme of arbitrary accuracy in space and time to solve linear hyperbolic conservation laws in two and three space dimensions, on unstructured grids through the advection-diffusion-reaction (ADER) approach. The improvement consisted of a new reconstruction operator using techniques originally developed in the discontinu-

ous Galerkin finite element fashion. In order to eliminate scaling effects and therefore to avoid ill-conditioned matrices, Dumbser (2007a) used hierarchical orthogonal basis to perform the reconstruction, which was done in a reference coordinate system rather than in physical coordinates. Dumbser (2007a) achieved non-oscillatory properties by proposing a new WENO reconstruction consisting of reconstruction of the entire polynomials, which can be easily evaluated and differentiated at any point, rather than point-value reconstruction. Later, Dumbser et al. (2007b) presented a quadrature-free essentially non-oscillatory finite volume scheme of arbitrary high order accuracy, in space and time, to solve nonlinear hyperbolic systems on unstructured grids, in two and three space dimensions. To achieve higher order discretization in space, the reconstruction technique provided the reconstruction polynomials in terms of a hierarchical orthogonal polynomials basis over a reference element. The Cauchy-Kovalewski procedure was applied to the reconstructed data that yielded, for each element, a space-time Taylor series for the evolution of the state, and was a low-cost and efficient way to obtain a quadrature-free formulation that avoided expensive numerical quadrature that arises mainly from high order finite volume schemes in three space dimensions. One of the features of this scheme was that it could easily be adapted to the one space dimension. In this thesis we apply the Dumbser et al. (2007b) scheme to solve fluid-structure interaction problems.

1.1.4 Fluid-Structural Interaction

In order to describe phenomena which cannot be modeled in an isolated way, multi-field models which include problems and processes from various kinds of fields, are needed. During recent decades, researchers have directed their efforts to multi-field problems, because understanding the interactions between various processes is of great importance in various fields of science and engineering (for example, aerospace, bio-engineering, civil engineering, and mechanical engineering). Multi-field problems can be classified as coupled-problems or boundary-coupled problems. The former concerns fields that are coupled inside the processing domain or volume, and the latter is with regard to problems where physical fields and processes are coupled through the boundaries of the domain, Helmig (2010). In this thesis we consider boundary-coupled problems. One of the challenges in boundary-coupled problems is fluid-structure interaction (FSI). Fluid-structure interaction occurs when a fluid (liquid or gas) interacts with a solid structure, exerting pressure on it, deforming the structure and therefore modifying the flow of the fluid itself. Fluid-structure interaction has its origin in 1828, when Friedrich Bessel proposed the concept of hydrodynamic or added mass. His work described findings regarding the motion of a pendulum in a fluid. He found that the period of a pendulum is higher if it moves in a fluid than if it moves in a vacuum, even when considering buoyancy effects, which indicated that the surrounding fluid increased the effective mass of the system, Helmig (2010). The concept of fluid-

structure interaction arose later in 1843, when George Gabriel Stokes investigated the uniform acceleration of an infinite cylinder moving in an infinite fluid medium. He found that the cylinder moving in the fluid had more effective mass. This was because the effect of the surrounding fluid multiplied by the quantity of added mass was equal to the mass of fluid that the cylinder displaced, Stokes (1851). Studies on fluid-structure interaction in pressure vessels and piping systems began in the 1960s. In 1966, Fritz and Kiss investigated the vibration response of a cantilever cylinder surrounded by an annular fluid. This study constituted the pioneering investigation on fluid-structure interaction, Wambsganss (1974). Since then, several researchers performed studies on the dynamics of the interaction between fluids and elastic shell systems, which include pipes, tubes, vessels, and co-axial cylinders.

Currently, several techniques to simulate strongly coupled fluid-structure systems, are being developed, Helmig (2010). Below we give an overview of some recent studies regarding fluid-structure interaction, from the 1990s until the present.

Piperno (1995) performed studies on partitioned procedures for the transient solution of coupled aero-elastic problems. In his work, several partitioned procedures were used to integrate the problem in time, and their merits discussed in terms of accuracy, stability, heterogeneous computing, $Input/Output$ transfers, sub-cycling, and parallel processing. Piperno (1997) presented a study concerning explicit/ implicit fluid/structure staggered procedures, with a structural predictor and fluid sub-cycling

for two space dimension inviscid aero-elastic simulations. In this study, new coupling staggered procedures, where the conservation of momentum was enforced at the interface, were presented.

Blom (1998) investigated the time marching computational model on fluid-structure interaction, by comparing the performance of staggered and monolithical approaches. He investigated linear acoustics as well as non-linear Euler equations for gas dynamics.

Farhat (2000) gave an overview of two sequential and parallel partitioned procedures, often used in computational nonlinear aero-elasticity, to discuss their limitation regarding accuracy and numerical stability. He proposed two alternative serial and staggered approaches to solve coupled transient aero-elasticity problems which showed superior performance.

Souli (2000) applied the Arbitrary Lagrangian Eulerian (ALE) approach to fluid-structure interaction problems, by explaining the underlying ideas of the method as well as a possible ways to control mesh deformation.

Guruswamy (2001) provided a technical overview of interfacing methods derived from the Euler/Navier-Stokes methods, with structural solutions by the nodal/ finite-element method. Michler et al. (2004), compared partitioned and monolithic procedures for FSI simulations and discussed the role of structural prediction for a partitioned approach. They investigated grid refinement to determine temporal accuracy of the schemes.

van Zuijlen (2004) applied a partitioned approach to FSI simulations, using higher order time integration schemes. He applied a mixed implicit/explicit time integration scheme to integrate the fluid and structure, and employed an explicit Runge-Kutta scheme to integrate the coupling terms. The implicit scheme that he used was the explicit singly diagonally implicit Runge-Kutta (ESDIRK).

Bathe (2009) presented a procedure to adapt and repair the grid for general solutions to Navier-Stokes incompressible and compressible fluid flows, including structural interactions. In this work, his concern was the need to adapt the fluid grid to pure computational fluid dynamics (CFD) solutions. He focused on FSI, taking into account the fact that large structural deformations were present. The procedure was considered a practical scheme for complex problems.

Lefrançois (2010) presented the basic knowledge required to construct and evaluate a coupling. His objective was to provide a grasp of both the numerics and the physics involving the FSI.

The work of Borsche (2010), was concerned with some theoretical aspects regarding a system of conservation laws coupled with a system of ordinary differential equations. They therefore presented analytical results to ensure the existence of solutions to the mixed system of ordinary and partial differential equations, using the technique supported by the classical theorems on the Cauchy problems for an ordinary differential equation, and by more recent results on the initial boundary-value

problems for systems of conservation laws, Filipov (1988), Colombo (2010). In their analytical as well as practical results, they emphasized the fact that a coupled mixed system of ordinary and partial differential equations may not be decoupled.

Fluid-structure interaction can be classified into three groups:

(1) *zero strain interactions*, such as the transport of suspended solids in a liquid matrix;

(2) *constant strain steady flow interactions*, such as the constant force exerted on an oil-pipeline, due to viscous friction between the pipeline walls and the fluid,

(3) *oscillatory interactions*, where the strain induced in the solid structure causes it to move such that the source of strain is reduced, and where the structure returns to its former state only for the process to repeat.

In the third group, we find one of the most popular applications of fluid-structural interaction, the piston problem, see Piperno (1995), Blom (1998), van Zuijlen (2004), Michler et al. (2004), Lefrançois (2010), Borsche (2010), and other references. A piston problem deals with a system of conservation laws coupled with a system of ordinary differential equations, Borsche (2010). The system of conservation laws models a fluid (gas) contained in a tube, closed on one side with a fixed wall, and closed on the other side with a moving piston which is generally modeled by a N degrees-of freedom mechanical system. The fluid can be modeled differently, according to as-

sumptions made for the fluid and the flow. Here we present an overview of some studies that have been done on the piston problem. In several fluid-structure interaction studies, the complete three-dimensional aero-elastic problem is very difficult to analyze mathematically, Piperno (1995).

Piperno (1995) investigated the one-dimensional piston problem to derive theoretical results. The linear dynamic equilibrium of the piston was modeled by a one degree freedom of motion mechanical system equation. The fluid (gas) was assumed to be perfect, and the flow isentropic. Therefore, by considering the response of the aero-elastic coupled system to small disturbances around the equilibrium position, they linearized the fluid flow equations, which was formulated in an arbitrary Lagrangian Eulerian approach with respect to a moving frame. Blom (1998) studied the piston problem by investigating linear acoustic-as well as nonlinear Euler equations for gas dynamics. van Zuijlen (2004) considered two cases of the piston problem. The classic one, that is modeled by a one degree of freedom mechanical system, and a modified piston problem that is modeled by a two degrees of freedom mechanical system. The flow was assumed to be isentropic and consequently the fluid equations were linearized by considering small disturbances from an equilibrium. Borsche (2010) also considered the flow to be isentropic.

Numerical Schemes for Fluid-Structural Interaction

There are two different approaches to solving a fluid-structure interaction (FSI) problem, namely the monolithic approach, and the staggered or partitioning procedure, see Piperno (1994), Blom (1998), van Zuijlen (2004). For the former, a single solver is employed to solve the complete system of equations modeling both the fluid and the structure, while for the latter, two solvers are used to deal with fluid and structure separately, with the coupling treated as a (explicit) force/boundary condition, van Zuijlen (2004), Blom (1998). The staggered scheme was introduced by Park (1977), and was used for transonic flutter computations by Prananta (1996), and for incompressible fluid-structure interaction by Mouro (1996). It was Piperno (1994, 1995) who included the staggering of fluid and structure solvers in the algorithm. This scheme uses the characteristic time scales in fluid and structure solvers by choosing different steps for both solvers, Blom (1998). Blom (1997), later adopted this scheme. Other different parallel versions of the partitioning scheme have been investigated by Piperno (1995) and by Farhat (1994). It is possible to improve the order of the error of a partitioning scheme by using prediction techniques, where the prediction may be applied for the position of the structural boundary at time $t + \Delta t$, instead of integrating the fluid based on the position of the structural boundary at current time t. This technique is based on extrapolating the solution from the current time level, see Piperno (2001), Piperno (1997), Michler et al. (2004), van Zuijlen (2004). Prananta

(1997) also presented an analysis of a predictor-corrector technique.

The dynamic response of a structure in a fluid flow has to be predicted, therefore the equations of the motion of the structure and the fluid have to be solved simultaneously. However there is a difficulty in numerically handling the fluid-structure coupling system, since the structural equations are usually formulated with material coordinates (Lagrangian), while the fluid equations are mainly written using spatial coordinates. For small displacements, a straightforward approach to the solution of the coupled fluid-structure dynamic equations, requires the movement at each time-step of at least the portions of the fluid mesh that are close to the moving structure. However for large displacements, this can lead to mesh distortions. Therefore several fluid flow formulations to deal with the moving mesh, have emerged as alternatives to re-meshing in transient aero-elastic computations. Among them are the arbitrary Lagrangian-Eulerian (ALE) formulation, the co-rotational approach, and the dynamic mesh, see Piperno (1995), Lefrançois (2010).

1.2 Strong coupling

An extremely important concept for fluid-structure interaction problems is strong coupling. One of the requirements for such a coupling is that the solution for all the physics have to be synchronized at every time step. When using a staggered approach, high order implicit schemes are not a condition to ensure strong coupling since as

the fluid and the structure domains move in time successively, there will always exist lags between solutions. However a solution can be achieved when various fluid and structural computations are performed at every time step, until synchronization is obtained between the solutions. This process is known as the strong-coupling staggered approach, Farhat (2000). Therefore strong coupling can be achieved even using explicit time marching schemes to integrate the equations for each domain, Jean et al. (2009). However for any case, it is necessary to ensure mass, momentum, and energy conservation at the fluid-structure interface, Jean et al. (2009), Lefrançois (2010).

1.3 Objectives

In this thesis a staggered approach is investigated in a structural predictor fashion. Explicit high order schemes to integrate fluid in time, and implicit high order schemes to integrate structure, are considered. Several tests are carried out separately to ensure the performance of the schemes. The aim is to investigate strong-coupling algorithm of the fluid-interaction problem, when applied to the piston problem, thus ensuring both the stability of the coupled algorithm, and energy conservation at the fluid-structure interface.

Applying a staggered approach with a structural predictor requires that at current time t the state of the fluid, the structure, and the mesh are known, the integration

in time of the fluid-structure system from the current time t to $t+\Delta t$, is achieved by:

(i) predicting the state of the structure at $t + \Delta t$,

(ii) using the predicted state of the structure to integrate the fluid at the next time step,

(iii) using the fluid pressure on the boundary to update the structure at the next time step.

This thesis fills some gaps in the literature.

A new numerical flux is proposed. Several numerical tests are carried out to show its non-oscillatory property when compared with traditional methods such as the local Lax-Friedrichs (LLF) method.

Since most fluid-structure interaction computations through a staggered approach are based on traditional fluid and structural solvers, such as finite element and finite volume and second order Newmark$_\beta$ schemes, we propose alternative schemes such as the WENO$_3$ for fluid, the second order TR-BDF2 and higher order ESDIRK schemes of order 3, 4 and 5 for structure, combined with selected structural predictors to obtain stable schemes.

1.4 Outline of the thesis

This thesis consists of six Chapters which are described as follows;

(1) In Chapter 2 we present high order schemes for hyperbolic conservation laws.

(2) In Chapter 3 we present an introduction to fluid-structure interaction and solvers.

(3) a high order finite volume method applied to a staggered approach for a FSI problem is given in Chapter 4.

(4) in Chapter 5 we present a family of high order explicit singly diagonally implicit Runge-Kutta (ESDIRK) methods and their application to FSI.

(5) finally, in Chapter 6 we present concluding remarks.

Chapter 2

HIGH ORDER SCHEMES FOR HYPERBOLIC CONSERVATION LAWS

2.1 Introduction

Hyperbolic conservation laws arise in many areas of science and engineering such as gas dynamics, shallow water, weather prediction, and diverse others, Zahran (2006). To solve practical problems, numerical methods are required since analytical solutions are available only in few a special cases.

Numerical methods replace by a finite set of discrete points the continuous problem modelled by partial differential equations (PDEs), Eymard (2006). In order to obtain these points, firstly the domain of the PDEs is discretized into a finite set of points or volumes via a mesh or grid, which results in discrete values. There are two, philosophically different, approaches: the finite difference and the finite volume methods. The first one regards these values as point values defined at grid points and the second one regards these discrete values as averages over finite volumes. Some of its essential characteristics are similar to those of the finite element method, Oden (1991). Since the finite volume method may be used on arbitrary geometries, using structured or unstructured meshes leads to robust methods. In the finite volume

method it is necessary to compute fluxes across the element interfaces, therefore numerical fluxes are used. An additional characteristic of the finite volume method is the local conservativity of the numerical fluxes, which means that the numerical flux is conserved from one discretization cell to its neighbor, Eymard (2006). This characteristic makes the finite volume method an ideal scheme when modelling problems for which the flux is crucial, such as in fluid mechanics, Stein (2004). In this thesis we are mostly interested in the finite volume method.

The concern for researchers is to improve this method by introducing correction terms. Godunov (1959), showed that all linear schemes which preserve solution monotonicity are at most first order accurate. The low order accuracy of these schemes served as motivation to develop higher order accurate schemes with the difference that these new schemes use nonlinearity so that monotone resolution of discontinuities and high order accuracy away from discontinuities are simultaneously achieved. A very important step forward in the generalization of Godunov's finite volume method to higher order accuracy is due to van Leer (1979). He employed linear solution reconstruction in each cell.

The construction of higher order accurate numerical schemes can be realized via the use of essentially non-oscillatory (ENO) and weighed essentially non-oscillatory (WENO) schemes.

WENO methods refer to a class of nonlinear finite volume or finite difference meth-

ods which can numerically approximate solutions of hyperbolic conservation laws and other convection dominated problems with high order accuracy in smooth regions and essentially non-oscillatory transition for solution discontinuities. The main advantage of such schemes is their capability to achieve arbitrarily high order formal accuracy in smooth regions while maintaining stable, non-oscillatory and sharp discontinuous transitions. The schemes are thus especially suitable for problems containing both strong discontinuities and complex smooth solution features.

The first WENO scheme was introduced by Liu et al. (1994) in their pioneering paper, in which a third order accurate finite volume WENO scheme was presented. Jiang (1996) provided a general framework for constructing arbitrary order accurate finite difference WENO schemes, which are more efficient for multi-dimensional calculations. However Dumbser et al. (2007b) considered the original point-wise WENO reconstruction difficult to be generalized to unstructured meshes in two and three dimensions because of the need to determine the optimal linear weights. They presented an alternative numerical scheme that could solve hyperbolic conservation PDEs with, at least theoretically, high order of accuracy in space and time in complex two and three dimensional domains. Dumbser (2007a), present a non-oscillatory finite volume scheme of arbitrary accuracy in space and time for solving linear hyperbolic systems on unstructured grids in two and three space dimensions using the arbitrary higher order derivatives (ADER) approach. Following this work, Dumbser et al. (2007b) pre-

sented a quadrature-free essentially non-oscillatory finite volume scheme of arbitrary high order accuracy both in space and time for solving nonlinear hyperbolic systems on unstructured meshes in two and three space dimensions. For high order spatial discretization, a WENO reconstruction technique provides the reconstruction polynomial in terms of a hierarchical orthogonal polynomial basis over a reference element. In this chapter, the general procedure to reconstruction of the arbitrary high-order non-oscillatory finite volume schemes for non-linear hyperbolic systems of Dumbser (2007a) and Dumbser et al. (2007b) is followed. Apart from the reconstruction, the main ingredient for these schemes is the definition of the numerical flux at the cell interfaces as functions of the cell averages, Titarev (2005c). There are several classical numerical fluxes defined for this problem such as the Lax- Friedrichs flux, the Lax-Wendroff flux, the Central flux and the first-order centered scheme (FORCE),Toro (2000). The main contribution of this section is a modification of fluxes which can improve the non-oscillatory properties of the scheme especially for systems of non-linear equations. As such a one-dimensional alternative scheme is introduced and tested. The modified numerical flux which reduces oscillations significantly and in some cases improves the resolution of the discontinuities is tested on one-dimensional systems of gas dynamic equations. It is believed that application of this scheme to higher-dimensional problems should be straight-forward. In this chapter we present:

- an overview of derivation of the equations of gas dynamics and of the finite

volume method.

- an overview of the WENO scheme that is used throughout this thesis as a fluid solver.

- the numerical flux method in this chapter proposed and the numerical experiments to test the performance of this scheme.

- concluding remarks.

2.2 Nonlinear equations for fluid dynamics: Euler equations

We gave a brief introduction to hyperbolic conservation laws in Section 1.1.3, where we presented the integral and the differential forms of the conservation laws. We introduce, without further detail, the equations for the conservation of mass, momentum and energy. We introduce additional details in relation to the Euler equations. In Chapter 1 we considered a one-dimensional pipe-flow. Let us, in that pipe, denote the density of the fluid by $\rho(x,t)$. In the case of an incompressible fluid, the density will be constant and in such case the problem is not of interest. However if we consider a compressible fluid (gas) it is expected that the density will vary. Assuming that the velocity u_c is constant, then the density $\rho(x,t)$ satisfies the advection equation

$$\frac{\partial}{\partial t}\rho(x,t) + u_c\frac{\partial}{\partial x}\rho(x,t) = 0. \tag{2.1}$$

However, from a physical point of view, if the gas is compressed it is expected that the velocity will change due to the variation in density, Leveque (2002). In that case, the velocity becomes an unknown and depends on the position and time, $u(x,t)$. Therefore the conservation law (2.1) takes the form

$$\frac{\partial}{\partial t}\rho(x,t) + \frac{\partial}{\partial x}\{\rho(x,t)u(x,t)\} = 0. \tag{2.2}$$

Equation (2.2) is the so-called continuity equation in fluid dynamics, modeling the conservation of mass. In addition to this equation we need another equation for velocity. The velocity is not a conservative quantity but the momentum is. If the density of momentum is described by the product $\rho(x,t)u(x,t)$, then the total momentum in the interval $[x_1, x_2]$ is given by $\int_{x_1}^{x_2} \rho(x,t)u(x,t)dt$, and it can change only due to the flux of momentum through the end-points x_1 and x_2. The momentum past any point x can be divided in two points,

(1) the momentum carried past any point x along with the moving fluid. For any density function q this flux takes the form qu, and since the momentum is $q = \rho u$, then the advection equation is $qu = (\rho u)u = \rho u^2$. Since the quantity to be advected is the momentum of the fluid, this phenomenon is called convection.

(2) Additionally, to this macroscopic convective flux, there is also a microscopic momentum flux as a result of the pressure of the fluid. It leads to the momentum

flux

$$\text{momentum flux} = \rho u^2 + p, \tag{2.3}$$

where $p = p(x,t)$ is the pressure. Taking into account that $q = \rho(x,t)u(x,t)$ the equation (1.8) becomes

$$\frac{d}{dt}\int_{x_1}^{x_2} \rho u dx = -[\rho u^2 + p]\Big|_{x_1}^{x_2}. \tag{2.4}$$

Assuming the smoothness of the functions ρ, u and p we get the differential equation

$$\frac{\partial}{\partial t}\rho u + \frac{\partial}{\partial x}(\rho u^2 + p) = 0, \tag{2.5}$$

which describes the conservation of momentum.

It is reasonable to think that there is a need for a third equation, for pressure. But pressure is not a conservative quantity. Therefore we introduce an additional variable for energy, which is a conservative quantity, and the additional equation for conservation of energy. Its density is denoted by $E(x,t)$. Since we need to determine the pressure it is necessary to close the system by adding an equation of state, which is an algebraic equation that determines the pressure at any point in terms of the mass, momentum and energy at the point. The total energy E takes the form

$$E = \rho e + \frac{1}{2}\rho u^2, \tag{2.6}$$

where e is the specific internal energy (energy per unity mass), ρe is the internal energy and $\frac{1}{2}\rho u^2$ is the kinetic energy. For the Euler equations it is assumed that

the gas is in local chemical and thermodynamical equilibrium and that the internal energy is a known function of pressure and density. The equation of state for a gas is

$$e = e(p, \rho), \tag{2.7}$$

where this depends on the particular gas under consideration.

The total energy advects with the flow, leading to a macroscopic energy flux term Eu. In addition, the microscopic flux measured by pressure gives the flux in kinetic energy which is given by pu. When there are no external forces, the conservation law for total energy takes the differential form

$$\frac{\partial}{\partial t}E + \frac{\partial}{\partial x}\{(E+p)u\} = 0. \tag{2.8}$$

Putting together equations (2.2), (2.5) and (2.8), we get the system of Euler equations

$$\begin{cases} \frac{\partial}{\partial t}\rho + \frac{\partial}{\partial x}(\rho u) = 0 & \text{(conservation of mass)} \\ \frac{\partial}{\partial t}(\rho u) + \frac{\partial}{\partial x}(\rho u^2 + p) = 0 & \text{(conservation of momentum)} \\ \frac{\partial}{\partial t}E + \frac{\partial}{\partial x}\{(E+p)u\} = 0 & \text{(conservation of energy)} \end{cases} \tag{2.9}$$

Additional information on these equations can be found in Section 1.1.3.

2.2.1 Entropy: Isentropic flow

In Chapter 1, we made a brief reference to isentropic flow, more details with some derivations will be provided here. Entropy is a fundamental thermodynamic property. It is a function of thermodynamics variables, such as temperature, pressure, or

composition that indicates the measure of the energy that is not available for work during a thermodynamic process, Leveque (2002). The entropy is denoted by s, and the specific entropy is given by

$$s = c_v \log(p/\rho^\gamma) + \text{constant} \tag{2.10}$$

where c_v is a specific heat at constant volume.

Solving equation (2.10) with respect to p we have

$$p = k e^{\frac{s}{c_v}} \rho^\gamma, \tag{2.11}$$

where k is a constant. Manipulating equations (2.9) we can derive the relation

$$\frac{\partial s}{\partial t} + u \frac{\partial s}{\partial x} = 0, \tag{2.12}$$

which shows that the entropy is constant along particle paths in domains of smooth flow, Leveque (2002). Equation (2.12) together with the equations of conservation of mass and conservation of momentum lead to an alternative system of Euler equations for smooth flows,

$$\begin{cases} \frac{\partial}{\partial t}\rho + \frac{\partial}{\partial x}(\rho u) = 0 \\ \frac{\partial}{\partial t}(\rho u) + \frac{\partial}{\partial x}(\rho u^2 + p) = 0 \\ \frac{\partial s}{\partial t} + u \frac{\partial s}{\partial x} = 0 \end{cases} \tag{2.13}$$

We recommend Chapter 14 in Leveque (2002) for further details. Taking into account small smooth perturbations around some background state, there will be not shocks

over reasonable time periods. For this reason it often makes sense to use the non-conservative equations (2.13) which give equivalent results as the conservative Euler equations (2.9). However s simply advects with the flow and if s is initially uniform throughout the gas, then it will remain constant. Hence it is often not necessary to solve the third equation in (2.13), and the isentropic equations for small perturbations reduce to

$$\begin{cases} \frac{\partial}{\partial t}\rho + \frac{\partial}{\partial x}(\rho u) = 0 \\ \frac{\partial}{\partial t}(\rho u) + \frac{\partial}{\partial x}(\rho u^2 + \hat{k}\rho^\gamma) = 0 \end{cases} \tag{2.14}$$

Taking s as a constant, equation (2.11) leads to the equation of state

$$p = \hat{k}\rho^\gamma, \tag{2.15}$$

where $\hat{k} = ke^{\frac{s}{c_v}}$ is a constant that depends only on the initial entropy particle. Hence the pressure p is a function of the density ρ only and satisfies

$$\frac{dp}{d\rho} = c^2, \tag{2.16}$$

where c denotes the sound speed. For details of applications to linear acoustics see Piperno (1995), Blom (1998), Leveque (2002), van Zuijlen (2004) and other references.

2.3 Finite volume methods

In this section we give an overview of finite volume schemes. Further details of the method, in the context of linear systems, nonlinear scalar and nonlinear systems, can

be found in Leveque (2002) and Toro (1999).

For the conservation laws (see Section 1.1.3) it is essential that the scheme is written in a conservative form. This ensures the correct approximation for the weak solutions, Leveque (2002). When the solution is discontinuous, the integral form is the correct form to model conservation laws. Therefore the conservation form of the method for conservation laws is derived directly from its integral form. Here we present this derivation.

We consider the following initial-boundary value problem

$$\begin{aligned} &\text{PDE: } \tfrac{\partial}{\partial t}Q + \tfrac{\partial}{\partial x}f(Q) = 0, \quad x \in [x_L, x_R], \quad Q \in \Omega_Q \subset R^m \\ &\text{IC: } Q(x,0) = h(x), \\ &\text{BC: } Q(x_L,t) = B_L(t), \quad Q(x_R,t) = B_R(t), \end{aligned} \tag{2.17}$$

where Q is the vector of the conservative variables, $f(Q)$ is the flux vector, h is the initial condition and $B_{L,R}$ are the boundary conditions on the left and the right.

Here we restrict our consideration to the essential properties that we need to apply numerical methods to conservation laws. In short, we restrict our consideration to simple model problems, assuming that the physical principles of conservation of mass, momentum and energy are satisfied. As in Section 1.1.3, the partial differential equation

$$\frac{\partial}{\partial t}Q + \frac{\partial}{\partial x}f(Q) = 0 \tag{2.18}$$

is called the differential form of the conservation laws. In one-dimensional, the finite volume method consists of subdividing the spatial domain into intervals called finite volumes or grid cells and keeping path of an approximation to the integral of Q over each of these cells. Therefore, we have to update these values at each time step by using approximations to the flux through the endpoints on the grid cells.

Denoting the i grid cell by

$$\mathcal{C}_i = [x_{i-\frac{1}{2}}, x_{i+\frac{1}{2}}],$$

the value Q_i^n is the approximation of the average value over the i grid cell at current time $t = t^n$ and reads

$$Q_i^n \approx \frac{1}{\Delta x} \int_{\mathcal{C}_i} Q(x, t^n) dx, \qquad \text{where} \qquad \Delta x = x_{i+\frac{1}{2}} - x_{i-\frac{1}{2}}. \tag{2.19}$$

Now, our concern is to derive the integral form of the conservation laws. Integrating the PDE (2.18) over the spatial grid cell:

$$\int_{x_{i-\frac{1}{2}}}^{x_{i+\frac{1}{2}}} \frac{\partial}{\partial t} Q dx + \int_{x_{i-\frac{1}{2}}}^{x+\frac{1}{2}} \frac{\partial}{\partial x} f(Q) dx = 0 \tag{2.20}$$

Assuming the smoothness of Q and $f(Q)$ we have

$$\frac{\partial}{\partial t} \int_{x-\frac{1}{2}}^{x+\frac{1}{2}} Q dx + f(Q)\Big|_{x-\frac{1}{2}}^{x+\frac{1}{2}} = 0, \tag{2.21}$$

which gives

$$\frac{\partial}{\partial t} \int_{x-\frac{1}{2}}^{x+\frac{1}{2}} Q dx = f\Big(Q(x_{i-\frac{1}{2}}, t^n)\Big) - f\Big(Q(x_{i+\frac{1}{2}}, t^n)\Big). \tag{2.22}$$

The expression (2.22) means that the temporal variation of the conservation variables $Q(x,t)$ inside the grid cell $\mathcal{C}_i$ is due only to the difference of the fluxes on its boundaries. Since the averages Q_i^n are known at the current t^n, we are concerned with approximating the cell average at the next time t^{n+1}, denoted by Q_i^{n+1}. Therefore the expression (2.22) can be used to develop a time marching algorithm. Defining the grid cell in time $[t^n, t^{n+1}]$ we obtain

$$\int_{t^n}^{t^{n+1}} \Big[\frac{\partial}{\partial t}\int_{x-\frac{1}{2}}^{x+\frac{1}{2}} Q dx\Big] dt = \int_{t^n}^{t^{n+1}} \Big[f\Big(Q(x_{i-\frac{1}{2}}, t^n)\Big) - f\Big(Q(x_{i+\frac{1}{2}}, t^n)\Big)\Big] dt, \qquad (2.23)$$

Using basic derivative rules, we have from (2.23) that

$$\Big[\int_{x-\frac{1}{2}}^{x+\frac{1}{2}} Q(x,t) dx\Big]_{t^n}^{t^{n+1}} = \int_{t^n}^{t^{n+1}} \Big[f\Big(Q(x_{i-\frac{1}{2}}, t^n)\Big) - f\Big(Q(x_{i+\frac{1}{2}}, t^n)\Big)\Big] dt, \qquad (2.24)$$

which gives

$$\begin{aligned}\int_{x-\frac{1}{2}}^{x+\frac{1}{2}} Q(x,t^{n+1}) dx - \int_{x-\frac{1}{2}}^{x+\frac{1}{2}} Q(x,t^n) dx = \\ \int_{t^n}^{t^{n+1}} \Big[f\Big(Q(x_{i-\frac{1}{2}}, t^n)\Big) - f\Big(Q(x_{i+\frac{1}{2}}, t^n)\Big)\Big] dt, \qquad (2.25)\end{aligned}$$

Re-arranging the terms in the expression (2.25) we get

$$\begin{aligned}\int_{x-\frac{1}{2}}^{x+\frac{1}{2}} Q(x,t^{n+1}) dx = \int_{x-\frac{1}{2}}^{x+\frac{1}{2}} Q(x,t^n) dx - \\ \Big[\int_{t^n}^{t^{n+1}} f\Big(Q(x_{i+\frac{1}{2}}, t^n)\Big) dt - \int_{t^n}^{t^{n+1}} f\Big(Q(x_{i-\frac{1}{2}}, t^n)\Big) dt\Big], \qquad (2.26)\end{aligned}$$

Dividing (2.26) by Δx we obtain

$$\frac{1}{\Delta x}\int_{x-\frac{1}{2}}^{x+\frac{1}{2}} Q(x,t^{n+1})dx = \frac{1}{\Delta x}\int_{x-\frac{1}{2}}^{x+\frac{1}{2}} Q(x,t^{n})dx - \frac{1}{\Delta x}\Big[\int_{t^n}^{t^{n+1}} f\Big(Q(x_{i+\frac{1}{2}},t^n)\Big)dt - \int_{t^n}^{t^{n+1}} f\Big(Q(x_{i-\frac{1}{2}},t^n)\Big)dt\Big], \tag{2.27}$$

As (2.19) defines the cell-average value computed at time t^n, similarly, we can define the time-average flux computed at the cell interface $x_{i+\frac{1}{2}}$ as

$$f_{i+\frac{1}{2}} \approx \frac{1}{\Delta t}\int_{t^n}^{t^{n+1}} f\Big(Q(x_{i+\frac{1}{2}},t^n)\Big)dt \tag{2.28}$$

Substituting (2.19) and (2.28) into (2.27) we can therefore derive the exact relation, which is the reformulation of the principle of the integral conservation:

$$Q_i^{n+1} = Q_i^n - \frac{\Delta t}{\Delta x}\Big(f_{i+\frac{1}{2}}^n - f_{i-\frac{1}{2}}^n\Big) \tag{2.29}$$

The Equation (2.29) tells us how the cell-average of Q from (2.19) should be updated exactly in one time step. Therefore while no numerical scheme is introduced, the exact solution of (2.27) satisfies also (2.29). However, in general, we can not evaluate the time integrals on the right-hand side of (2.27) since $Q(x_{i-\frac{1}{2}})$ and $Q(x_{i+\frac{1}{2}})$ vary with time along each edge of the cell, and on the other hand there is not the exact solution to work with. Therefore it is reasonable to consider the study of numerical methods that are in conservation form (2.29). So we use this formulation to construct a discrete method to solve the IBVP (2.17). The scheme is called finite volume method

since it is based on the integral conservation over finite control volumes. In the finite volume fashion we discretize the weak integral form of the partial differential equation and the essential feature is to define the numerical flux at the cell interfaces $f_{i\pm\frac{1}{2}}$ as a function of the cell-averages Q_i^n and $Q_{i\pm1}^n$, once only the cell-average solution is known. It means that in the finite volume framework instead of to get a discrete value of Q at a spatial point x, we get its integral average over the spatial control volume. But in order to compute the flux at the element interfaces, we need the so-called reconstruction step which consists in defining the values of Q at the interfaces $x_{i\pm\frac{1}{2}}$. In the most simple case the solution is supposed to be piece-wise constant with $Q_i^n \in \mathcal{C}_i$, which leads to discontinuities at the cell interfaces, since the numerical solution has two values at the interface namely $Q_{i+\frac{1}{2}}^- = Q_i^n$ and $Q_{i+\frac{1}{2}}^+ = Q_{i+1}^n$, where $Q_{i+\frac{1}{2}}^-$ and $Q_{i+\frac{1}{2}}^+$ denotes the solution at the left and at the right of the interface $x_{i+\frac{1}{2}}$, respectively.

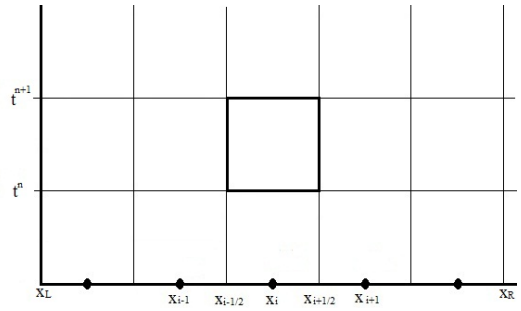

Figure 2.1: The $x-t$ space discretization and the $x-t$ control volume $\mathcal{C}_i \times T^n$ referred to as the finite volume method

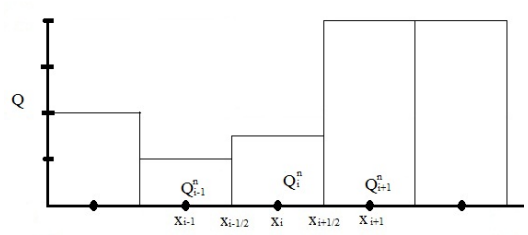

Figure 2.2: Piece-wise control solution.

So it is reasonable to suppose that to solve these discontinuities we need a function $f_{i+\frac{1}{2}}$ of both states $Q^-_{i+\frac{1}{2}}$ and $Q^+_{i+\frac{1}{2}}$, called numerical flux. We might use the formula of the form

$$f^n_{i+\frac{1}{2}} = f(Q^-_{i+\frac{1}{2}}, Q^+_{i+\frac{1}{2}}) = f(Q^n_i, Q^n_{i+1}) \tag{2.30}$$

The method (2.29) then becomes

$$Q^{n+1}_i = Q^n_i - \frac{\Delta t}{\Delta x}\Big(f(Q^n_i, Q^n_{i+1}) - f(Q^n_{i-1}, Q^n_i)\Big). \tag{2.31}$$

Basic Numerical Fluxes

Referring to the general form of finite volume method (2.29) for a hyperbolic system of conservation laws, here we consider several ways in which the numerical flux might be defined.

(1) Central flux. Let us define the average flux at the point $x_{i+\frac{1}{2}}$ on the basis of data Q^n_i and Q^n_{i+1} to the left and to the right, respectively, of the referred point.

Attempting the simple arithmetic average can lead to

$$f^c_{i+\frac{1}{2}} = f(Q^n_i, Q^n_{i+1}) = \frac{1}{2}\Big(f(Q^n_i) + f(Q^n_{i+1})\Big), \tag{2.32}$$

the so-called central flux. Using it in (2.29) we get the Central scheme

$$Q^{n+1}_i = Q^n_i - \frac{\Delta t}{2\Delta x}\Big(f(Q^n_{i+1}) - f(Q^n_{i-1})\Big) \tag{2.33}$$

In general this method is unstable for hyperbolic problems even for small time steps such that the CFL condition is satisfied, Leveque (2002).

(2) The Lax-Friedrichs flux, is defined as

$$f^{LF}_{i+\frac{1}{2}} = f(Q^n_i, Q^n_{i+1}) = \frac{1}{2}\Big(f(Q^n_{i+1}) + f(Q^n_i)\Big) + \frac{\Delta x}{2\Delta t}\Big(Q^n_{i-1} - Q^n_i\Big) \tag{2.34}$$

which leads to the Lax-Friedrichs method

$$Q^{n+1}_i = \frac{1}{2}\Big(Q^n_{i-1} + Q^n_{i+1}\Big) - \frac{\Delta t}{2\Delta x}\Big(f(Q^n_{i+1}) - f(Q^n_{i-1})\Big) \tag{2.35}$$

It is possible to see that this flux looks like the central flux plus an additional term, and the resulting Lax-Friedrics method is similar to the central scheme with the only difference that the value Q^n_i is replaced by the average $\frac{1}{2}\Big(Q^n_{i-1} + Q^n_{i+1}\Big)$. The additional term, in the LxF flux, is interpreted as numerical diffusion to damp the instabilities concerned with the central scheme and makes the method to be stable for a CFL number up to 1. However we need to

use a very refined grid otherwise the scheme produces more diffusion than it is required and leads to badly smeared numerical results.

(3) Local Lax-Friedrichs flux. An improvement for the Lax Friedrichs scheme can be reached by replacing the value $a = \frac{\Delta x}{\Delta t}$ by a locally determined value. So we obtain

$$f^{LxF}_{i+\frac{1}{2}} = f(Q^n_i, Q^n_{i+1}) = \frac{1}{2}\Big[\Big(f(Q^n_{i+1}) + f(Q^n_i)\Big) + a\Big(Q^n_{i-1} - Q^n_i\Big)\Big] \tag{2.36}$$

where $a = max\Big(\Big|f'(Q_i)\Big|, \Big|f'(Q_{i+1})\Big|\Big)$. The resulting method is known as Rusanov's method or the local Lax-Friedrichs method, Toro (1999), Leveque (2002).

(4) The Lax Wendroff flux. There are two possible versions of this scheme. The first one consists of

$$f^{LW_1}_{i+\frac{1}{2}} = \frac{1}{2}\Big(f(Q^n_{i+1}) + f(Q^n_i) - \frac{\Delta t}{2\Delta x} A^n_{i+\frac{1}{2}}(Q^n_{i+1} - Q^n_i)\Big), \tag{2.37}$$

where $A^n_{i+\frac{1}{2}}$ is an averaged Jacobian matrix defined at $x_{i+\frac{1}{2}}$. It can be computed by the arithmetic average of the two Jacobians calculated on basis of the left and right states, respectively. The second Lax-Wendroff flux is given by two stage procedure

$$f^{LW_2}_{i+\frac{1}{2}} = f(Q^{LW}_{i+\frac{1}{2}}), \tag{2.38}$$

where the state $Q^{LW}_{i+\frac{1}{2}} = \frac{1}{2}\Big(Q^n_{i+1} + Q^n_i\Big) - \frac{\Delta t}{2\Delta x}\Big(f(Q^n_{i+1}) - f(Q^n_i)\Big)$

(5) First-order centered flux (FORCE).The FORCE flux was introduced by Toro (2000). It is the arithmetic average of the Lax-Friedrichs and Lax-Wendroff fluxes, namely

$$f_{i+\frac{1}{2}}^{FORCE} = \frac{1}{2}\Big(f_{i+\frac{1}{2}}^{LF} + f_{i+\frac{1}{2}}^{LW}\Big). \tag{2.39}$$

2.3.1 Properties of the finite volume methods

(1) **Exact conservation**

A essential characteristic of the finite volume schemes is that they are exactly conservative. A method is conservative when can be written in the form

$$Q_i^{n+1} = Q_i^n - \frac{\Delta t}{\Delta x}\Big(f_{i+\frac{1}{2}} - f_{i-\frac{1}{2}}\Big). \tag{2.40}$$

Hou and Lefloch (1994) have proven that a nonconservative scheme converges to the wrong solution with wrong shock speed and the wrong states at the shock wave.

(2) **Consistency, stability and convergence**

A conservative method (2.40) is consistent if

$$f_{i+\frac{1}{2}}(Q, Q, ..., Q) = f(Q). \tag{2.41}$$

Lax Equivalence Theorem:

The main application of stability is in the Lax Equivalence Theorem which is concerned with well-posed linear problems and states that:

$Stability + Consistency \longrightarrow Convergence \longrightarrow Weak\ solution$

Further details of proof of this theorem can be found in Colella and Puckett (1998).

(3) **Monotonicity**

Consider a numerical method written in the compact form, Toro (1999)

$$Q_i^{n+1} = H(Q_{i-l}^n, Q_{i-l+1}^n, ..., Q_{i-1}^n, Q_i^n, Q_{i+1}^n, ..., Q_{i+r-1}^n, Q_{i+r}^n), \tag{2.42}$$

where H is a *linear* or *nonlinear* operator. The method is called monotone if H is a non-decreasing function with respect to all its arguments, i.e. when

$$\frac{\partial H}{\partial Q_k^n} \geq 0, \qquad i - l \leq k \leq i + r. \tag{2.43}$$

2.4 High order Finite Volume schemes

2.4.1 Point-wise WENO reconstruction

In a finite volume scheme, we need to compute fluxes across the element interfaces. For this purpose, numerical flux functions are used, which need two point values of the numerical solution at the cell interface, $x_{i+\frac{1}{2}}$, one extrapolated to the interface

from the left-side and another one from the right-side. The WENO method produces a higher order accurate point-wise reconstruction of the solution at the cell interface, $x_{i+\frac{1}{2}}$.

The general idea of a WENO scheme given by Jiang (1996) is as follows: In order to obtain a k-th order accurate WENO scheme, called WENO k, it is necessary to employ a piecewise reconstruction polynomial of degree $M = k-1$ for each cell, $\mathcal{C}_i = [x_{i-\frac{1}{2}}, x_{i+\frac{1}{2}}]$. To calculate the unknown coefficients of the reconstruction polynomial from the known cell averages U_j^n one needs a *reconstruction stencil* or a *stencil*

$$S_i^M = \bigcup_{j=i-e}^{i+e} I_j, \tag{2.44}$$

composed of $k = 2e+1$ elements, where e is the extension of the stencil to the left and the right, M is the degree of the reconstruction polynomial and i is the $i-$th grid cell. The reconstruction stencil must always include the cell $\mathcal{C}_i$ itself. The resulting reconstruction polynomial has k coefficients and is of degree $M = k-1$. According to the relative position of the stencil elements with respect to the cell $\mathcal{C}_i$ for which the reconstruction is undertaken, a stencil is called *centered* (with subscript $(0, e)$), left-sided (with subscript $(-, e)$, the minus sign denoting "left") or right-sided (with subscript $(+, e)$, the plus sign denoting "right"), henceforth. For instance, if we take $k = 5$, according to the $WENO_5$ reconstruction procedure for the interface $x_{i+\frac{1}{2}}$, we obtain: The big stencil (refer to Figure 2.3)

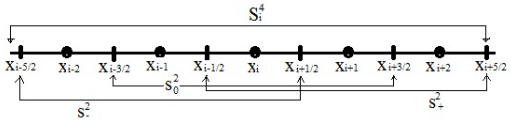

Figure 2.3: $WENO_5$ reconstruction procedure for $x_{i+\frac{1}{2}}$. The Figure shows the big stencil S_i^4 needed to reconstruct a $4-$th degree polynomial which is divided into three smaller sub-stencils. On each sub-stencil a degree 2 polynomial is reconstructed.

$$S_i^4 = \{I_{i-2}, I_{i-1}, I_i, I_{i+1}, I_{i+2}\}, \tag{2.45}$$

needed to reconstruct a $4-$th degree polynomial, which is sub-divided into three smaller sub-stencils:

$$S^2(-,e) = \{I_{i-2}, I_{i-1}, I_i\}, \quad S_2(0,e) = \{I_{i-1}, I_i, I_{i+1}\}, \quad S^2(+,e) = \{I_i, I_{i+1}, I_{i+2}\} \tag{2.46}$$

where the superscript is the degree of the piece-wise polynomial to be constructed on these sub-stencils. From now on we will not explicitly use e in the subscript for ease of notation. It will only be used where it is felt necessary. The reconstruction polynomial $P_i^M(x,t^n)$ of degree M is obtained from the known cell averages, Q_j^n, by imposing integral conservation i.e., the following must hold:

$$\frac{1}{\Delta x}\int_{\mathcal{C}_i} P_i^M(x,t^n)dx = Q_j^n, \quad \forall \mathcal{C}_j \in S_i^M. \tag{2.47}$$

Therefore, for the WENO method of order k in one space dimension, one needs one big central reconstruction stencil S_i^M of $k = M+1$ elements and $\frac{M}{2}+1$ small sub-

stencils $S_s^{M/2}$, $s \in \{0, \pm\}$ composed of $\frac{M}{2}+1$ elements to reconstruct several lower order polynomials of degree $\frac{M}{2}$. Here s is the stencil-shift with respect to the central element I_i, denoted by the sign of the shift, $\{0, \pm\}$. The linear WENO reconstruction at the element interface, $x_{i+\frac{1}{2}}$, is then given as a linear combination of the lower order reconstruction polynomials, $P_s^{M/2}(x, t^n)$, obtained from the sub-stencils $S_s^{M/2}$ using the same integral conservation principle (2.47) above. The linear weights, λ_s are chosen in such a way that the linear combination of the lower order polynomials is identical to the one obtained via the reconstruction polynomial on the big stencil S_i^M. The weights λ_s obviously depend on the position x for which the reconstruction is to be done. For consistency purposes the sum of the weights must always be equal to unity. Furthermore, the weights $\lambda_s$should be positive and must not depend on the solution Q_j^n .

Alternatively, for non-smooth solutions, the point value $Q_{i+\frac{1}{2}}^n = Q(x_{i+\frac{1}{2}}, t^n)$ is then given by a suitable non-linear combination of the reconstruction polynomials obtained on the sub-stencils. In order to make the WENO scheme non-linear, i.e. data-dependent, the reconstruction at point $x_{i+\frac{1}{2}}$ is obtained by using a nonlinear combination of the lower order reconstruction polynomials of the sub-stencils by substituting the linear weights with nonlinear weights ω_s, which are defined as

$$\omega_s = \frac{\tilde{\omega}_s}{\sum_s \omega_s}, \quad \tilde{\omega}_s = \frac{\lambda_s}{(\sigma_s + \epsilon)^r}, \quad s \in \{0, \pm\}. \tag{2.48}$$

where σ_s denotes the so-called smoothness or oscillation indicator, ϵ is a small

number to prevent division by zero and r is an exponent for which Jiang (1996) always choose as $r = 2$. For the smoothness indicator value of ϵ

$$\sigma_s = \sum_{l=1}^{M/2} \int_{x_{i-\frac{1}{2}}}^{x_{i+\frac{1}{2}}} h^{2l-1} \Big(\frac{\partial^l}{\partial x^l} P_s^{M/2} \Big)^2 dx \tag{2.49}$$

where $h = \Delta x$ and $P_s^{M/2}(x)$ are polynomials of degree $M/2$ on the sub-stencils, the term $(h)^{2l-1}$ is used to remove scaling effects from the derivatives as proposed in Jiang (1996).

For clarifying the computation of the weights we present an example.

Example: Computing linear weights λ concerned with WENO3 scheme, performing the reconstruction at point $x_{i+\frac{1}{2}}$.

There is one big central stencil with three elements denoted as $S_i^2 = \{I_{i-1}, I_i, I_{i+1}\}$ and two sub-stencils both composed of two elements, denoted as $s_-^1 = \{I_{i-1}, I_i\}$ for the left-sided , and $s_+^1 = \{I_i, I_{i+1}\}$ for the right-sided, respectively.

In order to compute the reconstruction polynomial on the big stencil S_i^2 we use the integral conservation principle (Eq. 13) which leads to the second order reconstruction polynomial

$$P_i^2(x) = \frac{1}{2}Q_{i-1}^n + \frac{5}{6}Q_i^n - \frac{1}{6}Q_{i+1}^n + (Q_i^n - Q_{i-1}^n)\xi + \Big(\frac{1}{2}Q_{i-1}^n - Q_i^n + \frac{1}{2}Q_{i+1}^n\Big)\xi^2, \tag{2.50}$$

where $x = x_{i-1} + \xi \Delta x$.

On the two sided sub-stencils we obtain the following first order polynomials

$$p_{-1}^{1}(x) = \frac{1}{2}Q_i^n + \frac{1}{2}Q_{i-1}^n + (Q_i^n - Q_{i-1}^n)\xi, \quad \text{and}$$
$$p_{1}^{1}(x) = \frac{3}{2}Q_i^n - \frac{1}{2}Q_{i+1}^n + (Q_{i+1}^n - Q_i^n)\xi, \tag{2.51}$$

respectively, on the left and right side.

The conditions to obtain the linear weights λ_{-1} and λ_1 are then the following equation:

$$\begin{cases} \lambda_{-1} + \lambda_1 = 1 \\ p_{-1}^{1}(x_{i+\frac{1}{2}})\lambda_{-1} + p_{1}^{1}(x_{i+\frac{1}{2}})\lambda_1 = P_i^2(x_{i+\frac{1}{2}}) \end{cases} \tag{2.52}$$

which, after some algebraic computations, result in the following linear weights: $\lambda_{-1} = \frac{1}{3}$ and $\lambda_1 = \frac{2}{3}$. These results are then used to compute the nonlinear weights for each sub-stencil. For instance, to compute the nonlinear weight for the left-sided sub-stencil the procedure should be:

$$\omega_{-1} = \frac{\tilde{\omega}_{-1}}{\sum \omega_s}, \qquad \tilde{\omega}_{-1} = \frac{\lambda_{-1}}{(\sigma_{-1} + \epsilon)^r} = \frac{1/3}{(\sigma_{-1} + \epsilon)^r}, \tag{2.53}$$

where $\sum \omega_s$ is the sum of all the nonlinear weights computed for each sub-stencil and

$$\sigma_{-1} = \int_{x_{i-\frac{1}{2}}}^{x_{i+\frac{1}{2}}} h\Big(\frac{d(p_{-1}^{1}(x))}{dx}\Big)^2 dx, \tag{2.54}$$

with $h = \Delta x$ and $x = x_{i-1} + \xi\Delta x$.

This original WENO reconstruction of Jiang (1996) for one dimension, described in Section 2.4.1, is rather difficult to be generalized to unstructured triangular and

tetrahedral meshes in two and three dimensions because of the need to determine the optimal linear weights. For more details, we recommend, Hu (1999), Shi (2002) and Zhang (2009). Therefore, we present, in the next section, a different idea that can be extended, more easily, to unstructured meshes.

2.4.2 Polynomial WENO reconstruction

In this section, we present an alternative reconstruction procedure for the one dimensional case on the basis of a new reconstruction technique, called the arbitrary high order finite volume scheme, proposed by Dumbser (2007a), which makes use of techniques developed originally in the discontinuous Galerkin framework. The polynomial WENO reconstruction operator produces entire polynomials, $P_i(x, t^n)$, as in the ENO approach proposed by Harten et al. (1987).

However, the method is formally written like a WENO scheme given in Shu (1997) and Liu et al. (1994) with a particularly simple choice for the linear weights. The most important difference between this scheme and the classical WENO scheme of Shu (1997) is that standard WENO methods reconstruct point values at the Gaussian integration points instead of an entire polynomial valid inside each control volume, $\mathcal{C}_i = [x_{i-\frac{1}{2}}, x_{i+\frac{1}{2}}]$. The reconstruction is done for each element on a reconstruction stencil $S_i^{(s)}$, which is given by the following union of the elements $\mathcal{C}_i$ and its neighbors

$\mathcal{C}_j$,

$$S_i^{(s)} = \bigcup_{j=i+s-e}^{i+s+e} \mathcal{C}_j, \tag{2.55}$$

where s is now the stencil shift with respect to the central cell I_i and e is the spatial extension of the stencil to the left and the right. A central reconstruction stencil ($s = 0$), an entirely left-sided stencil ($s = -e$) and an entirely right-sided stencil ($s = e$) are given, respectively, by

$$S_i^{(0)} = \bigcup_{j=i-e}^{i+e} \mathcal{C}_j, \quad S_i^{(-e)} = \bigcup_{j=i-2e}^{i} \mathcal{C}_j, \quad \text{and} \quad S_i^{(+e)} = \bigcup_{j=i}^{i+2e} \mathcal{C}_j, \tag{2.56}$$

which are the three fixed reconstruction stencils adopted in this Chapter. As usual for finite volume schemes, data is represented by the cell averages of a conserved quantity, Q, inside cell $\mathcal{C}_i$. Now that the stencils have been established, the use of e will be dropped for ease of notation. In order to achieve high order accuracy for the spatial discretization, one looks for a spatial reconstruction polynomial P obtained from $S_i^{(s)}$ at time t^n. The reconstruction polynomial for element I_i is written as

$$P_i^{(s)}(\xi, t^n) = \sum_{l=0}^{M} \phi_l(\xi) \hat{w}_l^{(s)}(t^n) \tag{2.57}$$

where ξ is the coordinate in a reference coordinate system. On the righthand side of (2.57) the standard tensor index notation is used. For each element I_i, a reference coordinate $\xi \in [0, 1]$ is used. The transformation from the physical coordinate system

x into the reference coordinate system ξ is defined by

$$x = x_{i-\frac{1}{2}} + \xi \Delta x. \tag{2.58}$$

The reconstruction basis, $\phi_l(\xi)$, is composed of polynomials of degree M and depends on space. As basis functions the Legendre polynomials,

$$\phi_l(\xi) = (2^l l!)^{-1} \frac{d^l}{d\xi^l} \Big[(\xi^2 - 1)^l \Big] \tag{2.59}$$

are used on the unit interval, which form an orthogonal basis with respect to the inner product:

$$< \phi_i(\xi), \phi_k(\xi) >= \int_0^1 \phi_i(\xi)\phi(\xi) d\xi. \tag{2.60}$$

In the following, the standard tensor index notation is used, implying summation over indices appearing twice. The number of polynomial coefficients (degrees of freedom) is $k = M + 1$, where M is the degree of the reconstruction polynomial and k is the spatial order of accuracy of the scheme in space. To compute the reconstruction polynomial, $P_i(\xi, t^n)$, valid for element I_i, one requires the integral conservation for all elements I_j inside the stencil $S_i^{(s)}$, i.e.

$$\int_{I_j} P_i^{(s)}(\xi, t^n) d\xi = \int_{I_j} \phi_l(\xi) d\xi . \hat{w}_l^{(s)}(t^n) = Q_j^n, \quad \forall I_j \in S_i^{(s)}. \tag{2.61}$$

Equation (2.61) yields a system of linear equations for the unknown coefficients $\hat{w}_l^{(s)}(t^n)$ of the reconstruction polynomial on stencil $S_i^{(s)}$ that can be easily solved.

To obtain the final non-oscillatory reconstruction polynomials for each element I_i at

the time t^n, a data-dependent nonlinear combination of the polynomials $P_i^{(0)}(\xi, t^n)$, $P_i^{(-)}(\xi, t^n)$, and $P_i^{(+)}(\xi, t^n)$ obtained from the central, left-sided and right-sided stencils is constructed as follows:

$$P_i(\xi, t^n) = \hat{w}_l(t^n)\phi_l(\xi), \quad \text{where} \quad \hat{w}_l(t^n) = \omega_0 \hat{w}_l^{(0)}(t^n) + \omega_- \hat{w}_l^{(-)} + \omega_+ \hat{w}_l^{(+)}(t^n). \quad (2.62)$$

Hence

$$P_i(\xi, t^n) = \omega_- P_i^{(-)}(\xi, t^n) + \omega_0 P_i^{(0)}(\xi, t^n) + \omega_+ P_i^{(+)}(\xi, t^n). \quad (2.63)$$

The nonlinear weights $\omega_{(s)}$, $s \in \{0, \pm\}$ are given by the relations

$$\omega_s = \frac{\tilde{\omega}_s}{\sum_s \omega_s}, \quad \tilde{\omega}_s = \frac{\lambda_s}{(\sigma_s + \epsilon)^r}; \quad s \in \{0, \pm\}. \quad (2.64)$$

The oscillation indicators σ_s are computed as for point-wise WENO reconstructions:

$$\sigma_s = \sum_{l=1}^{M} \int_0^1 \Big(\frac{\partial^l}{\partial \xi^l} P_i^{(s)}(\xi, t^n)^2 d\xi \Big). \quad (2.65)$$

The parameters ϵ and r are constants for which one typically chooses $\epsilon = 10^{-14}$ and $r = 8$. Unlike the nonlinear weights used in the usual point-wise WENO reconstruction, the linear weights λ_s are simply defined by $\lambda_- = \lambda_+ = 1$ and a very large linear weight λ_0 on the central stencil, typically $\lambda_0 = 10^5$. Jiang (1996), show that the numerical solutions are quite insensitive to the WENO parameters ϵ and r. Dumbser (2007a) show that the numerical results are also insensitive to the linear weights on the central stencil λ_0.

Typically, in order to avoid spurious oscillations that may appear when applying ENO or WENO reconstruction operators component-wise to non-linear hyperbolic conservation systems, the reconstruction needs to be done on characteristic variables, Harten et al. (1987). The result of reconstruction is a non-oscillatory spatial polynomial $P_i(\xi, t^n)$ defined at t^n inside each spatial element I_i.

The advantage of the polynomial WENO reconstruction is its straightforward extension to general unstructured meshes. The inconvenience is that at a given order of accuracy k the total stencil needed for the reconstruction is wider than the one of the classical point-wise WENO.

In this chapter, the alternative polynomial WENO reconstruction described in this section is applied. Specifically, the third order polynomial WENO reconstruction is employed, the rescaled Legendre polynomials up to degree two are used as reconstruction basis functions, which according to equation (2.59) are

$$\phi_0(\xi) = 1, \quad \phi_1(\xi) = 2\xi - 1, \quad \text{and} \quad \phi_2(\xi) = 1 - 6\xi + 6\xi^2 \tag{2.66}$$

It can be easily checked that the set of non-zero functions $\{\phi_l(\xi) : l = 0, 1, 2\}$, given above, is mutually orthogonal on the unit interval $[0, 1]$. Following equations (2.62)-(2.65), we obtain the following expansion coefficients (note that $e = 1$):

- for the left-sided stencil

$$\hat{w}_0^{(-1)} = Q_i^n, \;\; \hat{w}_1^{(-1)} = \frac{1}{4}Q_{i-2}^n - Q_{i-1}^n + \frac{3}{4}Q_i^n, \;\; \hat{w}_2^{(-1)} = \frac{1}{12}Q_{i-2}^n - \frac{1}{6}Q_{i-1}^n + \frac{1}{12}Q_i^n, \tag{2.67}$$

- for the central stencil

$$\hat{w}_0^{(0)} = Q_i^n, \;\; \hat{w}_1^{(0)} = -\frac{1}{4}Q_{i-1}^n + \frac{1}{4}Q_{i+1}^n, \;\; \hat{w}_2^{(0)} = \frac{1}{12}Q_{i-1}^n - \frac{1}{6}Q_i^n + \frac{1}{12}Q_{i+1}^n, \tag{2.68}$$

- and for the right-sided stencil

$$\hat{w}_0^{(1)} = Q_i^n, \;\; \hat{w}_1^{(1)} = -\frac{3}{4}Q_i^n + Q_{i+1}^n - \frac{1}{4}Q_{i+2}^n, \;\; \hat{w}_2^{(1)} = \frac{1}{12}Q_i^n - \frac{1}{6}Q_{i+1}^n + \frac{1}{12}Q_{i+2}^n. \tag{2.69}$$

- The oscillation indicator is given by

$$\sigma_{(s)} = 156(\hat{w}_2^{(s)})^2 + 4(\hat{w}_1^{(s)})^2, \quad s \in \{-, 0, +\}. \tag{2.70}$$

2.4.3 The Cauchy-Kovalewski procedure in the reference element

Consider a general nonlinear system of conservation laws as in equation (2.17) where Q is a vector of conserved variables and $F(Q)$ is a vector of nonlinear fluxes. Since all basis functions are given in the reference coordinate, we apply the Cauchy-Kovalewski procedure in the reference element, rewriting the generic nonlinear hyperbolic system of conservation laws (2.17) directly as

$$\frac{\partial Q}{\partial t} + \Delta t \frac{\partial}{\partial \xi} F^*(Q) = 0 \tag{2.71}$$

with

$$F^* = F\xi_x. \tag{2.72}$$

Further information can be found in Dumbser (2007a) and Dumbser et al. (2007b). The iterative steps can be summarized as follows:

(1) Compute the flux $F(q)$,

(2) Compute the flux F^* in the reference space,

(3) Perform the local space-time discontinuous Garlekin interaction.

2.4.4 The ADER-Finite Volume One step Scheme

For time integration, it is important to take into account the efficiency and accuracy of time integration schemes. Several studies focus on the efficiency of Runge-Kutta (RK) time discretization schemes, Bijl (2001). However it is found that the efficiency of these schemes decreases substantially if, due to the so-called Butcher barriers, Butcher (1987), the order of accuracy becomes greater than four, which makes the number of intermediate RK stages larger than the formal order of accuracy.

Therefore, in order to achieve an arbitrarily accurate time discretization, in this work, we apply the arbitrary high order derivation (ADER) approach, developed originally and introduced by Toro (2001), to the semi-discrete form of the system resulting from the integration in the reference system. The ADER approach consists

of a Taylor expansion in time, the solution of generalized Riemann problems (GRP) to approximate the space derivatives at the interface and the Cauchy-Kovalewski procedure for replacing the time derivatives in the Taylor series by space derivatives. Throughout the work presented in this Chapter, the approach in Dumbser (2007a) with regards to the ADER for high order time integration of the finite volume method on unstructured grids, called ADER-FV scheme, was followed. The difference is that in Dumbser (2007a) the ADER is simplified for general linear hyperbolic systems. Here the original approach for the general nonlinear hyperbolic systems is applied. Further details of the approach can be found in, Titarev (2002), Titarev (2005b), Titarev (2005a), and other references.

2.5 Numerical Flux and Schemes

We formulate the conservative finite volume schemes of the form

$$Q_i^{n+1} = Q_i^n - \frac{\Delta t}{\Delta x}\Big(f_{i+\frac{1}{2}} - f_{i-\frac{1}{2}}\Big) \tag{2.73}$$

to solve systems of hyperbolic conservation laws

$$\frac{\partial Q}{\partial t} + \frac{\partial f(Q)}{\partial x} = 0, \tag{2.74}$$

which in that case are the Euler equations. Here we need to specify the numerical flux $f_{i+\frac{1}{2}}$. In this chapter an explicit method is applied. Thus for stability a constraint on the time step, Δt, needs to be imposed. The flux can be written in conservative

form as

$$f_{i+\frac{1}{2}} = f(Q_{i+\frac{1}{2}}), \tag{2.75}$$

and the time step satisfies:

$$\Delta t \leq \frac{\Delta x}{S_{max}}, \tag{2.76}$$

where S_{max} is the largest wave speed present throughout the domain at time $t = t^n$, Toro (1999), Leveque (2002). For instance, for scalar problems this is approximated as $S_{max} = max(|f'(q)|)$, over all q between Q_i^n and Q_{i+1}^n. The size of the spatial discretization Δx is chosen according to the desired accuracy. However the size of the time step Δt has to be chosen on the basis of the condition, Toro (1999):

$$\Delta t = CFL\frac{\Delta x}{S_{max}}, \tag{2.77}$$

where CFL is the Courant number, which satisfies

$$0 < CFL \leq 1. \tag{2.78}$$

Proposed Numerical Flux

For finite volume schemes, the main feature is to define the numerical flux $f_{i+\frac{1}{2}}$ at the cell interfaces as functions of the cell-averages Q_i^n since for the finite volume framework only the cell-averages are known, Toro (1999), Stein (2004). Therefore, the specific method depends on how we choose the numerical flux function. In this chapter we consider two numerical fluxes:

(1) The numerical flux of two states Q^n_{i+1} and Q^n_i for the Local Lax-Friedrichs Method

$$f^{LLF}_{i+\frac{1}{2}} = f^{LLF}_{i+\frac{1}{2}}(Q^n_{i+1}, Q^n_i) = \frac{1}{2}\Big[f(Q^n_{i+1}) + f(Q^n_i)\Big] - \frac{1}{2}a_{i+\frac{1}{2}}\Big[Q^n_{i+1} - Q^n_i\Big]; \quad (2.79)$$

where $a_{i+\frac{1}{2}}$ is a locally determined value defined as $a_{i+\frac{1}{2}} = max(|S_{i-\frac{1}{2}}|, |S_{i+\frac{1}{2}}|)$, where $S_{i-\frac{1}{2}}$ and $S_{i+\frac{1}{2}}$ are, respectively, the left and the right characteristic speed at the interface.

(2) The numerical flux of two states Q^n_{i+1} and Q^n_i for the first Lax-Wendroff method (LW1)

$$f^{LW1}_{i+\frac{1}{2}} = f^{LW1}_{i+\frac{1}{2}}(Q^n_{i+1}, Q^n_i) = \frac{1}{2}\Big[f(Q^n_{i+1}) + f(Q^n_i)\Big] - \frac{1}{2}\frac{\Delta t}{\Delta x}A^2_{i+\frac{1}{2}}\Big[Q^n_{i+1} - Q^n_i\Big] \quad (2.80)$$

where $A_{i+\frac{1}{2}}$ is an averaged Jacobian matrix defined at $x_{i+\frac{1}{2}}$.

The numerical flux that we propose takes the form:

$$f^{PF}_{i+\frac{1}{2}} = \frac{1}{2}\Big[f^{LLF}_{i+\frac{1}{2}}(Q^n_{i+1}, Q^n_i) + f^{LW1}_{i+\frac{1}{2}}(Q^n_{i+1}, Q^n_i)\Big] \quad (2.81)$$

where $A^2_{i+\frac{1}{2}}$ is chosen as a unit matrix. The flux (2.81) can be written as

$$f^{PF}_{i+\frac{1}{2}} = \frac{1}{2}\Big[f(Q^n_{i+1} + Q^n_i)\Big] - \frac{1}{2}\Big[\Big(\frac{a_{i+\frac{1}{2}} + \frac{\Delta t}{\Delta x}}{2}\Big)\Big(Q^n_{i+1} - Q^n_i\Big)\Big], \quad (2.82)$$

Therefore from (2.73) the numerical flux leads to the numerical method

$$Q^{n+1}_i = Q^n_i - \frac{\Delta t}{2\Delta x}\Big[(f_{i+1} + f_{i-1}) - \frac{1}{2}DQ^n_{i-1} + DQ^n_i - \frac{1}{2}DQ^n_{i+1}\Big], \qquad D = (a_{i+\frac{1}{2}} + \frac{\Delta t}{\Delta x}). \quad (2.83)$$

Recalling the properties for the finite volume methods (refer to Section 2.3.1) we can show that the method (2.83) is:

(1) Consistent:$f^{LLF}_{i+\frac{1}{2}}$ and $f^{LW1}_{i+\frac{1}{2}}$ are consistent, therefore $\frac{1}{2}\left\{ f^{LLF}_{i+\frac{1}{2}} + f^{LW1}_{i+\frac{1}{2}} \right\}$ is consistent. So the flux (2.81) satisfies the condition (2.41).

(2) Monotonicity: Consider a numerical method written in the compact form, Toro (1999):

$$Q_i^{n+1} = H(Q_{i-l}^n, Q_{i-l+1}^n, ..., Q_{i-1}^n, Q_i^n, Q_{i+1}^n, ..., Q_{i+r-1}^n, Q_{i+r}^n), \tag{2.84}$$

where H is a *linear* or *nonlinear* operator. The method is called monotone if H is a non-decreasing function with respect to all its arguments, i.e. when

$$\frac{\partial H}{\partial Q_k^n} \geq 0, \qquad i - l \leq k \leq i + r. \tag{2.85}$$

Further details can be found in Chapter 13 in Toro (1999).

Our aim here is to show that the finite volume scheme, (2.83), with our proposed numerical flux, (2.81), is monotone. For simplicity we recall the scalar PDE

$$Q_t + f_x = 0 \tag{2.86}$$

and as application we consider the advection equation

$$Q_t + \bar{u} Q_x = 0, \tag{2.87}$$

so that the flux $f = \bar{u}q$. As we referred above our proposed numerical flux takes the form

$$f^{PF}_{i+\frac{1}{2}} = \frac{1}{2}\Big[f^n_{i+1} + f^n_i\Big] - \frac{1}{4}\Big[\Big(a_{i+\frac{1}{2}} + \frac{\Delta t}{\Delta x}A^2_{i+\frac{1}{2}}\Big)\Big(Q^n_{i+1} - Q^n_i\Big)\Big], \tag{2.88}$$

for simplification purpose we denote $\Big(a_{i+\frac{1}{2}} + \frac{\Delta t}{\Delta x}A^2_{i+\frac{1}{2}}\Big) = D$.

Recalling the finite volume method

$$Q^{n+1}_i = Q^n_i - \frac{\Delta t}{\Delta x}(f^n_{i+\frac{1}{2}} - f^n_{i-\frac{1}{2}}), \tag{2.89}$$

our proposed numerical flux (2.88) leads to the following numerical method

$$Q^{n+1}_i = Q^n_i - \frac{\Delta t}{2\Delta x}\Big[(f^n_{i+1} - f^n_{i-1}) - \frac{1}{2}DQ^n_{i-1} + Dq_i - \frac{1}{2}DQ^n_{i+1}\Big], \tag{2.90}$$

and applied to the advection equation (2.87) becomes

$$Q^{n+1}_i = Q^n_i - \frac{\Delta t}{2\Delta x}\Big[(\bar{u}Q^n_{i+1} - \bar{u}Q^n_{i-1}) - \frac{1}{2}DQ^n_{i-1} + DQ_i - \frac{1}{2}DQ^n_{i+1}\Big]. \tag{2.91}$$

Factorizing (2.91) becomes

$$Q^{n+1}_i = \frac{1}{2}\Big[\frac{\Delta t}{\Delta x}\bar{u} + \frac{\Delta t}{2\Delta x}D\Big]Q^n_{i-1} + \Big[1 - \frac{\Delta t}{2\Delta x}D\Big]Q^n_i + \frac{1}{2}\Big[\frac{\Delta t}{2\Delta x}D - \frac{\Delta t}{\Delta x}\bar{u}\Big]Q^n_{i+1}. \tag{2.92}$$

Now consider the operator H given by

$$H(Q^n_{i-1}, Q^n_i, Q^n_{i+1}) := \frac{1}{2}\Big[c + \frac{\Delta t}{2\Delta x}D\Big]Q^n_{i-1} + \Big[1 - \frac{\Delta t}{2\Delta x}D\Big]Q^n_i + \frac{1}{2}\Big[\frac{\Delta t}{2\Delta x}D - c\Big]Q^n_{i+1}, \tag{2.93}$$

where c is the Courant number, Toro (1999).

For monotonicity it is sufficient to have, assuming differentiability

$$\frac{\partial H}{\partial Q_{i-1}^n} > 0, \qquad \frac{\partial H}{\partial {Q_i}^n} > 0, \qquad \frac{\partial H}{\partial Q_{i+1}^n} > 0, \qquad \forall c : 0 < c < 1. \tag{2.94}$$

$$\frac{\partial H}{\partial Q_{i-1}^n} = \frac{1}{2}\Big[c + \frac{\Delta t}{2\Delta x} D\Big] > 0, \qquad \forall c : 0 < c < 1, \tag{2.95}$$

$$\frac{\partial H}{\partial Q_{i+1}^n} = \Big[1 - \frac{\Delta t}{2\Delta x} D\Big] > 0, \Rightarrow \frac{\Delta t}{2\Delta x} D < 1, \tag{2.96}$$

Note that the expression (2.96) does not depend on c.

$$\frac{\partial H}{\partial Q_{i+1}^n} = \frac{1}{2}\Big[\frac{\Delta t}{2\Delta x} D - c\Big] > 0 :\Rightarrow \Big[\frac{\Delta t}{2\Delta x} D - c\Big] > 0 :\Rightarrow c < \frac{\Delta t}{2\Delta x} D \tag{2.97}$$

But from (2.96) we have that

$$\frac{\Delta t}{2\Delta x} D < 1, \tag{2.98}$$

thus by transitivity property we have that

$$c < 1. \tag{2.99}$$

We conclude that a sufficient condition for monotonicity is satisfied under the CFL condition $0 < c < 1$.

2.6 NUMERICAL EXPERIMENTS

In this section, the proposed approach is tested. The inter-cell flux that we proposed in this work will be compared numerically with the Rusanov's flux popularly known as the local Lax-Friedrichs flux. The one dimensional system of Euler equations

$$Q_t + F(Q)_x = 0, \tag{2.100}$$

where $Q = (\rho, \rho u, \rho E)^T$ and $F(Q) = (\rho u, \rho u^2 + P, u(\rho E + P))^T$, will be solved. As already pointed out ρ is the density, u is the velocity, P is the pressure, $E = \frac{1}{2}\rho u^2 + \frac{P}{(\gamma-1)}$ is the total energy and γ is the ratio of specific heats, taken as 1.4 here. The following Riemann type initial conditions:

$$\mathbf{Q}(x,0) = \begin{cases} \mathbf{Q}_L & \text{if } x < 0 \\ \mathbf{Q}_R & \text{if } x > 0 \end{cases}$$

are imposed.

Four classical one dimensional shock tube problems were computed. These examples were also used in a fully three dimensional setting to test the quadrature-free non-oscillatory finite volume schemes on unstructured meshes for nonlinear hyperbolic conservation laws in Dumbser et al. (2007b).

Given the computational domain $[a, b]$ discretised into L computing cells with length Δx, conditions at the boundaries $x = a$ and $x = b$ are required. Therefore, we consider the transmissive boundary conditions for the problems tested below, Leveque

(2002), Toro (1999).

All the results are computed for a Courant number of CFL = 0.5.

2.6.1 Example 1: The Sod Shock tube Problem

The first test case corresponds to a modification of the standard Sod problem. The initial conditions are $(\rho, u_L, P_L) = (1, 0.75, 1)$ and $(\rho_R, u_R, P_R) = (0.125, 0.0, 0.1)$ separated by a discontinuity at $x = 0.5$. The solution in Figure 2.4 is computed at time $t = 0.20$. The computational domain length is taken as a unit ranging from $x = 0.0$ and $x = 1.0$ divided into 200 cells. In Figure 2.5, a magnified profile for energy is shown in order to emphasize the improvement brought about by the modified flux.

2.6.2 Example 2: The Lax Shock tube Problem

The second problem is the Riemann problem proposed by Lax and also appearing in, Jiang (1996). The initial conditions are $(\rho_L, u_L, P_L) = (0.445, 0.698, 3.528)$ and $(\rho_R, u_R, P_R) = (0.5, 0.0, 0.571)$ separated by a discontinuity at $x = 0.5$. The output presented in Figure 2.6 is computed at time $t = 0.14$. The computational domain length is taken as a unit ranging from $x = 0.0$ and $x = 1.0$ divided in 200 cells. In the following figure 2.7, a magnified profile for density and energy is shown in order to emphasize the improvement brought about by the modified flux.

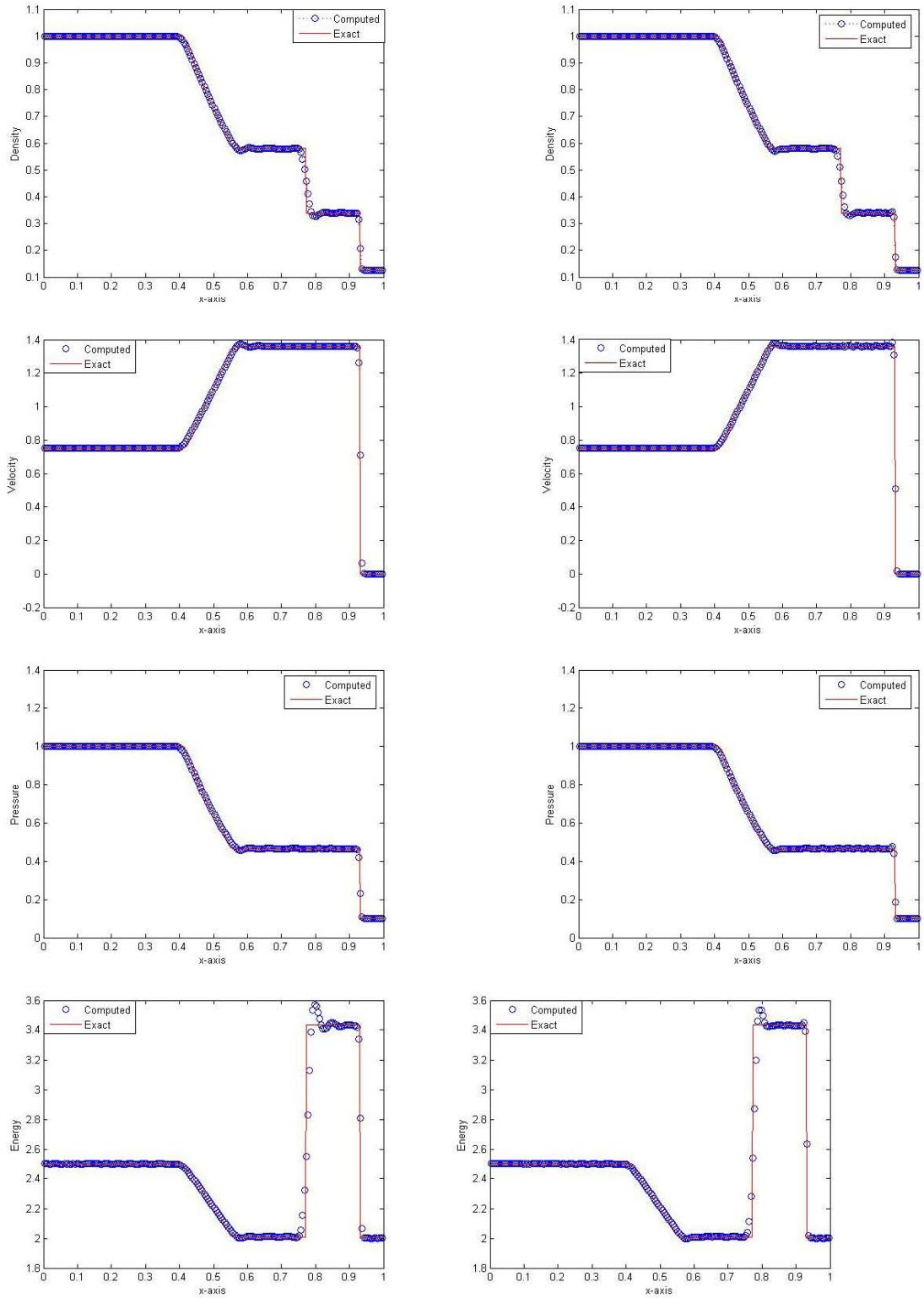

Figure 2.4: Results for a modified Sod's problem, Example 1, via LLF inter-cell flux (left) and the proposed inter-cell flux(right)

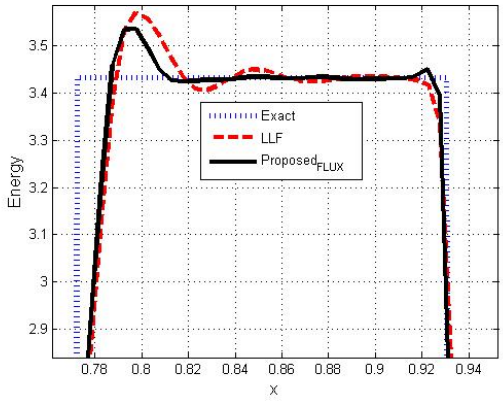

Figure 2.5: Energy for Sod's problem, Example 1, magnified.

2.6.3 Example 3: An Example with High Pressure Jump

The third problem is the more challenging Riemann test problem. It was introduced to show on the one hand the capability of the proposed scheme to capture discontinuities that are very close to each other and on the other hand to deal with very severe pressure jumps without producing negative pressures, since the initial condition jumps over five orders of magnitude from 10^3 to 10^{-2}.

The initial conditions are

$(\rho_L, u_L, P_L) = (1.0, 0.0, 1000)$, and

$(\rho_R, u_R, P_R) = (1.0, 0.0, 0.01)$.

The results presented in Figure 2.8 were computed at $t = 0.012$. The computational domain length is taken as a unit ranging from $x = 0.0$ and $x = 1.0$ divided in 200 cells.

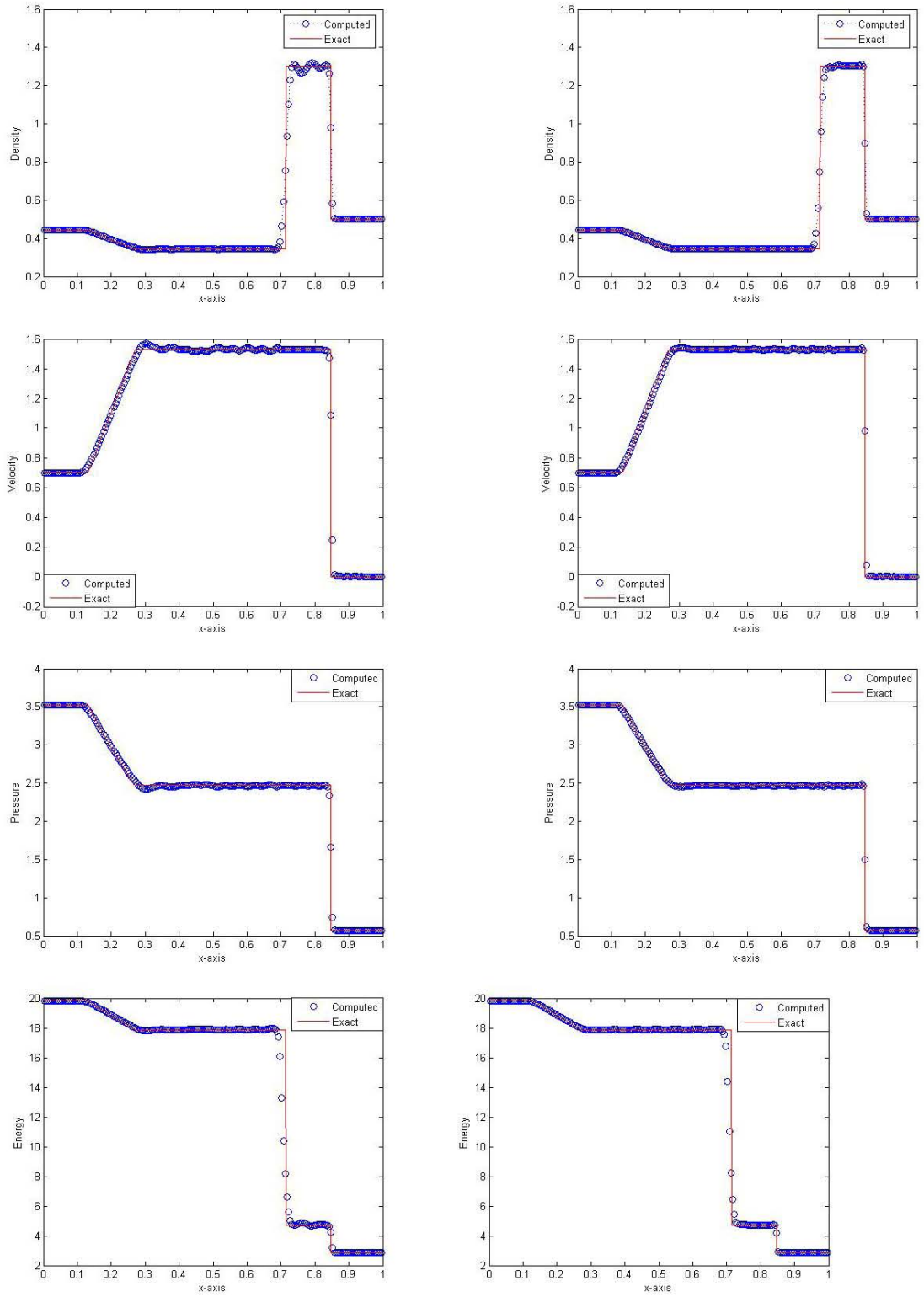

Figure 2.6: Results for a modified Lax's problem, Example 1, via LLF inter-cell flux (left) and the proposed inter-cell flux(right)

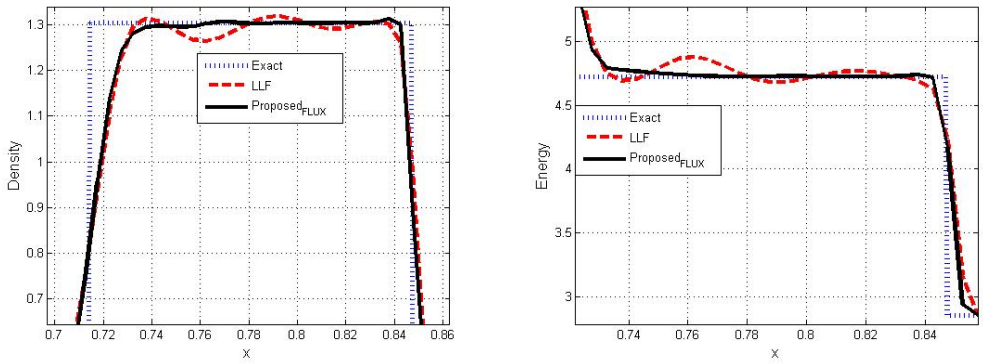

Figure 2.7: Density and Energy for Lax problem, Example 2, magnified.

In the following figure 2.9, a magnified profile for density and energy is shown in order to emphasize the improvement brought about by the modified flux.

2.6.4 Example 4: Slowly Moving Shock Wave

The fourth and last test is given by the Riemann problem:

$(\rho_L, u_L, P_L) = (5.99924, 19.5975, 1460.895)$, and

$(\rho_R, u_R, P_R) = (5.99242, -6.19633, 46.0950)$.

The results presented in Figure 2.10 are computed at $t = 0.035$. The computational domain length is taken as the interval $[0, 1.2]$ divided in 200 cells. This example exhibits a particular feature of a very slowly moving shock wave that can cause problems for numerical schemes and that can lead to spurious oscillations. In the following figure 2.11, a magnified profile for density and energy is shown in order to emphasize the improvement brought about by the modified flux.

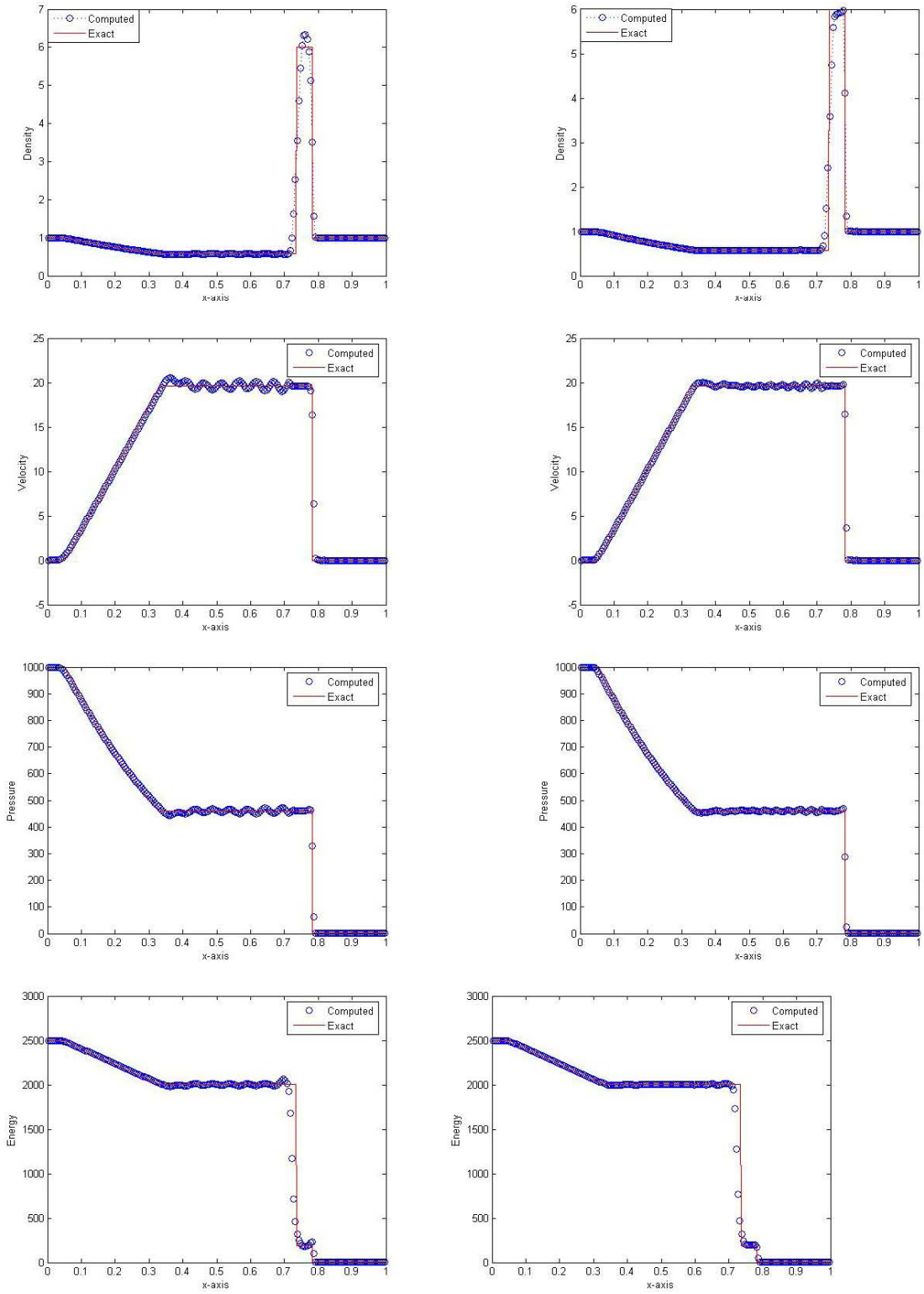

Figure 2.8: Results for test problem 3 via LLF inter-cell (left) and the proposed intercel flux (right)

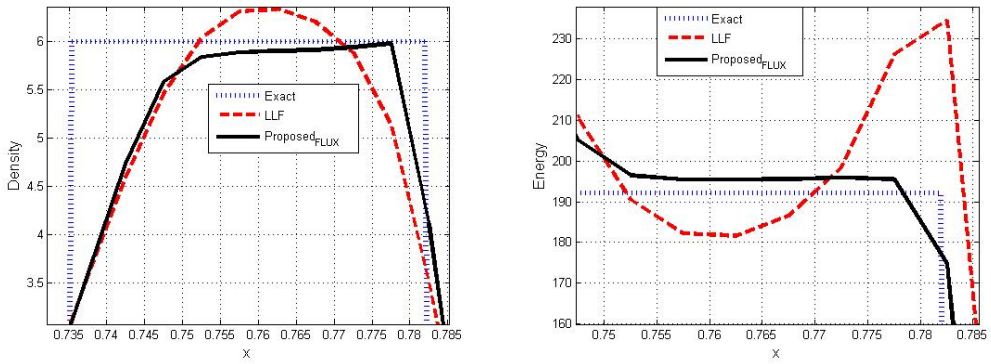

Figure 2.9: Density and Energy for Example 3 magnified.

2.6.5 Comparison of errors

In this section we undertake a comparison of absolute errors of the two numerical flux results in the region where we magnified. In this case, one sees clearly from figure 2.12 that the modified flux does produce smaller relative errors than LLF for energy in this case.

In the second example, the absolute errors were compared for density and energy for the regions were oscillations were observed as shown in Figure 2.13. Here too it is clear that the modified scheme performs better.

In the third and fourth example, the absolute errors were compared for density and energy for the regions were oscillations were observed as shown in Figure 2.14 and 2.15. Here too it is clear that the modified scheme performs better for density. In terms of energy it produces a greater error especially close to the shock front. This might be because the scheme might be producing more diffusion on the shock front.

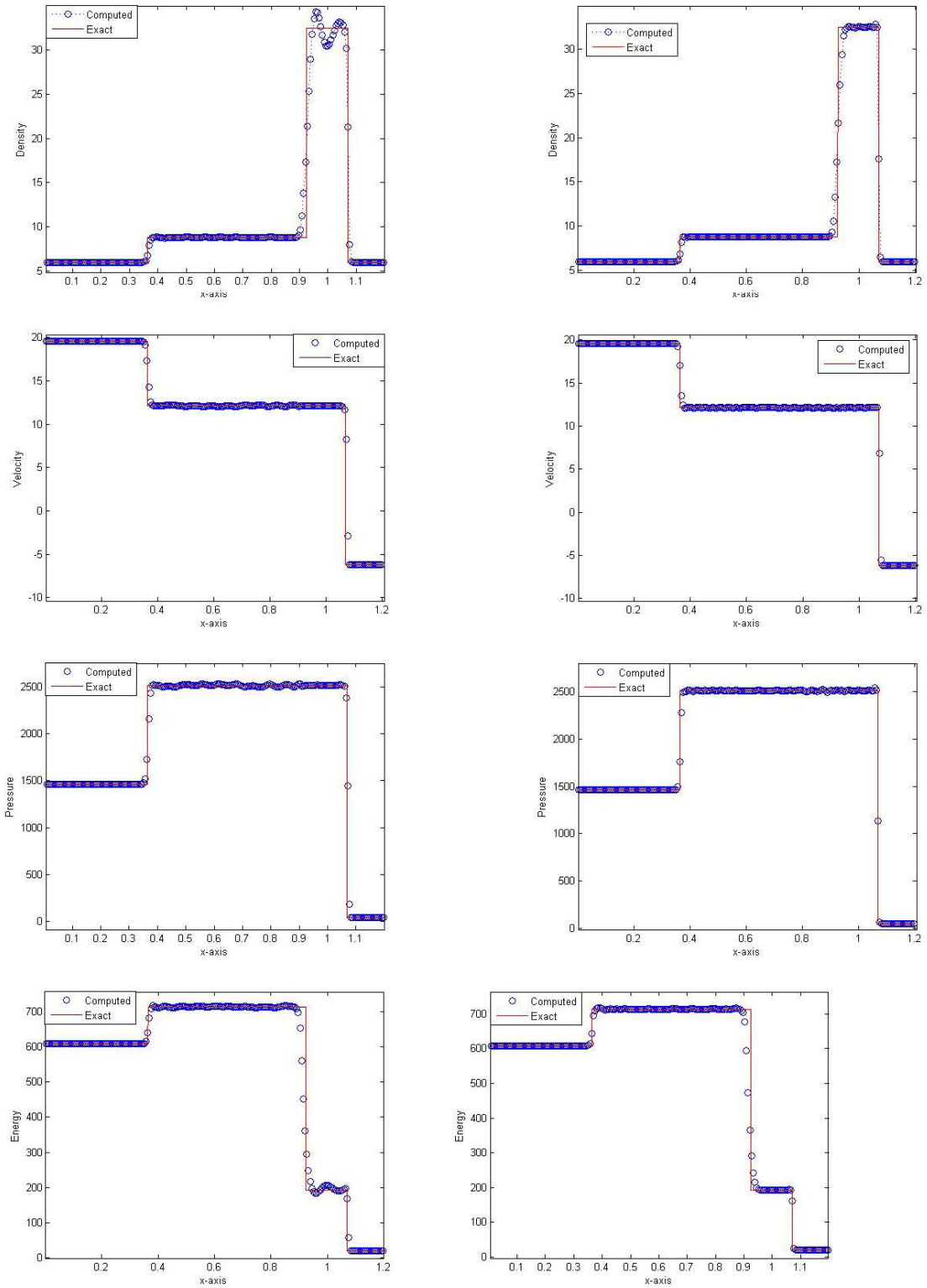

Figure 2.10: Results for the test problem 4 via LLF inter-cell (left) and the proposed intercel flux (right)

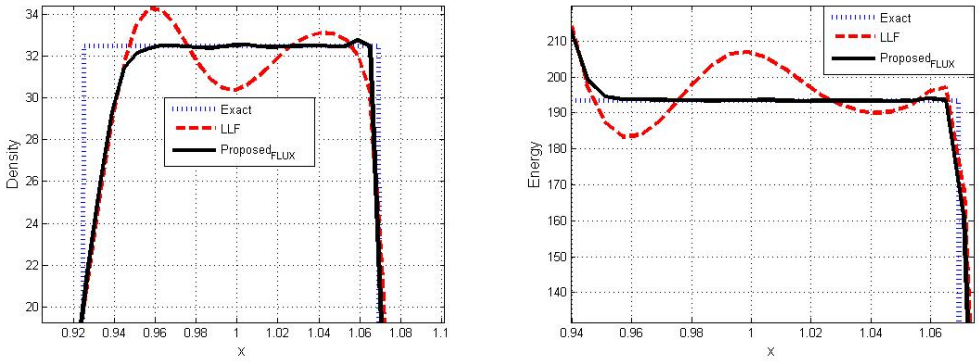

Figure 2.11: Density and Energy for Example 4 magnified.

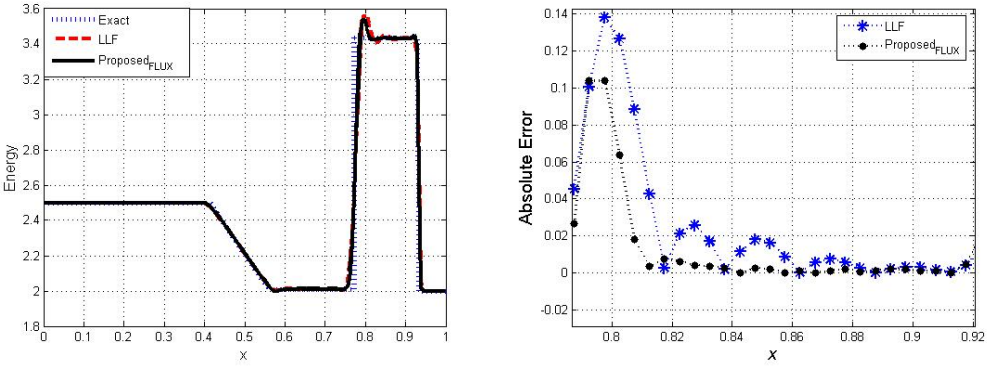

Figure 2.12: The performance of proposed scheme (left) and the respective absolute error (right) for Example 1, in the points where LLF scheme oscillates considerably.

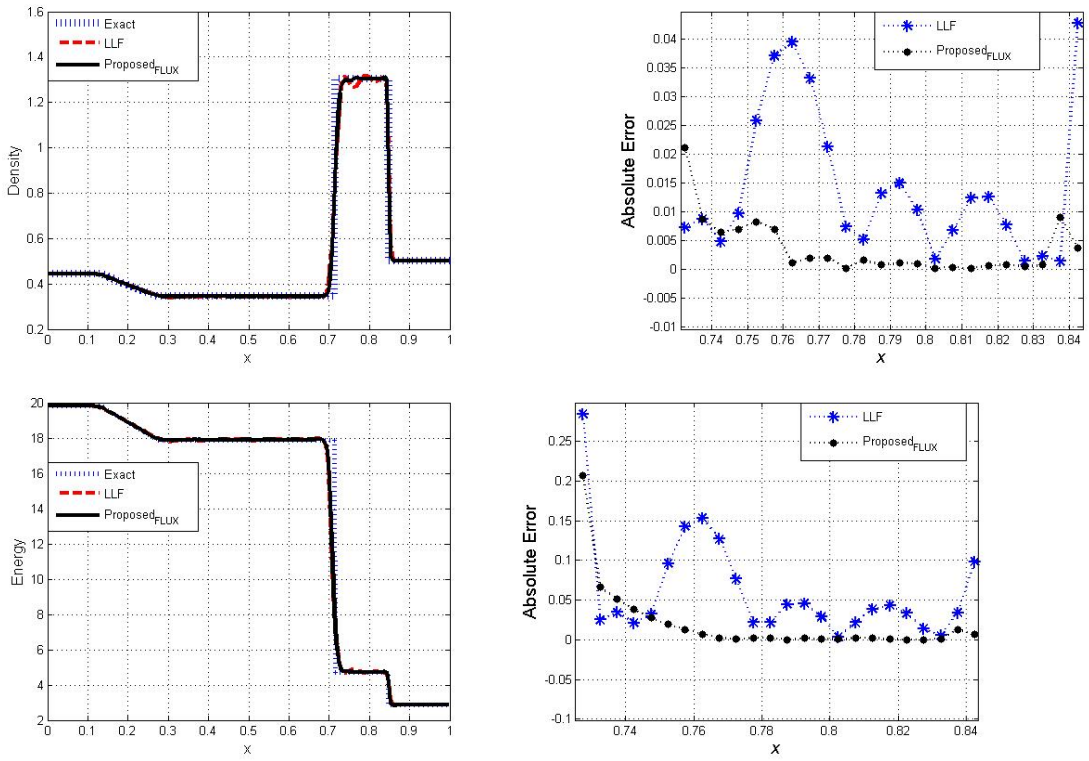

Figure 2.13: The performance of proposed scheme (left) and the respective absolute error (right) for Example 2, in the points where LLF scheme oscillates considerably.

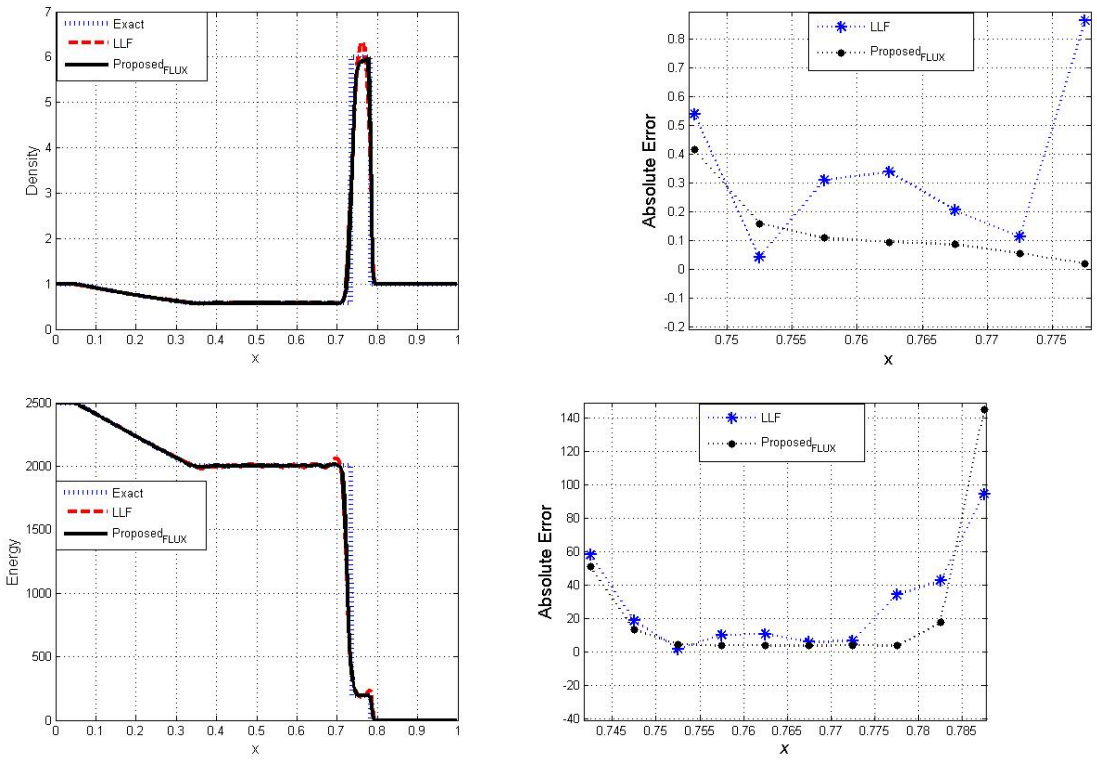

Figure 2.14: The performance of proposed scheme (left) and the respective absolute error (right) for Example 3, in the points where LLF scheme oscillates considerably.

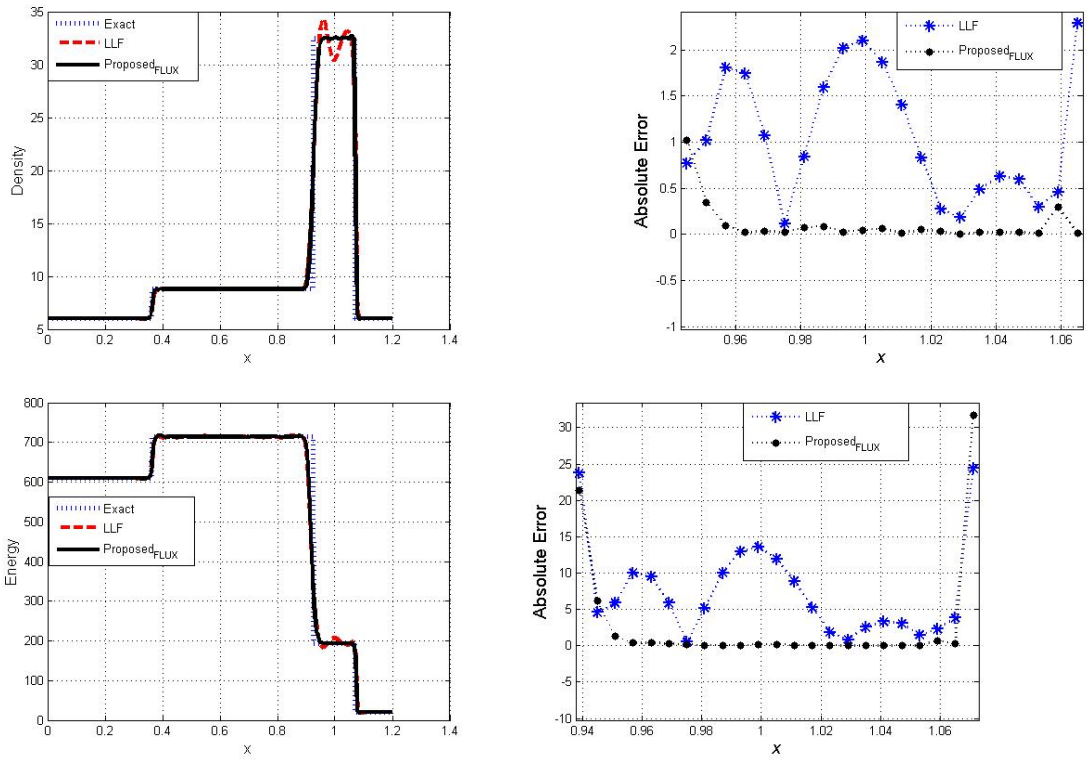

Figure 2.15: The performance of proposed scheme (left) and the respective absolute error (right) for Example 4, in the points where LLF scheme oscillates considerably.

As shown in Fig. 2.12, LLF scheme oscillates considerably in the points between the discontinuities. However, the modified scheme reduces oscillations significantly except in a few points. While the absolute error for LLF scheme oscillates between order 1 and order 4, the absolute error for proposed scheme practically keeps the order of oscillation constant between order 3 to order 4, meaning practically very reduced oscillations. The same observation can be practically made for test problem 2, as shown in Fig. 2.13. Here the modified scheme even behaves better than in the test problem 1.

The test problem 3 is considered the most challenging one, Dumbser et al. (2007b). However the modified scheme is capable of reducing the oscillations significantly. In the fourth test case it is possible to see the better performance of modified scheme since the order of magnitude of the absolute error is higher and practically non oscillatory compared with the order of magnitude of the absolute error for LLF, which is small and oscillates considerably.

2.6.6 Results and discussion

We can see that for all problems when we apply a basic numerical Rusanov flux there are oscillations present. However for the proposed flux, only few oscillations are notable which confirm in general the essentially non-oscillatory character of this approach. And also the discontinuities are, practically, well resolved. In particular, for

the Lax test problem the approach performs well. For the test Problem 3, the most challenging one, the modified approach behaves robustly although with some overshoots. For the fourth and last test problem we get also good non-oscillatory results. Taking into account only the density for all the test problems our approach almost compare with the computations obtained by applying the fully three-dimensional setting in Dumbser et al. (2007b).

2.7 Conclusions

In this chapter a review of arbitrary order WENO schemes has been made. A one-dimensional case was presented. The reconstruction is done for each element of a reconstruction stencil as given in Dumbser (2007a) and Dumbser et al. (2007b). A modified inter-cell flux is developed. Numerical examples were computed especially those with discontinuous solutions for Euler equations. In general WENO reconstructions yield oscillatory results but these oscillations can be reduced by using the modified numerical flux functions. In addition the accuracy of the solutions is not compromised. Hence for specific problems it might be necessary to apply a modified flux functions rather than application of expensive decompositions or refining the grid, Qiu (2002).

Chapter 3

INTRODUCTION TO FLUID-STRUCTURE INTERACTION: GOVERNING EQUATIONS, APPROACHES AND SOLVERS.

3.1 Introduction

In the past few decades easy access to fast computing capabilities has sparked a renewed interest in multi-physics problems. Such problems involving a coupling between two or more different interacting physical phenomena include, *inter alia*, fluid-structure interactions in aerodynamics, vibro-aeroacoustic problems, the modelling of solidification and melting processes, and soft tissue mechanics, Soulaïmani (2005). These problems are particularly challenging to solve since the combined demands for the use of different solvers in different parts of the solution domain, as well as different mesh requirements, increase the complexity of the computational effort. For fluid-structure interaction (FSI) problems, fluid flow induces forces and thermal fluxes on a solid structure. The motion of the two phases modifies not only the fluid domain, but also the velocity and the temperature fields at the fluid-structure interface. There are several practical and challenging examples of FSI, including for instance: the interaction between the sail of a boat or the wing of a plane and the surrounding aerodynamic flow; the interaction between a bridge and the wind; and the interaction

between vessels and blood flow. In these practical examples there are always technology gaps to be filled by numerical simulations, Weymouth et al. (2006), Weymouth (2008), Hou (2012). For instance, in an example of a sailing boat, for further study of the interaction between water waves and the motion of the boat, an efficient numerical algorithm has to be used. This kind of study is typically multidisciplinary. For instance, the performance of a boat results from the interaction between water hydrodynamics and structural dynamics, Hou (2012). The multidisciplinary nature of fluid-structure interaction problems, plus their strong nonlinearity, constitutes a motivation to study comprehensively such problems, and making such study a constant challenge, Hou (2012). Numerical simulations have been the way to investigate the fundamental physics of the complex interaction between fluids and structures because it is nearly impossible to obtain analytical solutions to the equations modelling most FSI problems, van Zuijlen (2004), Hou (2012). The numerical procedures commonly used to solve FSI problems may be essentially classified into two approaches: the *staggered or partitioned approach*; and the *monolithic approach*. The staggered approach treats the sub-domains-fluid and structure-with separate solvers, by solving each computational field with its respective mesh discretization and numerical scheme. The interface conditions are treated explicitly to interchange information between the fluid and the structure solutions, Farhat (2006), Farhat (2000), Garelli (2011). In contrast, the monolithic approach treats the fluid and structure dynamics

as a single system of equations, which is integrated simultaneously by an integrated scheme. The conditions at the interface are implicit in the solution approach, Blom (1998), Michler et al. (2004).

The monolithic approach is potentially more accurate for a multi-physics problem, however it may require significant resources and time to develop such a specialized algorithm, Hou (2012). Unlike the monolithic approach, the staggered approach combines available disciplinary codes, which reduces the time for its development since it takes advantage of existing numerical algorithms that have been used to solve fluid or structural problems. When a staggered approach succeeds, it can solve a fluid-structure interaction problem with complicated fluid and structural physics. Therefore the staggered approach is the most widely used. The staggered approach was introduced by Park (1977). Among several works regarding the staggered approach, we highlight the following: Piperno (1994) considered stability features of the staggered approach to integrate in time one-dimensional aero-elastic model problems. Various partitioned approaches were presented by Piperno (1995). Prananta (1996) used the staggered approach for transonic flutter calculations. Mouro (1996) treated incompressible fluid-structure interaction problems applying a staggered approach. Piperno (1997) presented a coupling staggered approach where momentum conservation is enforced at the interface. A staggered approach based on an estimation of the energy that is numerically created at the interface of fluid and structure, was considered by

Piperno (1997). Farhat (2000) proposed two alternative serial and parallel staggered approaches to solve a coupled transient aero-elastic problem. Piperno (2001) solved a large-scale nonlinear dynamic aero-elastic problem using a fluid/structure staggered procedure. Lefrançois (2010) provided a basic and solid grasp of numerics underlying the physics of fluid-structure interaction, using a staggered approach. Throughout this thesis the staggered approach is considered to solve fluid-structure interaction problems, using "Arbitrary Lagrangian Eulerian" formulation to ensure the use of moving meshes.

3.2 Governing equations for fluid and structure

In this section we present the governing equations for fluid dynamics, structure dynamics and mesh dynamics.

3.2.1 Fluid dynamics

The dynamics of fluid flow is governed by the Euler equations that model a compressible gas. These equations form a set of coupled conservation laws that can be enumerated as:

(1) Conservation of mass,

(2) Conservation of momentum,

(3) Conservation of energy,

and in order to consider the Arbitrary Lagrangian Eulerian (ALE) framework, another conservation law must be added,

(4) Geometric conservation law.

The Euler equations are a simplification of the *Navier-Stokes* equations. The Navier-Stokes equations are more realistic and also include the effects of fluid viscosity and heat conduction, Leveque (2002). In Chapters 1 and 2, the normal formulation of the Euler equations was presented. Here an emphasis is given to the Arbitrary Lagrangian Eulerian formulation of such equations.

Traditionally, the problems in structural mechanics use a Lagrangian coordinate system, in which the computational mesh moves with the material. For fluid mechanics, the traditional choice is an Eulerian coordinate system which has the mesh fixed in space. For fluid-structure interaction problems, neither the Lagrangian nor the Eulerian formulations are optimal for the whole domain, because for large deformations of the fluid, a Lagrangian formulation can lead to spurious results and an Eulerian formulation is less accurate when applied to the structure, Souli (2010).

In order to allow the mesh to move in an arbitrary way, the appropriate choice for the coordinate system is an Arbitrary Lagrangian Eulerian (ALE) formulation.

In what follows, the ALE formulation of a typical nonlinear system of conservation

laws

$$\frac{\partial}{\partial t}(Q) + \nabla_x.F(Q) = 0, \tag{3.1}$$

is presented, where Q is the vector of conserved quantities and F is the flux. Eq. (3.1) is the divergence form of the equation (2.18).

The ALE formulation of Eq. (3.1) is the case when the reference coordinates move at an arbitrary velocity which is characterized by both the Lagrangian and the Eulerian equations as subsets, Piperno (1997), Souli (2010).

Let $\Omega(x,t) \subset \mathbb{R}$ be the flow domain of interest, where x is the the coordinate of a point in space, and t denotes time, and a reference configuration is denoted as $\Omega(\xi,0)$, where ξ is the coordinate of a point in space. A mapping function between $\Omega(x,t)$ and $\Omega(\xi,0)$ is defined as

$$x = x(\xi,\tau); \qquad t = \tau. \tag{3.2}$$

The Jacobian J of the frame transformation $\xi \rightarrow x$ and the ALE mesh velocity v_x (that may be different from the fluid velocity and from zero) are defined by

$$J = det\Big(\frac{\partial x}{\partial \xi}\Big|_t\Big) \;\text{ and }\; v_x = \frac{\partial x}{\partial t}\Big|_\xi, \tag{3.3}$$

respectively.

The ALE formulation of Eq. (3.1) is given as follows, Piperno (1997), Farhat (2001)

$$\frac{\partial}{\partial t}(JQ)\Big|_\xi + J\nabla_x.\bar{F}(Q,v_x) = 0, \tag{3.4}$$

where

$$\bar{F}(Q, v_x) = F(Q) - v_x Q \tag{3.5}$$

denotes the corrected flow with respect to the moving space coordinate, while Q and $F(Q)$ remain fixed, Lefrançois (2010), Piperno (1997). In particular, for nonlinear Euler equations, the following equations apply

$$Q = \begin{pmatrix} \rho \\ \rho u \\ \rho E \end{pmatrix}, \tag{3.6}$$

$$\bar{F} = \begin{pmatrix} \rho\bar{u} \\ \rho u\bar{u} + p \\ \rho E\bar{u} + pu \end{pmatrix} \quad \text{and} \quad \bar{u} = u - v_x. \tag{3.7}$$

This set of equations is closed by an equation of state for an ideal polytropic gas

$$p = (\gamma - 1)[E - \frac{1}{2}\rho u^2], \tag{3.8}$$

where $\gamma = \frac{c_p}{c_v}$, is known as the *adiabatic exponent*. c_p and c_v denote, respectively, the *specific heat at constant pressure* and the *specific heat at constant volume*. Under normal conditions, air is constituted by N_2 and O_2, and therefore $\gamma \approx 1.4$, Leveque (2002).

3.2.2 Spatial discretization

In this section the discretization, in space, of Eq.(3.4) is presented.

Finite element semi-discretization

The finite element method requires a variational form of Eq.(3.1), by multiplying it by a test function $\psi = \psi(\xi, t)$ and integrating over a reference cell C_ξ

$$\int_{C_\xi} \Big[\frac{\partial (JQ)}{\partial t} + J\nabla_x.\bar{F}\Big]\psi d\xi = 0, \tag{3.9}$$

which may be written as

$$\int_{C_\xi} \psi \frac{\partial (JQ)}{\partial t} d\xi + \int_{C_\xi} J\nabla_x.\bar{F}\psi d\xi = 0. \tag{3.10}$$

In the above equation, the temporal derivative is evaluated at constant ξ. Switching back to the time varying elements, Eq.(3.10) above can be written as

$$\int_{C_x(t)} \psi \frac{\partial Q}{\partial t} dx + \int_{C_x(t)} \nabla_x.\bar{F}_i\psi dx = 0. \tag{3.11}$$

Spatial integration by parts of the last term yields, and considering Eqs. (3.2) and (3.3), the usual weak formulation

$$\int_{C_x(t)} \psi \frac{\partial Q}{\partial t} dx - \int_{C_x(t)} \bar{F}\nabla_x\psi dx + \int_{\partial C_x(t)} (\bar{F}.\vec{n})\psi ds = 0, \tag{3.12}$$

Finally, switching back again to constant ξ, we have

$$\int_{C_\xi} \psi \frac{\partial JQ}{\partial t} d\xi - \int_{C_\xi} \frac{\partial \psi}{\partial \xi}\bar{F}_i d\xi + \int_{\partial C_\xi} (\bar{F}.\vec{n})\psi ds = 0. \tag{3.13}$$

The time integration between t^n and t^{n+1} gives

$$\int_{C_\xi} \psi (JQ)^{n+1} d\xi - \int_{C_\xi} (JQ)^n d\xi - \Delta t\Big(\int_{C_\xi} \frac{\partial \psi}{\partial \xi}\bar{F}_i^{n+\frac{1}{2}} d\xi + \Big[\psi \bar{F}_i^{n+\frac{1}{2}}\Big]_{C_\xi}\Big) = 0. \tag{3.14}$$

The spatial discretization of the finite elements of the mesh followed by an assembling process gives

$$[M]^{n+1}\{Q\}^{n+1} - [M]^{n}\{Q\}^{(n)} - \Delta\{R\}^{n+\frac{1}{2}} = \{0\} \tag{3.15}$$

where $\{Q\}$ is the $(N \times 1)$ global vector of unknowns in (3.1), $[M]^n$ and $[M]^{n+1}$ are the global mass matrices at times t^{n+1} and t^n, respectively, and $\{R_i\}^{n+\frac{1}{2}}$ is an $(N \times 1)$ global residual vector calculated at the half way time step. The equation (3.15) is a system of equations to be solved at each time step.

Finite volume semi-discretization

The semi-discretization of Eq.(3.4) by a finite volume method is realized by integrating this equation over a reference cell C_ξ

$$\int_{C_\xi} \frac{\partial}{\partial t}(JQ)\Big|_\xi d\xi + \int_{C_\xi} J\nabla_x.\bar{F}(Q, v_x)d\xi = 0, \tag{3.16}$$

since the partial time derivative is evaluated at constant ξ, therefore, it is possible to move it outside of the integral

$$\frac{d}{dt}\int_{C_\xi} QJd\xi + \int_{C_\xi} \nabla_x.\bar{F}(Q, v_x)Jd\xi = 0. \tag{3.17}$$

Taking into account Eqs. (3.2) and (3.3) this can be transformed into

$$\frac{d}{dt}\int_{C_x(t)} Qdx + \int_{C_x(t)} \nabla_x\bar{F}(Q, v_x)dx = 0, \tag{3.18}$$

corresponding to the cell C_x in moving mesh, Farhat (2001), Piperno (1995), Piperno (1997), Lesoinne (1995).

Finally, integrating by parts the second term in Eq. (3.18) the integral equation gives

$$\frac{d}{dt}\int_{C_x(t)} Q dx + \int_{\partial C_x(t)} \bar{F}(Q, v_x).\mu ds = 0, \tag{3.19}$$

where μ denotes the unit normal vector perpendicular to the cell boundary $\partial C_x(t)$, pointing outward, van Zuijlen (2004), Farhat (2001).

3.2.3 Structural dynamics

Since in this thesis we focus on fluid-structure interaction (FSI), in this section an overview of structural dynamic equations is presented. Further details about these equations and their numerical approximations can be found in Craig (2006), Butcher (2003), Huges (1987), and Hairer (1993). We consider, in general, structural systems under the assumption of linear behaviour.

According to Hooke's law, we consider structural systems with the resilient elements (springs) that establish proportionality between displacements and restoring forces

$$F_S = -kx, \tag{3.20}$$

and the viscous dashpots (dampers) that establish proportionality between velocities and damping forces

$$F_R = -c\dot{x}. \tag{3.21}$$

k, c, x and $\dot{x}$ denote, respectively, the spring constant, the damping constant, the displacement, and the velocity of the mass. In addition to the forces F_S and F_R, we

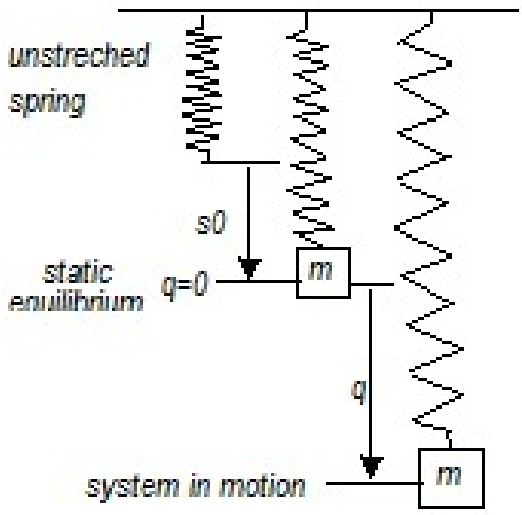

Figure 3.1: Vibrating system

assume that the mass is subject to an excitation force $F_E = F(t)$. From Newton's law or alternatively, from the so-called Lagrange's equations, the second order linear differential equation is obtained

$$m\ddot{q} + c\dot{q} + kq = F(t) \tag{3.22}$$

that governs the motion of the mass m.

3.3 Fluid-structure interaction

In Section 1.1.1 we introduced the fundamental principle of dynamics (FPD), or Newton's second law. The general equation for fluid-structure interaction (FSI) is

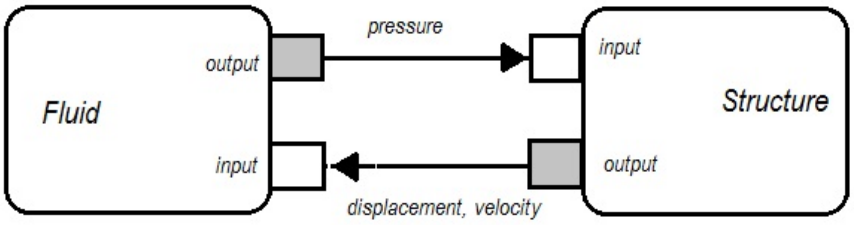

Figure 3.2: Principle of fluid-structure interaction

the result of this principle, producing the mechanical system

$$m\vec{\Gamma} = \sum_{forces} \vec{F}, \tag{3.23}$$

where m denotes the system mass, $\vec{\Gamma}$ the acceleration vector, and $\vec{F}$ the applied forces, Lefrançois (2010).

An approach consists of relating a determined solver with each side of the equation (3.23) by a coupling technique to provide an equality term. The solution of equation (3.23) can be divided into the following parts:

- left-side, that is computed by a fluid solver,
- right-side, that is computed by a structure solver,
- equality, where a coupling scheme is applied to update common data between the solvers. The common data are input and output for each of the solvers, as illustrated in Fig. 3.2.

In order to study staggered schemes, a general coupled system

$$\dot{x} = f(x) \tag{3.24}$$

can be written in a so-called partitioned way

$$\begin{cases} \dot{x}_1 = f_1(x_1, x_2) \\ \dot{x}_2 = f_2(x_1, x_2) \end{cases} \tag{3.25}$$

where the variables are split into two groups $x = (x_1, x_2)^T$, Piperno (1997). This decomposition is a feature of multi-physics problems.

For fluid-structure interaction problems, there is a spatial and a physical decomposition:

- the first equation denotes the fluid evolution x_1 (density, velocity and pressure),
- the second equation denotes the structure evolution x_2 (displacement and velocity),
- x_2 in the first equation denotes the displacement and velocity transferred to the fluid interface,
- x_1 in the second equation denotes the density, velocity and pressure transferred to the structure interface.

3.3.1 Fluid structure-coupling: the staggered algorithm

The coupling scheme is applied to regularly update common data between the fluid and structure solvers. The coupling scheme is realized by taking as a basis the staggered time integration method as illustrated in Figure 3.3. The description of the

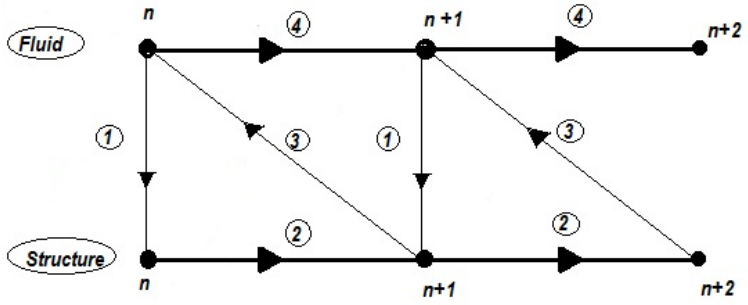

Figure 3.3: Coupling between structure and fluid solvers

algorithm is as follows, Piperno (1994), Lefrançois (2010)

- calculate the distribution of forces exerted by the fluid pressure p on the structure at time t^n,
- advance the structure using a structure solver, obtain the structure's displacement and the velocity at time t^{n+1},
- transfer the structure's displacement and velocity, computed at time $n+1$, to the fluid,
- fluid computation for the new pressure p at time $n+1$, and compute new fluid mesh location.

3.3.2 Structure prediction

In order to improve the staggered (partitioned) order of error, the coupling algorithm requires a structural predictor, Blom (1998), Michler et al. (2004). A predictor may

be employed for the position of the structural boundary at time t_{n+1}, on the basis of an extrapolation of the solution from the current level. This is to avoid integrating the fluid equations on the basis of the structural boundary at time t_n. The predictor techniques improve the accuracy of the partitioned scheme leading it to better stability, Piperno (1997), Blom (1998). They also allow a significant reduction in energy dissipation, Piperno (1997). Throughout this thesis we use several structural predictors according to structural solvers, as some predictors were designed to combine with specific time integration schemes to make them stable, van Zuijlen (2004). For instance, in this chapter two predictors are chosen. Predictor 1 that is given by the zero order prediction

$$\{\dot{q}^{n+1}\} = \{\dot{q}^{n}\}, \tag{3.26}$$

and predictor 2 given by the first order prediction

$$\{\dot{q}^{n+1}\} = \{\dot{q}^{n}\} + \Delta t\{\ddot{q}^{n}\}. \tag{3.27}$$

Regarding the structural predictors discussed below, their performance will be tested by numerical experiments in Section 3.5.

3.3.3 Conservation of the coupling scheme

The indicators to test the conservation capabilities of the arbitrary Lagrangian Eulerian formulation and the coupling approach, are obtained by integrating over the

domain $[0, L(t)]$ the mass, momentum, and energy, such that:

$$\frac{\partial}{\partial t}\int_0^{L(t)} Q\ dx + [F - v_x Q]_0^{L(t)} = 0 \tag{3.28}$$

where Q and F are defined as in Equation (2.9). Taking into account the boundary conditions

$$u(L(t)) = v_x(L(t)) = \dot{q(t)} \tag{3.29}$$

and

$$u(0,t) = v_x(0,t) = 0, \tag{3.30}$$

from Equation (3.28), the following indicators can be deduced:

(1) Conservation of Mass: The first indicator corresponds to the Conservation of Mass closed in the domain $[0, L(t)]$:

$$\frac{\partial}{\partial t}\int_0^{L(t)} \rho\ dx + [\rho(u - v_x)]_0^{L(t)} = 0. \tag{3.31}$$

Applying the boundary conditions (3.29) and (3.30), one obtains

$$\frac{\partial}{\partial t}\int_0^{L(t)} \rho A\ dx = 0. \tag{3.32}$$

Therefore

$$\int_0^{L(t)} \rho\ dx = \text{Constant} = \text{Initial Mass}. \tag{3.33}$$

(2) Conservation of Momentum: Proceeding in the same way as in (3.31), one has

$$\frac{\partial}{\partial t}\int_0^{L(t)} \rho u\ dx - p(0) = -p(L(t)) \equiv -kq(t) = F_p^s \tag{3.34}$$

where F_p^s is the piston force. This means that the force computed by the fluid solver is balanced by the force computed by the structure solver.

(3) Conservation of Energy: Finally, for the conservation of energy, one gets

$$I(t) = \int_0^{L(t)} \rho E \, dx - \int_0^{L(0)} \rho \, dx = - \int_0^t p(L,t)u(L,t) \, dt. \tag{3.35}$$

which corresponds to the impulsion $I(t)$, the total fluid energy variation (left-hand term), or the energy required by the piston for motion (right-hand term). On the other hand from (3.22) one can define the variation of the mechanical energy of the piston, given by

$$E(t) - E(0) \tag{3.36}$$

where $E(t) = \frac{1}{2} m \dot{q(t)}^2 + \frac{k}{2}(L_{se} - q(t) + L_{s0})^2$ and $E(0) = \frac{1}{2}k(L_{se} - q(0) + L_{s0})^2$. This would ensure the Conservation of Energy if $I(t) = E_t - E_0$ for $t \geq 0$. $I(t)$ is computed by the fluid solver and $E_t - E_0$ is computed by the structure solver.

For the numerical approaches discussed below, these properties will be tested in the numerical results, Section 3.5. In the following section the numerical schemes applied to solve the fluid flow and the structural dynamics will be described.

3.4 Coupling problem: Piston problem

In this thesis, for a staggered (partitioned) approach, several methods for fluid and structural dynamics are considered. The application is realized through the piston problem.

The piston problem is the most considered fluid-structure interaction application, to test the performance of numerical methods, Piperno (1995), Blom (1998), Michler et al. (2003), Michler et al. (2004), van Zuijlen (2004), Subramanian (2009), Borsche (2010), Lefrançois (2010).

Piperno (1995) presented several partitioned procedures and derived all the theoretical results for a one-dimensional piston model problem. Blom (1998) investigated the time-marching computational fluid-structure interaction algorithms. Michler et al. (2003) presented the relevance of maintaining conservation for a fluid-structure interaction model problem. Michler et al. (2004) compared partitioned and monolithic solution procedures for numerical simulations of fluid-structure interaction. van Zuijlen (2004) applied high order time integration schemes to structural and fluid-structure interaction simulations. In the partitioned FSI simulations on a one-dimensional piston test problem, a mixed implicit/ explicit (IMEX) time integration was employed, by using the implicit scheme to integrate fluid and structural dynamics. An explicit Runge-Kutta method was used to integrate the coupling terms. Subramanian (2009) investigated a blast pressure wave interaction with an elastic structure, using

a numerical analysis approach. Borsche (2010) was motivated by applications to the piston problem and by other applications, to investigate a coupling between a system of conservation laws and a system of ordinary differential equations. Lefrançois (2010) introduced a basic and solid grasp of the numerics underlying the physics of the fluid-structure interaction.

3.4.1 Physical Model

We consider the fluid contained in a chamber, closed on its right side by a moving piston and on its left by a fixed wall. The fluid in the chamber is modelled by the one-dimensional nonlinear Euler equations (2.9). This system of equations is closed by the state equation for an ideal polytropic gas (3.8). The configuration is depicted in Figure 3.4. The structure is modelled by a mass-spring system of one degree of freedom, (3.22), where $c = 0$ and

$$F(t) = A(p(x = L_0 + q(t)) - p_0). \tag{3.37}$$

A denotes the structure cross section, $p(x = L_0 + q(t))$ is the fluid pressure applied to the structure, and p_0 is the atmospheric pressure. The structure has a mass m and is attached to an external fixed point with a linear spring stiffness k. The spring is characterized by three different lengths, namely, the unstretched length L_{s0}, the length at rest under pressure L_{se}, and the length $L_s(t)$ at any given time during the interaction process. The displacement, velocity, and acceleration of the piston are

given, respectively, by $q(t)$, $\dot{q}(t)$, and $\ddot{q}(t)$ with regard to its position at rest.

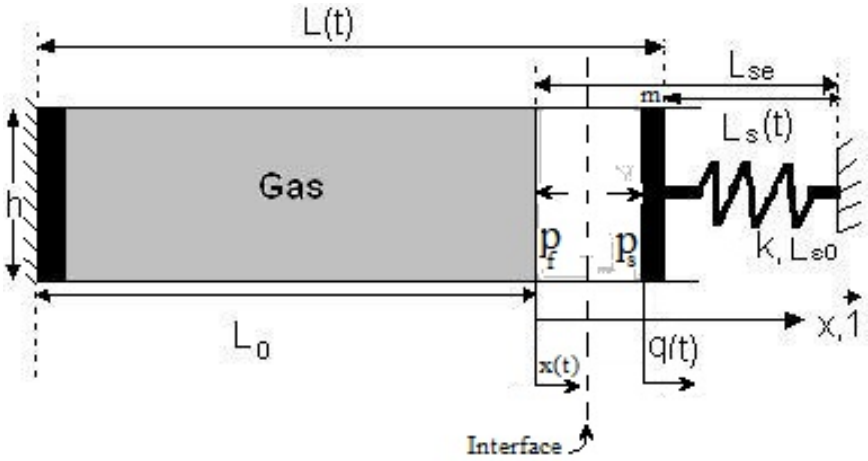

Figure 3.4: A gas enclosed in a chamber with a moving piston

Conditions at the interface

There are required interface conditions for the fluid-structure system. These conditions are: (one dynamic and two kinematic).

(1) dynamic equilibrium states that the pressure has to be the same at either side of the interface

$$p_f = p_s, \tag{3.38}$$

(2a) the first kinematic condition requires that the position of the moving fluid boundary is equal to its initial position plus the structural displacement

$$L(t) = L_0 + q(t), \tag{3.39}$$

(2b) the second kinematic condition requires that the velocity at the boundary is equal to the velocity of the moving boundary

$$u(t) = \dot{x}(t) = \dot{q}(t). \tag{3.40}$$

These conditions are required for the conservation of mass, momentum and energy.

Fluid mesh deformation technique

When coupling fluid and structure at each time step of the coupling method, a fluid mesh deformation technique is required. This technique ensures kinematic compatibility between the fluid domain and the structural position and avoids the situation in which the nodes near the structure can traverse. Fig.3.5 shows the mesh configurations at time t^n and t^{n+1}, respectively. The latter mesh configuration is the result of the structure motion to $\dot{q} \times \Delta t$, where $\dot{q}$ is the structure velocity. The new position for node x^n is given by a linear interpolation

$$x^{n+1} = x^n + v_x \Delta t. \tag{3.41}$$

From Eq.(3.41) we deduce the nodal velocity

$$v_x = \frac{x^{n+1} - x^n}{\Delta t}. \tag{3.42}$$

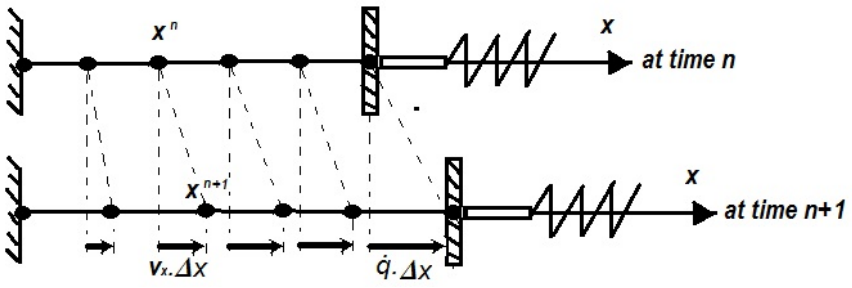

Figure 3.5: Mesh configurations at time t_n e t_{n+1}.

3.5 Numerical experiments

In this section the numerical experiments undertaken to test the numerical algorithm will be presented. The characteristic time-scales will be evaluated and the parameters for the problem are obtained as follows:

(a) the undamped angular frequency and the characteristic time scale for the structural sub-system are

$$\omega_s = \sqrt{\frac{k}{m}} \quad \text{and} \quad T_s = 2\pi\sqrt{\frac{m}{k}}, \tag{3.43}$$

respectively;

(b) the characteristic time scale for the fluid-subsystem is given by

$$T_f = \frac{L}{c}, \quad \text{where} \quad c = \sqrt{\frac{\gamma p}{\rho}}, \tag{3.44}$$

describes the speed of sound.

The characteristic time scale for the structure is the natural period, and for the fluid it is the time that it takes a pressure wave to cross the chamber from side to side. The relation $\frac{T_s}{T_f}$ determines the importance of the transient effects on the fluid behaviour, Lefrançois (2010). If both characteristic times are similar, the fluid and the structure face each other. In that case the coupling is considered strong. In the case where $T_s \gg T_f$ or $T_f \gg T_s$, the fluid or the structure can be considered quasi-steady. In that case, the coupling is weak. Another important feature is the mass ratio between the fluid and the structure

$$\mu = \frac{\rho L}{m}, \tag{3.45}$$

which describes the problem with respect to non-dimensional quantities. When $\mu \ll 1$, the fluid can be neglected. In that case only the structural mass is taken into account for the dynamic of the system. If μ is of order 1 the fluid and the structure have an equal contribution to the dynamic of the coupled system. For this test case, the physical parameters used in the piston problem are given in Table 3.1 and were chosen as in Pedro (2012).

The characteristic time scales for fluid and structure are $T_f \approx 3.6 \times 10^{-3} s$, and

Table 3.1: Numerical values of the parameters for the piston problem

k	m	L_0	q^0	L_{s0}	A	γ	p_0	$\mathbf{T}_0$	$\mathcal{R}$	c_0
$10^7 N/m$	0.8 Kg	1 m	0.20 m	1.2 m	1	1.4	10^5Pa	300K	287	334.7m/s

$T_s = 1.8 \times 10^{-3} s$ respectively. T_f, and T_s are of the same order, therefore the fluid and the structure see each other and the coupling is strong.

In this test problem the spatial discretization of the fluid domain is realized by the finite element method. This involves computing the solution at discrete nodes within the fluid domain, such that two successive nodes form a finite element. A Lax-Wendroff scheme is used for temporal resolution. For numerical approximation of the flux, the explicit two stage Lax-Wendroff procedure, Toro (1999)

$$\tilde{F}^{LW2}_{i+\frac{1}{2}} = \tilde{F}\Big(U^{LW}_{i+\frac{1}{2}}\Big), \tag{3.46}$$

where the state $U^{LW}_{i+\frac{1}{2}}$ is computed from

$$U^{LW}_{i+\frac{1}{2}} = \frac{1}{2}\Big(U^n_{i+1} + U^n_i\Big) + \frac{1}{2}\frac{\Delta t}{\Delta x}\Big(\tilde{F}(U^n_i) - \tilde{F}(U^n_{i+1})\Big), \tag{3.47}$$

is applied to solve the system (3.15) for each new time step t^{n+1}. The temporal stability criteria is given by the CFL condition as

$$\Delta t = \text{CFL}\times\min\Big(\frac{L^e}{|u + c + w_x|}\Big), \qquad \text{with} \qquad \text{CFL} < 1, \tag{3.48}$$

where $c = \sqrt{\frac{\gamma p}{\rho}}$ is the local speed of sound.

Since the fluid flow has a moving boundary, a node attached to a movable boundary, such as the piston at $x = L(t)$, must follow it, van Zuijlen (2004); Blom (1998); Lefrançois (2010). In order to prevent nodes impinging or traversing, interior nodes must be moved, except for the node attached to the fixed boundary located at $x = 0$,

Lefrançois (2010). This concept of moving coordinates is illustrated in Figure 3.6, where we consider a mesh composed of five nodes located at regular intervals along the domain and indexed from 1 to 5. Here the bullet symbol (•) depicts the position at time t^n and a circle symbol (∘) depicts the position at time t^{n+1}.

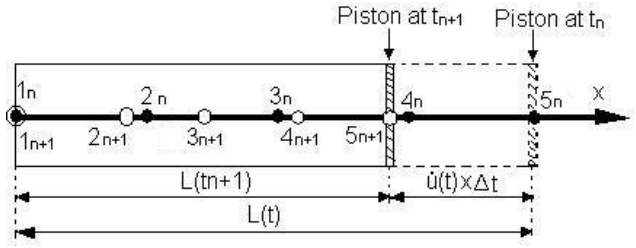

Figure 3.6: Moving physical space $x(t)$ representation

It is essential to be able to move nodes in order to avoid the traversing node effect, visible in Figure 3.6 between nodes 4 and 5 wherein if nodes 4 and 5, are fixed, then they will be outside the problem domain at time t^{n+1}.

3.5.1 Structure solver

We apply an implicit finite difference Newmark-Wilson scheme for time integration of equation (3.37). Further information about this method can be found in Blom (1998); Bardella (2005); Lefrançois (2010) This scheme is based on the time series expansion of q and $\dot{q}$;

$$q^{n+1} = q^n + \Delta t \dot{q}^n + \frac{\Delta t^2}{4}\left(\ddot{q}^n + \ddot{q}^{n+1}\right) \qquad \text{and} \qquad \dot{q}^{n+1} = \dot{q}^n + \frac{\Delta t}{2}\left(\ddot{q}^n + \ddot{q}^{n+1}\right), \quad (3.49)$$

where n and $n+1$ correspond to times t and $t+\Delta t$, respectively, and Δt is the time step between two successive solutions. From the first relation in (3.49) we have that

$$\ddot{q}^{n+1} = \frac{4}{\Delta t^2}\Delta q - \frac{4}{\Delta t}\dot{q}^n - \ddot{q}^n, \tag{3.50}$$

where the variation between two successive times, $\Delta q = q^{n+1} - q^n$, is obtained by substituting (3.49) and (3.50) into equation (3.37). The variables are updated at time t^{n+1}:

$$\Delta q = \frac{1}{4m + k\Delta t^2}\Big[A\Delta t^2\Big(p^n - p_0\Big) + m\Big(4\Delta t\dot{q}^n + \Delta t^2\ddot{q}^{n+1}\Big) - \Delta t^2 k q^n\Big]. \tag{3.51}$$

This relation allows the new piston position, q^{n+1} to be computed from q^n, $\dot{q}^n$ and $\ddot{q}^n$. Thus the structural position is updated according to

$$q^{n+1} = q^n + \Delta q \tag{3.52}$$

and the velocity $\dot{q}^{n+1}$ and acceleration $\ddot{q}^{n+1}$ are updated according to (3.49) and (3.50), respectively. For the first step q^1 of (3.52), the initial conditions are $q(0) = q^0$, $\dot{q}(0) = \dot{q}^0$ and $\ddot{q}(0) = \ddot{q}^0$. The first two initial conditions are given in (3.37) and it is easy to show, also from (3.37), that

$$\ddot{q}^0 = \frac{1}{m}\Big(- kq^0 + A(p(0) - p_0)\Big), \tag{3.53}$$

where $p(0)$ is the uniform pressure in the chamber resulting from an adiabatic variation entailed by the initial change in the piston position q^0.

3.6 Numerical results

In Blom (1998), the fluid domain was discretised in space by the finite volume method and integrated in time using an implicit upwind scheme. It is found that in the case of acoustic equations, the predictor 2 algorithm given by (3.27) performed better than the predictor 1 algorithm given by (3.26). We compared the performance of these two predictors by discretizing the fluid domain using the finite element method, and by integrating in time using the explicit two stage Lax-Wendroff procedure.

3.6.1 Results

Firstly, in order to test the performance of the two coupling approaches with respect to the amplitude of the piston, the fluid flow is solved by means of the finite element method. The fluid is discretised with 100 finite elements and 101 nodes. The initial conditions for the piston are taken as $q(0) = 0.2m$ and $\dot{q}(0) = 20m/s$.

We compared the amplitude of the piston for the two coupling algorithms and different CFL numbers. Figure 3.7 shows the amplitude of the piston for the two coupling algorithms at CFL = 0.80. Apparently there is not too much difference between the solutions, but one can see that the second curve, obtained by applying the predictor 2 algorithm, is slightly more damped than the first one. The difference between the two algorithms becomes more noticeable as the CFL number increases. Figures 3.8 and 3.9 show the amplitude of the piston computed by predictors 1 and

2 algorithms, respectively, as the CFL number increases. It is found that as the CFL number increases, the curve becomes more damped. The damping is more pronounced in the curves shown in Figure 3.9, which are obtained by the predictor 2 algorithm. From the structure solver given in Section 3.5.1, we find that there is no damping, so the damping of the signal comes from the fluid solver. As the CFL number increases, the deviation of the solution from the equilibrium position also increases. This deviation is larger for the predictor 1 algorithm since it is less accurate.

Secondly, since we did not find a discussion in the literature regarding the performance of the above coupling approaches with respect to the fluid, we tested them. In order to do so, the fluid was discretized with 100 finite elements and then with 200 finite elements, respectively. Figures 3.10 and 3.11 show the results for density and pressure, respectively, obtained via predictor 1, left-side, and via predictor 2, right side. It is possible to see that the results obtained by applying prediction 2 with 100 finite elements compared favorably with the results obtained by predictor 1 with 200 finite elements, showing the efficiency of predictor 2.

3.7 Conclusions

A numerical analysis of different time marching fluid-structure interaction algorithm has been presented. The relatively simple piston problem was chosen in order to

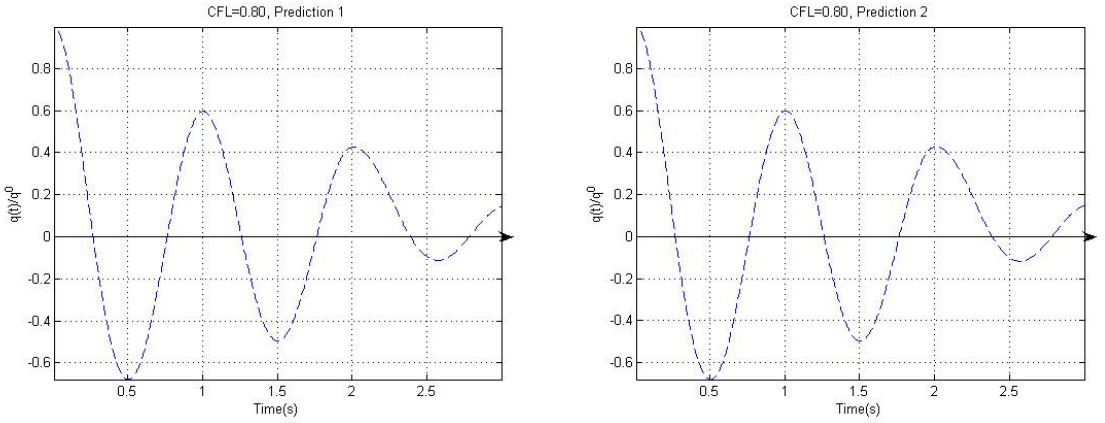

Figure 3.7: Amplitude of the piston at $CFL = 0.80$

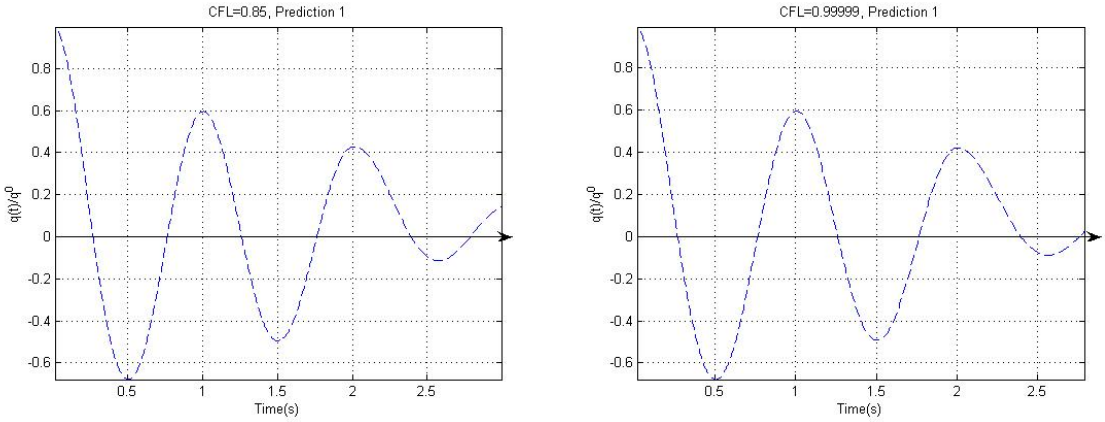

Figure 3.8: Amplitude of the piston by predictor 1 algorithm

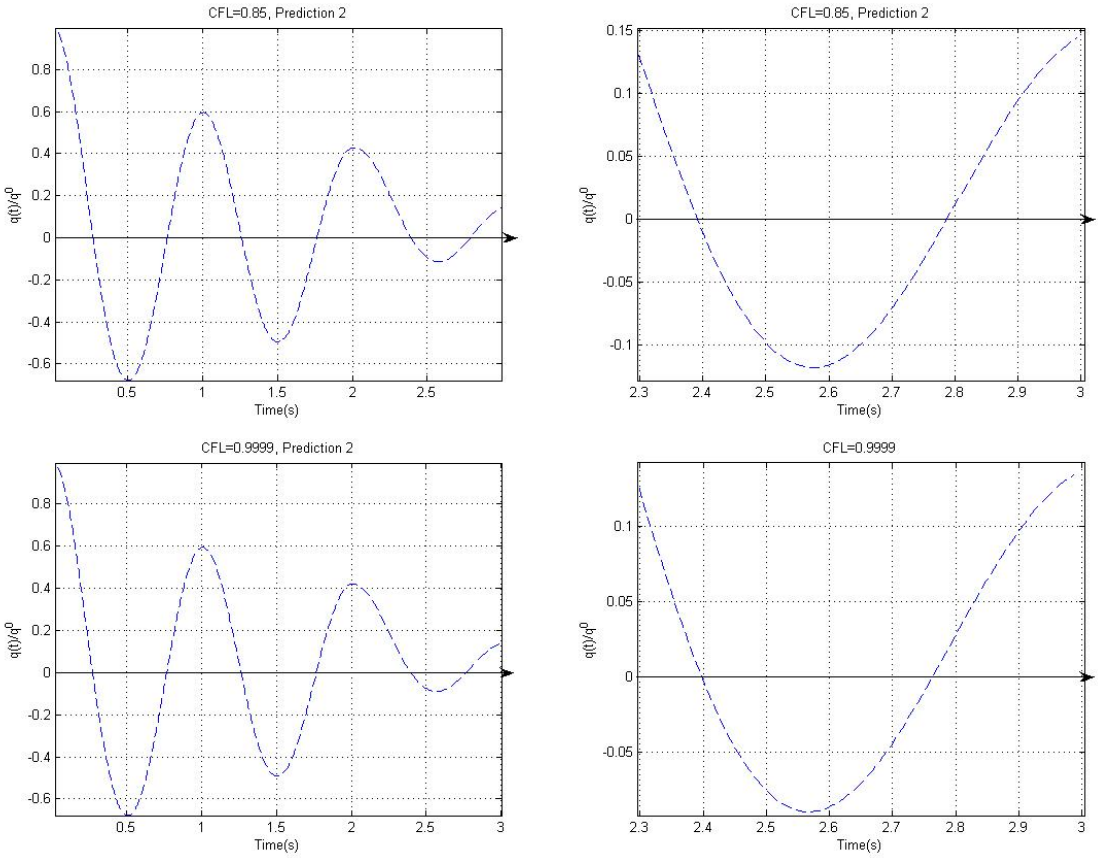

Figure 3.9: Amplitude of the piston by predictor 2 algorithm at $CFL = 0.85$ and $CFL = 0.99999$ respectively (*left*). Zoom to emphasize the damping (*right*).

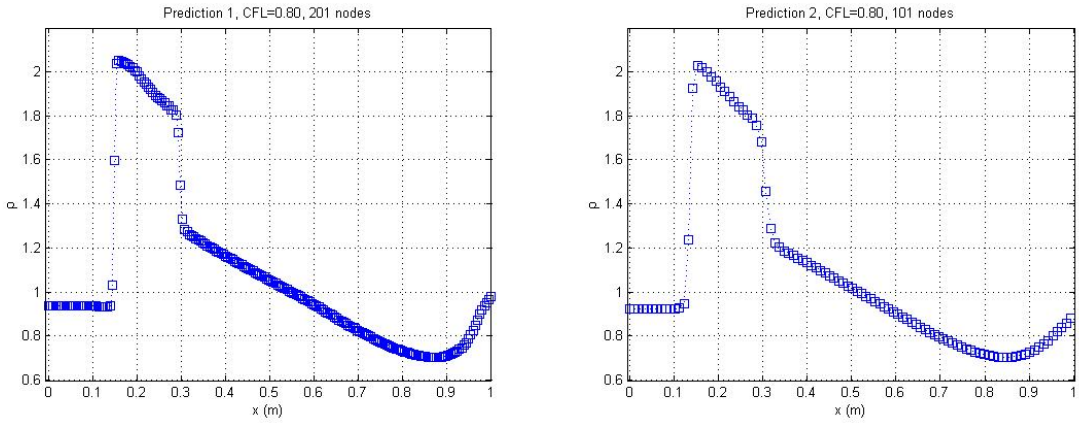

Figure 3.10: Density ρ at $T_{max} = 3 \times \mathcal{T}_0$, staggered algorithm, via predictor 1 (right)and predictor 2 (right)

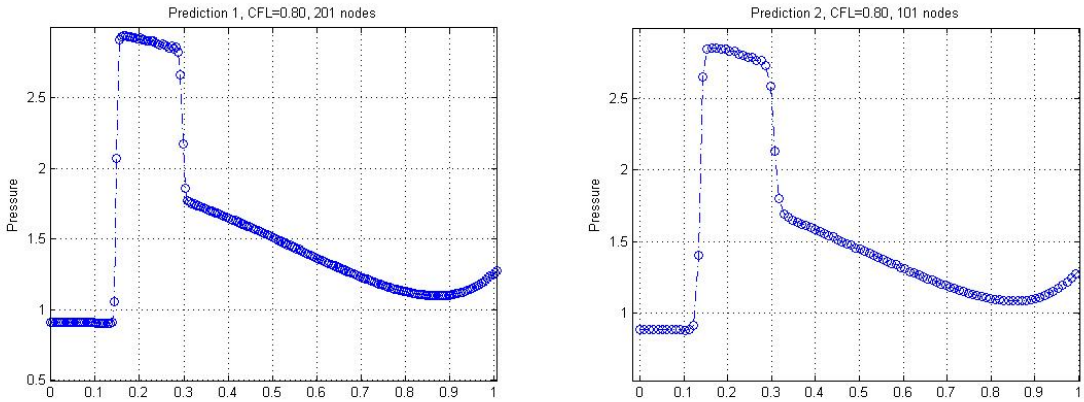

Figure 3.11: Pressure p at $T_{max} = 3 \times \mathcal{T}_0$, staggered algorithm, via predictor 1 (left) and predictor 2 (right)

gain an understanding of coupling algorithms. The one dimensional fluid is modelled by the nonlinear Euler equations which were presented in moving mesh coordinates using the arbitrary Lagrangian Eulerian (ALE) approach, discretised in space by the finite element method, and integrated in time by an explicit method. The structure was integrated in time by an implicit finite difference Newmark-Wilson scheme. The fluid and the structure were integrated in time using separate solvers. The coupling between the fluid and structure solvers was realized by applying the staggered approach. Since the staggered approach suffers from a time lag, the influence of the time lag was studied by comparing two different predictions for the structure. The computations show that the differences between the two coupling algorithms become noticeable as the CFL number increases. The predictor 2 algorithm gave a higher accuracy.

Chapter 4

HIGH ORDER FINITE VOLUME WENO SCHEME: APPLICATION IN FLUID-STRUCTURE INTERACTION FOR GAS DYNAMICS

4.1 Introduction

Over the last few decades there has been active interest among researchers in computational fluid dynamics, as well as in the computational structural mechanics fields, in developing efficient fluid and structure solvers taking into account, respectively, flows around complex geometries and structural deformations under a given load. Fluid-structure interactions, known as FSI, can be identified in many engineering applications, thus FSI simulations have gained in importance, Hou (2012). It has been demonstrated that for flow applications, higher order time integration schemes are computationally more efficient, van Zuijlen (2004). Therefore, it is reasonable to suppose that high order fluid solvers can perform better when applied to fluid-structure interaction problems. In this chapter, a third-order scheme based on the weighted essentially nonoscillatory (WENO) idea has been proposed for the fluid solver. The precursor of this high-order scheme for hyperbolic flow problems was first proposed in, Dumbser (2007a); Dumbser et al. (2007b). The realization applied in this chapter was presented in Chapter 2. The choice of this scheme has been made due to its proper-

ties of being high-order accurate as well as for its ease of application for unstructured grids. The reader is referred to Dumbser et al. (2007b), and Dumbser (2007a) for more details on multidimensional formulations. So far, this scheme has only been used for fixed domains. Since for the FSI case the fluid domain boundaries are time dependent, in this Chapter the quadrature-free essentially non-oscillatory finite volume scheme of arbitrary high order for nonlinear hyperbolic systems is adapted and extended to dynamic meshes, based on the arbitrary Lagrangian Eulerian (ALE) formulation for the nonlinear Euler equations. For the integration of the structure, the same scheme used in Lefrançois (2010), and Pedro (2012) will be employed. In addition, other schemes that have been applied elsewhere and which have been documented to have better energy and momentum conservation properties for similar structure problems, will also be tested, for example the TR-BDF2, scheme Bank et al. (1985), Bathe (2007), Bathe (2012). The essence of this chapter will be an application of high-order schemes (higher than second-order) based on the WENO formulation which have been extensively applied to hyperbolic conservation laws on fixed domains, but not yet on problems in FSI. It has been demonstrated that higher-order schemes could be more efficient in FSI, since there is no requirement for sub-iterations needed at the interface, Hou (2012). For example, second-order schemes have demonstrated better accuracy and stability, Farhat (2006), Zhang et al. (2007). In this Chapter, the performance of the scheme is compared to the results from the Finite Element

formulation in Chapter 3. In particular, the results of the scheme for the amplitude of the piston, conservation properties as well as dissipation production, are compared.

4.2 Numerical schemes and solvers

4.2.1 Fluid solver

Our aim in this chapter is to apply a high order finite volume weighted essential non-oscillatory scheme described in chapter 2, as thus far we did not disacover from the literature the application of the referred scheme to fluid-structure interaction problems. The scheme is employed as a fluid solver in a staggered approach. Further details regarding this method can be found in chapter 2 and in Dumbser (2007a); Dumbser et al. (2007b).

Arbitrary Lagrangian Eulerian formulation

Since the original scheme was applied to fluid problems on fixed meshes, when applied to fluid-structure interaction problems, it is required to reformulate the fluid flow equations in order to ensure moving meshes. Therefore the equations are formulated in an ALE framework. Further details concerning ALE formulation are presented in chapter 3.

0	0	0	0
γ	d	d	0
1	w	w	d
	w	w	d
	$(1-w)/3$	$(3w+1)/3$	$d/3$

4.2.2 Structure solver

Several structure dynamic time integration schemes of equation (3.37), which have been documented to have better energy and momentum conservation properties, are applied. Coupling will be investigated in terms of its relationship to the accuracy of the structure solver. The aim is to test the performance of time integration schemes for the structure relating to solving a fluid-structure interaction problem. For this study the following schemes are considered:

- **trapezoidal-rule backward differentiation formulae of order 2 (TR-BDF2)**

  The TR-BDF2 scheme was derived by Bank et al. (1985) and can be considered as a Singly Diagonal Implicit Runge-Kutta, SDIRK, 2(3) pair, where $\gamma = 2-\sqrt{2}$, $d = \gamma/2$, $w = \sqrt{2}/4$. Further details about this method can be found in Bank et al. (1985), Hosea (1996).

- **Newmark's family of methods: Average acceleration**

A family of single-step integration schemes to solve structural dynamic problems for both blast and seismic loading was presented by Newmark, Newmark (1959). During the past decades, the Newmark's scheme has been employed for dynamic analysis for many practical engineering structures. Additionally, many modifications and improvements by many other researchers have been contributed.

Assuming that the time step Δt is constant, and also that the solution has been computed up to time t; therefore all the solution variables up to t are known. The time-stepping scheme will compute the solution for time $n+1$. The algorithm can then be used to recursively calculate the solution at all discrete points. The direct use of Taylor's series provides us the following time series expansion on q and $\dot{q}$:

$$q^{n+1} = q^n + \Delta t \dot{q}^n + \frac{\Delta t^2}{2}\ddot{q}^n + \frac{\Delta t^3}{6}\dddot{q}^n + \dots \tag{4.1}$$

$$\dot{q}^{n+1} = \dot{q}^n + \Delta t \ddot{q}^n + \frac{\Delta t^2}{2}\dddot{q}^n \dots \tag{4.2}$$

These equations were truncated by Newmark and expressed in the form

$$q^{n+1} = q^n + \Delta t \dot{q}^n + \frac{\Delta t^2}{2}\ddot{q}^n + \alpha \Delta t^3 \dddot{q} \tag{4.3}$$

$$\dot{q}^{n+1} = \dot{q}^n + \Delta t \ddot{q}^n + \delta \Delta t^2 \dddot{q} \tag{4.4}$$

Assuming that the acceleration is linear within the time step, the following equation can be written

$$\dddot{q} = \frac{(\ddot{q}^{n+1} - \ddot{q}^n)}{\Delta t} \tag{4.5}$$

Substituting Equation (4.5) into Equations (4.3) and (4.4) yields

$$q^{n+1} = q^n + \dot{q}^n \Delta t + \left[\left(\frac{1}{2} - \alpha\right)\ddot{q}^n + \alpha \ddot{q}^{n+1}\right]\Delta t^2 \tag{4.6}$$

$$\dot{q}^{n+1} = \dot{q}^n + \left[(1-\delta)\ddot{q}^n + \delta \ddot{q}^{n+1}\right]\Delta t. \tag{4.7}$$

where α and δ are integration parameters.

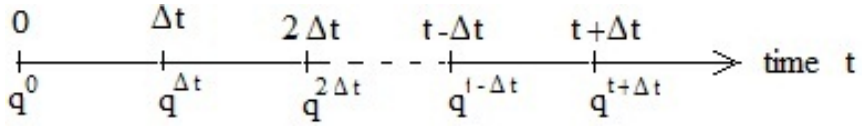

Figure 4.1: Time axis discretization and the respective q solutions

Figure 4.1 illustrates the indexes corresponding to times t^{n-1}, t^n and t^{n+1}, where Δt is the time step between two successive solutions.

From (4.6) it is deduced that the acceleration at time $n+1$ can be computed by the relation

$$\ddot{q}^{n+1} = \frac{1}{\alpha}\Delta q - \frac{1}{\alpha\Delta t}\dot{q}^n - \frac{1}{\alpha}\Big(\frac{1}{2} - \alpha\Big)\ddot{q}^n. \tag{4.8}$$

Hence in the single step the equations (3.37) are solved at time $n+1$

$$m\ddot{q}^{n+1} + kq^{n+1} = F(t)^{n+1} \tag{4.9}$$

The variation between two successive times $\Delta q = q^{n+1} - q^n$ is obtained by substituting (4.8) and (4.6) in (4.9), yielding

$$\Big(\frac{m}{\alpha\Delta t^2} + k\Big)\Delta q = F(t)^{n+1} - kq^n + m\Big(\frac{1}{\alpha\Delta t}\dot{q}^n + \frac{1}{\alpha}\Big(\frac{1}{2} - \alpha\Big)\ddot{q}^n\Big) \tag{4.10}$$

The average acceleration method is identical to equations (4.6) and (4.7) with $\delta = \frac{1}{2}$ and $\alpha = \frac{1}{4}$. Because of its unconditional stability, the average acceleration method is the optimal case of the Newmark method to be used for the step-by-step dynamic analysis of large complex structural systems, in which a large number of high frequencies, (short periods), are present, Craig (2006).

- **explicit central difference scheme**

Further details of this method can be found in Craig (2006). The foundation of

the central difference scheme is the simple finite-difference expression

$$\dot{q}^n = \frac{q^{n+1} - q^{n-1}}{2\Delta t}. \tag{4.11}$$

The value of the second derivative is computed as the difference of first-order forward and backward finite differences,

$$\ddot{q}^n = \frac{q^{n+1} - 2q^n + q^{n-1}}{\Delta t^2}. \tag{4.12}$$

The discrete governing equation is obtained when the finite difference expressions (4.11) and (4.12) are substituted into the equation (3.37). This scheme is excellent for small Δt and unstable for large Δt, Craig (2006). We use this scheme for comparison purposes only, to establish the relationship between the accuracy of structural solvers and the coupling fluid/structure.

4.3 Numerical Experiments

The numerical experiments are realized taking into account relevance of the transient effects on the fluid behaviour (see Chapter 3). Therefore, we consider two test cases.

The parameters for the piston problem are obtained as follows, Piperno (1995); Michler et al. (2004); Garelli (2011):

- the undamped angular frequency and the characteristic time scale for the mass-spring system are

$$\omega_s = \sqrt{\frac{k}{m}}, \quad T_s = \frac{2\pi}{\omega_s}, \tag{4.13}$$

respectively,

- the characteristic time scale for the fluid subsystem is

$$T_f = \frac{L_0}{c}, \quad c = \sqrt{\frac{\gamma p_0}{\rho_0}}. \tag{4.14}$$

where c is the speed of sound.

- the characteristic time-scale of fluid-structure interaction is

$$T_{fs} = \frac{2\pi}{\omega_{fs}}, \tag{4.15}$$

where ω_{fs} is the approximated oscillating frequency of the coupled system.

TEST PROBLEM CASE 1: STRONG COUPLING

For the first case, the physical parameters used in the piston problem are given in Table 4.1.

$$\frac{T_s}{T_f} = \frac{1.8 \times 10^{-3}}{3.0 \times 10^{-3}} = 0.6 \Rightarrow T_s \approx T_f. \tag{4.16}$$

Here, T_s and T_f are of the same order, therefore the coupling is strong, and only the structural mass is considered into the dynamic coupled system.

We start by testing the performance of the structure solvers, set out in section 4.2.2, without the fluid.

The following experimental examples will be considered:

(1) the first experimental example is the free-mass $m = 1$, $k = 0$, under period forcing $f(t) = A\sin(\omega t)$, where $A = 100$. The initial conditions are $q(0) = \dot{q}(0) = -A$.

(2) the second experimental example is also a forced free mass $m = 1$, $k = 4$, $f(t) = -B\sin(\omega t) + C\cos(\omega t)$, where $B = 5$, $C = 3$ and $\omega = 2$. Subject to the initial conditions $q(0) = -1$ and $\dot{q}(0) = 1$.

(3) the third and last experimental example is an unforced free mass $m = k = 1$. The initial conditions are given by $q(0) = 1$ and $\dot{q}(0) = 0$. These test examples can be found in van Zuijlen (2004); Bardella (2005); Zill (1989).

The results in Figure 4.2 show that the explicit central scheme is obviously the

Table 4.1: Numerical values of the parameters for the piston problem

m	$0.8[Kg]$
k	$10^7[N/m]$
ρ_0	$1.1614[Kg/m^3]$
p_0	$10^5[P_a]$
T_s	$0.0018[s]$
T_f	$0.0030[s]$
L_0	$1[m]$

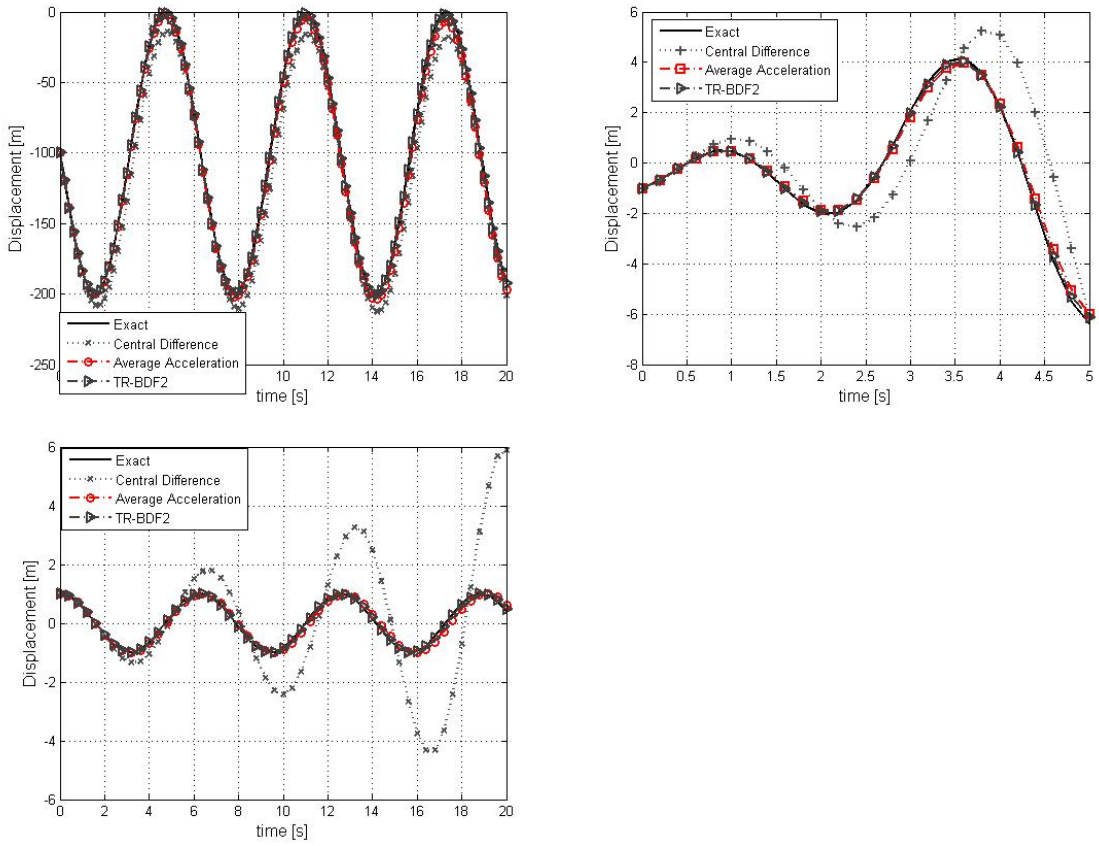

Figure 4.2: Displacement q for different schemes applied to Examples 1, 2, and 3, respectively.

least accurate and least stable. The second order average acceleration and TR-BDF2 are the schemes that perform better, however the TR-BDF2 performs slightly better than the acceleration average.

Since the performance of the schemes for structure dynamics was tested separately,

without fluid, the tests are extended to fluid-structure interaction problems. The aim is to test the performance of these schemes using a partitioned approach for an FSI problem, where they are applied as structure solvers.

Because an explicit scheme is used; which is conditionally stable, to integrate fluid, the stability criteria is given by the CFL condition:

$$\Delta t = \text{CFL} \times \min\Big(\frac{L^e}{|u + c_0 + v_x|}\Big), \qquad \text{with} \qquad \text{CFL} < 1 \tag{4.17}$$

where $c_0 = \sqrt{\frac{\gamma p}{\rho}}$. The flow is computed using 100 grid cells.

Figure 4.3 shows the results obtained by using these structural solvers on a partitioned approach. It can be observed clearly that the weakest coupling between fluid and structure is obtained with the explicit central difference. Apparently, all the implicit second-order schemes perform in the same way. However it is possible to observe that for longer times, the TR-BDF2 performs slightly better than the average acceleration which is traditionally used as a structure solver a lot of research. See for instance Blom (1998), Lefrançois (2010). Therefore, the strongest coupling is obtained with the TR-BDF2, as shown by zoomed Figure 4.3, at right. It follows that with the results obtained from the structure as well as from FSI, one can observe that the more accurate the structure solver, the stronger is the coupling between the fluid and the structure. The accuracy of the TR-BDF2 has also been extensively reported in Bathe (2007, 2012). Next, we consider the partitioned procedure with structure predictor. Two predictors (3.26), and (3.27), are considered and compared.

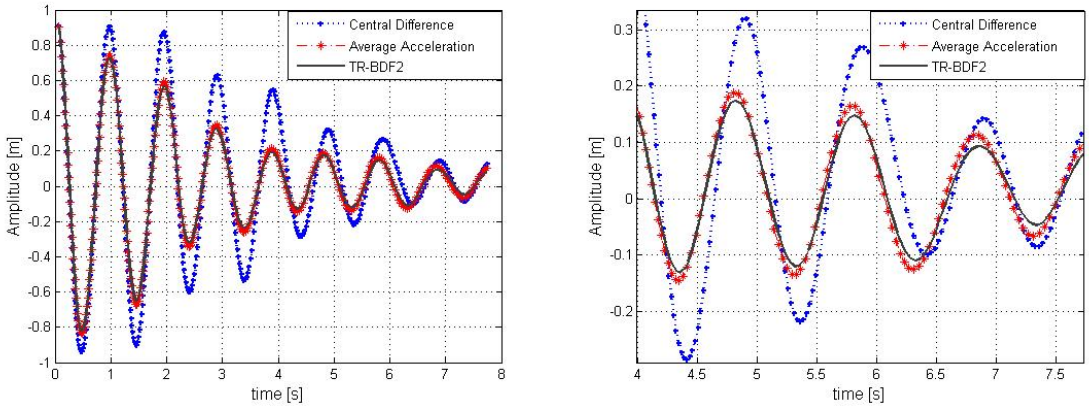

Figure 4.3: Amplitude of the piston for various structure solvers

Figure 4.4 shows the performance of the referred structure predictors at different CFL numbers. Comparing the results, it is visible that for both cases, as the CFL number increases, the profiles become more damped. From the figures, one can observe that the profiles obtained by applying the first order predictor are more damped. As observed in Chapter 3, these results validate the theory presented in Blom (1998) which, consequently, validates our scheme. In addition, the high-order scheme demonstrates more damping which qualitatively implies more accuracy.

As in Chapter 3, we applied a finite element method (FEM) to discretize fluid and in this Chapter we proposed a high order finite volume scheme (QFENOFV) as fluid solver, now we compare the results obtained in both cases using a predictor (3.27).

In both cases the structure is integrated by an implicit finite difference, Newmark

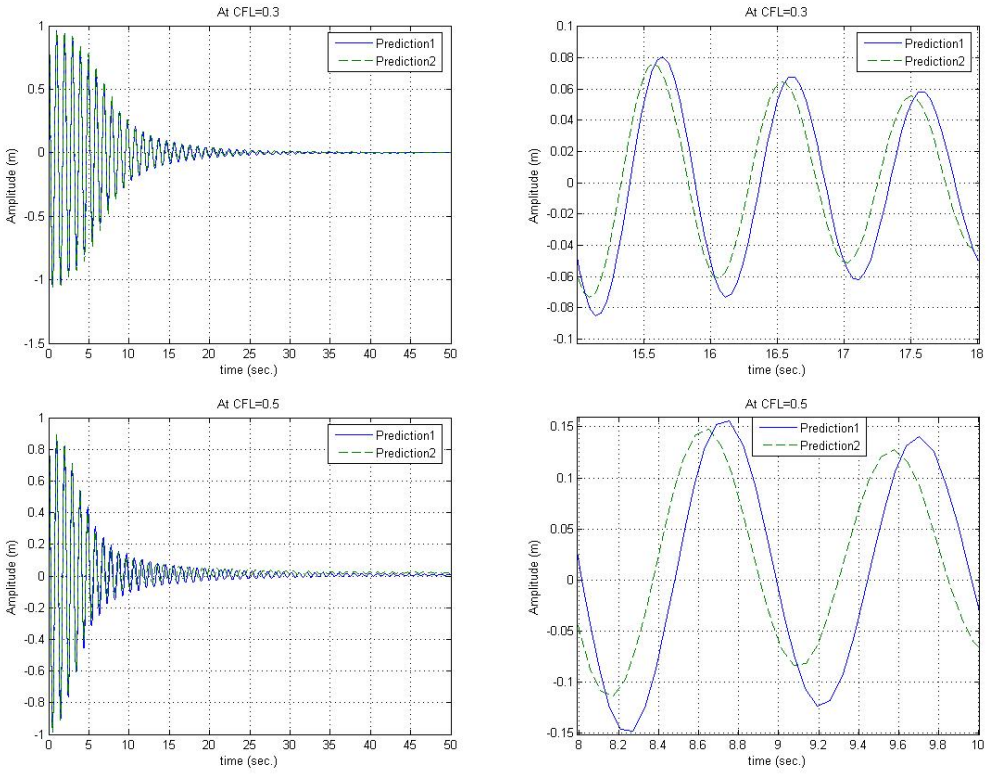

Figure 4.4: The figures show the amplitude of the piston for a zero order predictor and for a first order predictor scheme at different CFL numbers

(average acceleration). This procedure is to show that the damping signal comes from the fluid solver. The performance of the scheme derived in this chapter, referred to as QFENOFV henceforth, will be compared with the scheme in Chapter 3, referred to as FEM.

In Figure 4.5, the comparison of the results obtained by the finite element and the finite volume method is presented. It clearly shows that the solution obtained by the

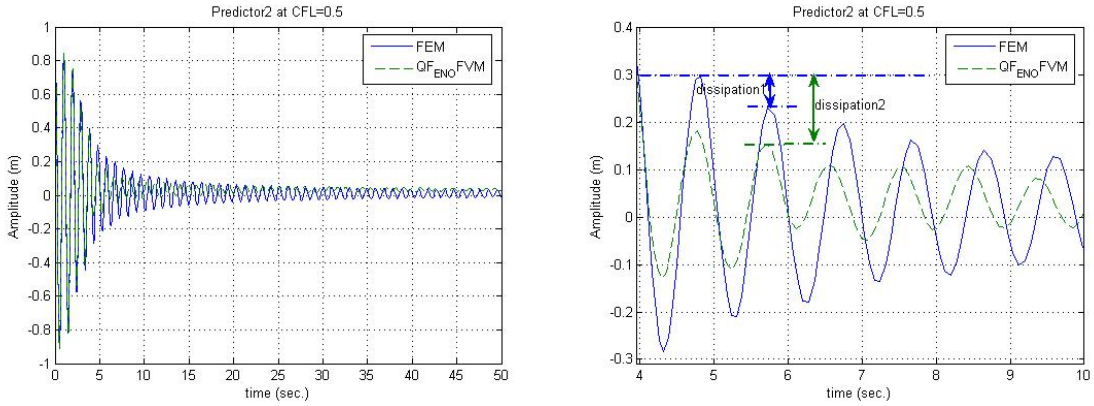

Figure 4.5: The Figs show: (Left-side) The amplitude of the piston, obtained by using FEM (line) and QFENOFV (symbols) and (right-side) the dissipation effects over time between the results obtained by using FEM (line) and QFENOFV (symbols).

finite volume method (QFENOFV) is more damped than that obtained by the finite element (FEM) solution. This is clear evidence of the accuracy of the scheme. Figure 4.5 (right-side), shows the dissipation effect, over time, as the FEM and QFENOFV are applied using first order prediction. The dissipation effect is more visible when QFENOFV is applied, which means, again, that the oscillations lose more amplitude over time in that case. The dissipation comes from the energy transfer from the piston to the fluid. As the dissipation effect increases over time, the stronger is the coupling between the fluid and the piston. In addition, it is shown that the higher-order does not oscillate perfectly around the equilibrium position. The source of this error might be caused by an inherent effect of the partitioned formulation as postulated in Blom (1998).

Finally, as in Lefrançois (2010), the transfer and conservation of energy is presented according to the conservation properties presented in Chapter 3. In Figure 4.6, the results corresponding to $f_0 = 50Hz$ and maximum simulation time equal to twice the period of the piston ($\mathcal{T}_0$) are presented. The graphs on the left side were calculated by using FEM and the graphs on the right side by using QFENOFV. From top to bottom the normalized forces and the normalized energy, respectively, are presented. The results obtained using QFENOFV agree perfectly with the expected results, since for the piston force, it is clear that the integration of the fluid momentum (3.34) corresponds to the fluid pressure. On the other hand, the energy conservation is always satisfied. From Figure 4.6 (bottom) it can be seen that the variation of mechanical energy ($E_t - E_0$) and the impulsion $I(t)$ move in opposite directions, satisfying the principle that what is lost by one is taken by the other. A calculation of the fluid mass variation gives variations of 0.0032% and 0.0021% for the FEM and QFENOFV approaches, respectively.

4.3.1 Piston pressure

Table 4.2: Natural frequency for the piston

m(Kg)	100	10	0.8
f_0(Hz)	50	159	562.698
$\mathcal{T}_0$(s)	0.0021	0.006281	0.00177715

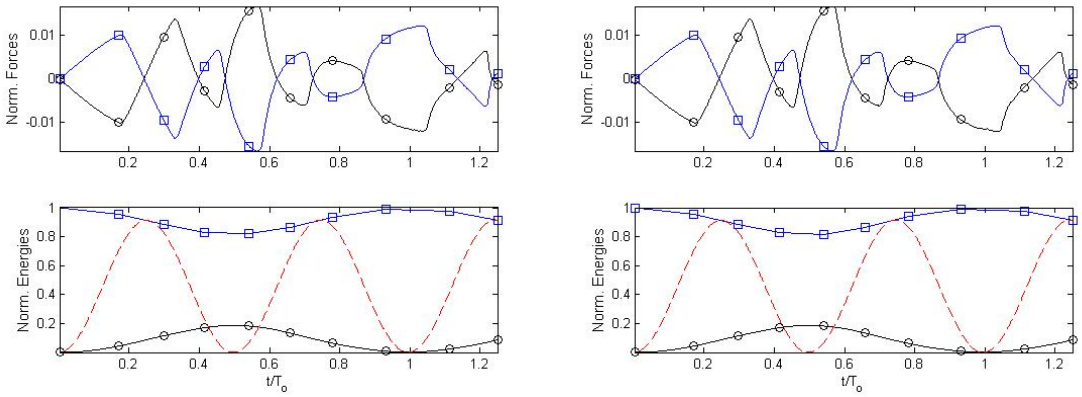

Figure 4.6: Piston Force and Energy transfer signals by using FEM and QFENOFM. These results correspond to $f_0 = 50$ Hz (m = 100)

In Figure 4.7, piston pressure variations are compared by applying different schemes and by taking the natural frequency of the piston, f_0, as a function of mass (m) and by keeping the spring k as constant. Three frequencies are considered as illustrated in Table 4.3.1. Unlike in Lefrançois (2010), where the comparison is done taking into account different flow models, here the same flow model is integrated but different integration schemes are employed. It is clear that the results show a strong overlap agreement between those obtained by the QFENOFV and the FEM schemes, except for the highest frequency where a slight difference is produced.

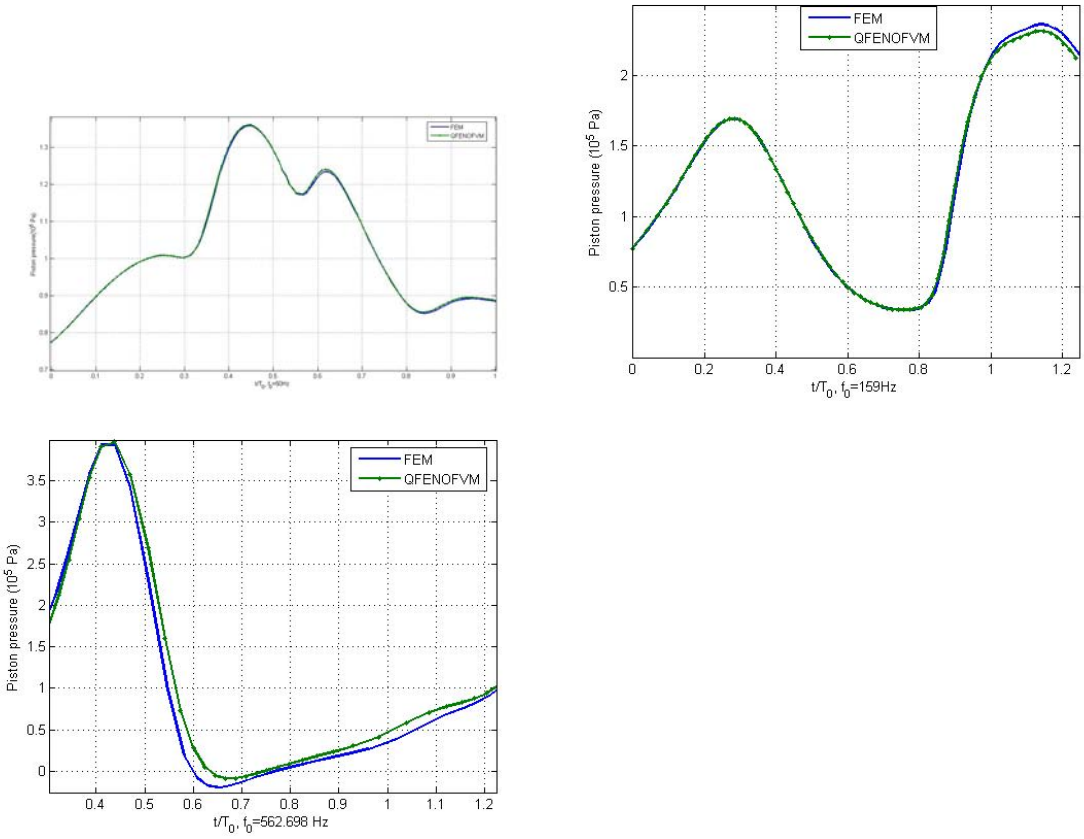

Figure 4.7: The figures show the piston pressure variations, by using FEM (left) and QFENOFVM (right)

4.4 Mesh refinement

Previous studies have proved that the order of temporal accuracy of fluid-structure interaction depends on the fluid and structure discretization separately, as well as on their coupling, Michler et al. (2003, 2004). In the following, the order of temporal

accuracy for the partitioned fluid-structure coupling will be studied.

In this Chapter, for fluid we use the one-dimensional case of a finite volume WENO scheme derived from the high order quadrature-free non-oscillatory finite volume schemes, used for two and three dimensional problems, which uses the techniques developed originally in the discontinuous Galerkin (DG) framework, see Dumbser (2007a); Dumbser et al. (2007b). And for structural dynamics we use implicit schemes which are second order of accuracy, see Blom (1998); Michler et al. (2004); Craig (2006). Therefore, the coupled system can be regarded as having high order accuracy. Here we determine the observed order of temporal accuracy by

$$p = \ln\Big(\frac{\|q_{4\tau} - q_{2\tau}\|}{\|q_{2\tau} - q_{1\tau}\|}\Big) / \ln(2), \tag{4.18}$$

Table 4.3: Order estimation p

Mesh sequences	Average acceleration	TR-BDF2
2×10^{-3}, 2×10^{-4}, 2×10^{-5}	3.4937	3.4937
2×10^{-4}, 2×10^{-5}, 2×10^{-6}	3.2081	3.1808
2×10^{-5}, 2×10^{-6}, 2×10^{-7}	3.8774	3.8774

Table 4.4: CPU time in sec.

CFL	Average acceleration	TR-BDF2
0.5	0.344 sec.	0.328 sec.
0.7	0.344 sec.	0.327 sec.

as in Michler et al. (2003, 2004). p denotes the observed order of temporal accuracy and q denotes the calculated structural displacement on grids of different time-steps, τ, 2τ and 4τ. We take the L_2 norm to measure the differences. Table 4.3 shows the order estimation p, for a partitioned approach with a predictor (3.27). Here, we consider the two structure solvers that are demonstrably more accurate: the average acceleration and the TR-BDF2 schemes. It is clear that although the TR-BDF2 performs better than the average acceleration, both schemes have formally the same order of accuracy. However, from Table 4.4, we observe that TR-BDF2 is the less CPU time consuming in comparison to the average acceleration, which confirms its efficiency in the partitioned method that we propose in this Chapter.

PISTON PROBLEM CASE 2: WEAK COUPLING

Table 4.5: Numerical values of the parameters for the piston problem case 2

m	$0.8[Kg]$
k	$7911[N/m]$
ρ_0	$1.3[Kg/m^3]$
p_0	$10^5[P_a]$
T_s	$0.063[s]$
T_f	$0.0061[s]$
L_0	$1[m]$

In the second case, the parameters for the piston are taken as in Piperno (1995), Michler et al. (2004), and Blom (1998) and are presented in Table 4.5

$$\frac{T_s}{T_f} = \frac{6.3 \times 10^{-2}}{6.1 \times 10^{-3}} \approx 10.33 \Rightarrow T_s \gg T_f, \quad \mu \approx 1.63. \tag{4.19}$$

Therefore, the piston does not see the pressure waves, which means that the *coupling is weak*; the fluid can be considered as *quasi-steady*; and its mass will impact on the oscillation frequency of the coupled system. Here, we have to estimate the oscillation frequency on the coupled system by adding the fluid mass and stiffness to the mass-spring system, Garelli (2011)

$$(m + m_f)\ddot{q(t)} + (k + k_f)q(t) = 0, \tag{4.20}$$

where m_f and k_f are the mass and stiffness contributions from the fluid, so that the fluid behaves as a mass-spring system. Parameters used in Garelli (2011) are considered: $m_f = 43.33 \times 10^2[Kg]$ and $k_f = 14 \times 10^4[N/m]$, $\omega_{fs} = 346.3[rad/s]$ and $T_{fs} = 0.0181$. As in Garelli (2011), we impose the initial conditions $q_0 = 0.05,$ and $\dot{q}_0 = 0$. The goal is to verify the structural solver, by making comparisons between the estimated oscillation frequency and the oscillation frequency computed using (4.13). Both must agree. As it can be verified from figures 4.8, the estimated oscillation frequency T_s,indicated by the arrows, agree with the oscillation frequency computed by equation (4.13) and presented in Table 4.5.

In Garelli (2011) they applied Newmark (average acceleration) scheme, and two dif-

ferent time steps:

$$\Delta t_1 = 3.05 \times 10^{-4}[s] \text{ and } \Delta t_2 = 2.43 \times 10^{-3}[s]. \tag{4.21}$$

We use the same time steps, but apply the TR-BDF2 scheme. The figures 4.8 represent the results. Since the structural solver was verified, we solve the coupled system.

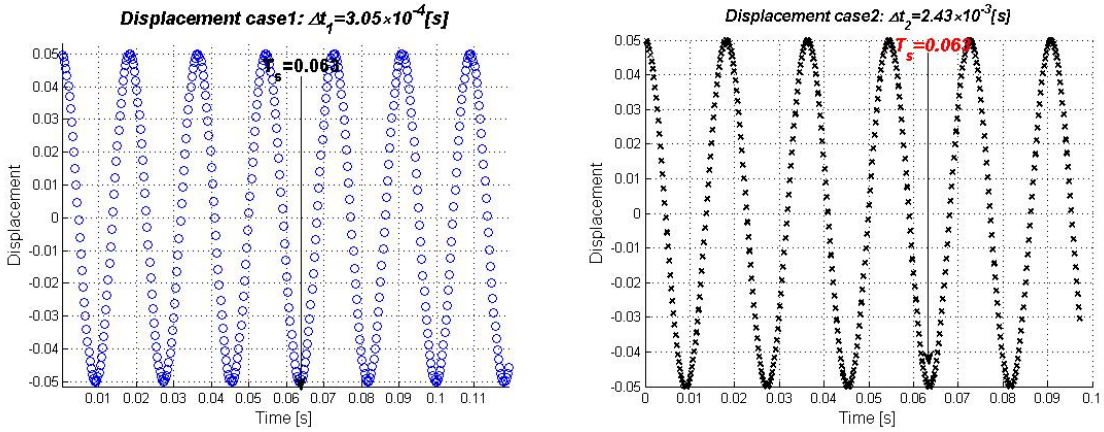

Figure 4.8: Structural displacement obtained by TR-BDF2 scheme, using $\Delta t_1 = 3.05 \times 10^{-4}[s]$ and $\Delta t_2 = 2.43 \times 10^{-3}[s]$, respectively.

Again, we apply the TR-BDF2 scheme. Firstly, we solve the coupled system for Courant number $CFL \in \{0.1; 0.5; 0.9\}$, using the structural predictor 1 given by (3.26). Figure 4.9 shows the growing of the amplitude of the oscillations with time, when increases the CFL number. The reason for this is the increasing of the structural total energy (Potential+Kinetic) in time, as shown in Figure 4.10.

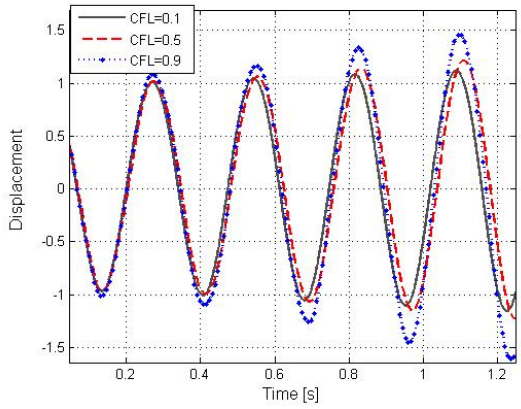

Figure 4.9: Structural displacement computed using structural predictor 1

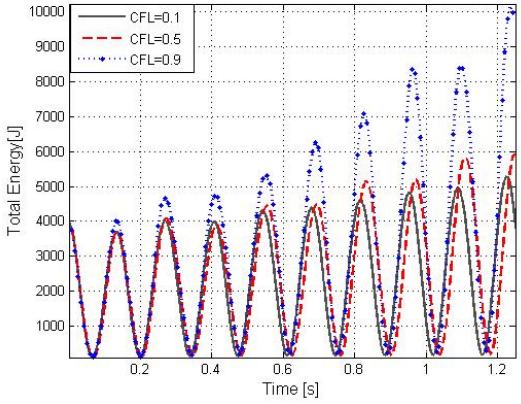

Figure 4.10: Structural total energy computed using structural predictor 1

Alternatively, to decrease the spurious additional energy, we apply the structural predictor 2, given by (3.27). As shown in Figure 4.11, the artificial additional energy decreases significantly and for $CFL = 0.5$ and $CFL = 0.9$, the solutions practically compare. Figure 4.12 shows the structural total energy for different CFL numbers, and it demonstrates that the energy does not increase too much, as in the previous

case.

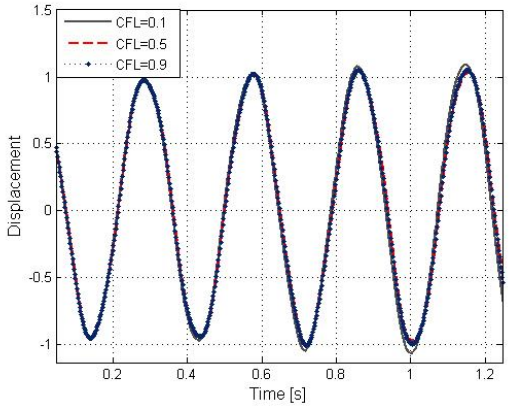

Figure 4.11: Structural displacement computed using structural predictor 2

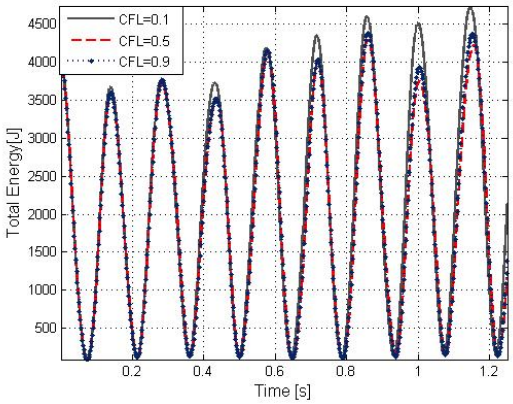

Figure 4.12: Structural total energy computed using structural predictor 2

Finally, we show the coupled system computed using Newmark (average acceleration) and TR-BDF2 schemes. Figure 4.13 clearly shows the good performance of the TR-BDF2 scheme compared with the most preferred scheme by several researchers: the average acceleration scheme.

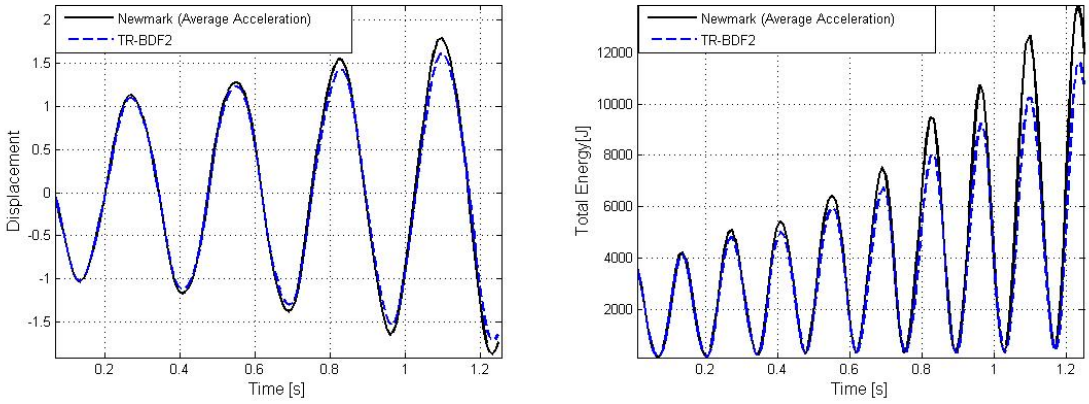

Figure 4.13: Structural displacement and structural total energy computed using Newmark and TR-BDF2 schemes

4.5 Concluding Remarks

A numerical investigation of different fluid-structure interaction algorithms has been presented. The one-dimensional piston problem was chosen as a test bed. The one dimensional fluid is modelled by the nonlinear Euler equations which were discretized by the finite element method as in Lefrançois (2010), and by a one-dimensional arbitrary high order quadrature-free essentially non-oscillatory finite volume scheme, reformulated for moving mesh coordinates using the arbitrary Lagrangian Eulerian (ALE) approach. The structure was integrated in time by various time integration schemes. The fluid and the structure were integrated in time using separate solvers. The coupling between the fluid and structure solvers was realized by applying the partitioned approach. Since the partitioned approach suffers from a time lag, the

influence of the time lag was studied by comparing two different predictions for the structure, a zero order and a first order prediction. Numerical experiments were carried out and the computations show that the differences between the two coupling algorithms become noticeable as the CFL number increases. The first order prediction algorithm gave a higher accuracy. These results agree with the theory presented in Blom (1998).

On the other hand, the performance of the QFENOFV scheme was tested by comparing it with the numerical results obtained by using FEM as in Lefrançois (2010). It is found that the dissipation effects over time is greater by applying QFENOFV than FEM. Showing that applying QFENOFV scheme the coupling between the fluid and the piston is stronger than by FEM.

Chapter 5

HIGH ORDER IMPLICIT RUNGE-KUTTA SCHEMES AS STRUCTURE SOLVER FOR A STAGGERED APPROACH

5.1 Introduction

Thus far we have found from the existing literature, that for a staggered approach, the solution of structure is based on at most second-order time accurate schemes. In general, the Newmark schemes are the most preferred, as we describe next.

Piperno (1995) predicted the dynamic response of a flexible structure in a fluid flow, solving the structure by the second-order accurate *midpoint rule*. Piperno (1997) simulated the supersonic flutter of a flat panel, using the *trapezoidal rule*(Newmark with parameters $\beta = \frac{1}{4}$, $\gamma = \frac{1}{2}$) for the structure. Blom (1998) investigated the time marching computational fluid-structure interaction algorithms, in which the structure was integrated numerically by the average acceleration scheme. This scheme is the optimal case of the Newmark's method, Bathe (1976), with no numerical damping and is unconditionally stable. Farhat (2000) solved coupled transient aeroelastic problems with the flutter analysis of the AGARD Wing 445. In his work the structural system is advanced by the second-order time accurate *midpoint rule*. Michler et al. (2003) investigated the relevance of maintaining conservation for a model fluid-

structure interaction problem, using the Newmark method with the parameter choice $\beta = \frac{1}{4}$, $\gamma = \frac{1}{2}$ for structure. The same scheme was used again by Michler et al. (2004) to compare partitioned and monolithic solution procedures for the numerical simulations of fluid-structure interactions. Lefrançois (2010) provided a basic and solid grasp of numerics underlying the physics of fluid-structure interaction, employing the Newmark-Wilson scheme as a structure solver. Garelli (2011), when it came to investigating the coupling strategies for fluid-structure interaction, used the average acceleration scheme to integrate the structure in time. Rarely, the implicit high order of the family of explicit singly diagonal implicit Runge-Kutta (ESDIRK) schemes are applied to FSI problems. In our information, from the literature, ESDIRK schemes have only been applied with success to FSI problems in a partitioned coupling approach, in which the scheme is used to integrate, in time, both fluid and structure. In these problems, the fluid flow was considered isentropic, and by looking to small perturbations, the governing Euler equations were linearized, van Zuijlen (2004).

In this Chapter, high order, explicit single diagonal implicit Runge-Kutta (ESDIRK) schemes in the order of three to five are proposed as the structure solver, and an arbitrary high order finite volume scheme as the fluid solver. In order to decrease the additional fictitious energy, a structure prediction is considered and tested for different natural frequencies of the structure.

5.2 Structure dynamics high-order integration Schemes

The structural high-order time integration we consider in this Chapter is the Explicit single diagonal implicit Runge-Kutta (ESDIRK), which is an L-stable implicit scheme, with an explicit first stage. These characteristics ensure that the implicit stages are second-order accurate. The scheme works as such:

We consider any system of the form

$$\dot{q} = F(q, t), \tag{5.1}$$

describing structural dynamics. For every k stage we solve

$$q^{(n)} = q^n + \Delta t \sum_{i=1}^{k} a_{ki} F^{(i)}, \qquad k = 1, ..., s, \tag{5.2}$$

here $F^{(i)} = F(q^{(i)})$ is the flux at stage i. After calculating the s stages, we calculate the solution at the next time level by

$$q^{n+1} = q^n + \Delta t \sum_{i=1}^{s} b_i F^{(i)} \tag{5.3}$$

In this Chapter, third-to fifth-order ESDIRK schemes are considered, which consist of four, six, and eight stages, respectively. The coefficients a_{ki} and b_i are presented in a Butcher tableau, which in Table 5.1 is represented by $s = 4$:

The Butcher tableau we use in this work can be found in Kennedy (2003). At stage $k = i$ the time level $t^{(i)}$ follows from $t^{(i)} = t^n + c_i \Delta t$, where the coefficient

$c_i = \sum_j a_{ij}$. As shown by the Butcher tableau, when applying ESDIRK schemes, because the first stage is explicit, there are $s-1$ implicit stages-which implies solving $s-1$ implicit systems in one time step.

5.3 Structural Dynamics Simulations

In this Section, we test the performance of ESDIRK, for the structure dynamics simulations, compared with the second-order Newmark ($\beta = \frac{1}{4}$, $\gamma = \frac{1}{2}$). As we referred to in Section 4.2.2, the Newmark ($\beta = \frac{1}{4}$, $\gamma = \frac{1}{2}$) is most used to integrate structure when it comes to applying a staggered approach for fluid-structure interaction problems. This scheme is the optimal version of the Newmark methods, with no numerical damping and is unconditionally stable, Bathe (1976). However Bardella (2003) found that this scheme is affected by a significant drift error, for which the

Table 5.1: Butcher Tableau

c_1	a_{11}	a_{12}	a_{13}	a_{14}
c_2	a_{21}	a_{22}	a_{23}	a_{24}
c_3	a_{31}	a_{32}	a_{33}	a_{34}
c_4	a_{41}	a_{42}	a_{43}	a_{44}
	b_1	b_2	b_3	b_4

following formulae

$$d_2 = \frac{\omega^2 \Delta t}{A} \lim_{T \to \infty} \left[\frac{1}{T} (q^{exact}(T) - q^{alg}(T)) \right] \tag{5.4}$$

was proposed to measure it, where ω is the undamped angular frequency, A is the amplitude of the system, and T is the total time integration. van Zuijlen (2004) found that this drift reduces for ESDIRK schemes.

In this Section, we directly integrate the harmonic oscillator (3.22).

As test examples, we resume those considered in Bardella (2003) and van Zuijlen (2004).

(1) the first test example is a free mass with a period forcing $m\ddot{q} + kq = f_{ext}(t)$, with $m = 1$, $k = 0$, and under a periodic loading $f_{ext}(t) = Asin(\omega t)$. This example was tested in Bardella (2003) and in van Zuijlen (2004). Therefore, similarly to those those two papers, we also use $A = 100$ and $\omega = 1$. The initial conditions are given by $q(0) = -A$ and $\dot{q}(0) = -A$, where A is the amplitude of the vibrations.

(2) the second test example is an unforced mass-spring system $m\ddot{q} + kq = 0$, with $m = k = 1$, under initial conditions $q(0) = 1$, and $\dot{q}(0) = 0$. This example served as a test in van Zuijlen (2004).

Figure 5.1 shows the results for the displacement in time by the Newmark$_\beta$ scheme and by the ESDIRK schemes from third to fifth order. In these figures,it can be seen

that the drift error is more distinctive for the Newmark$_\beta$ scheme, which is exactly the same as the cases reported in Bardella (2003), van Zuijlen (2004).

Table 5.2 shows the drift error that affects the Newmark$_\beta$ scheme and the ESDIRK schemes, for the data $A = 100$, $\omega = 1$, $\Delta t = 1$, and $\Delta t = 0.1$, by setting $T = 100$. The parameter p, which denotes the observed order of accuracy, was computed by

$$p = \ln\Big(\frac{\|d_{4\tau} - d_{2\tau}\|}{\|d_{2\tau} - d_{1\tau}\|}\Big) / \ln(2), \tag{5.5}$$

where d is the computed structural displacement on meshes of different time-step sizes, denoted by τ, 2τ and 4τ, and the L_2 norm is used to measure the differences. In the last column of the table the CPU times needed by the code is presented. The code was developed using MATLAB 7.0 and executed on a processor with Intel(R) Core(TM)2 Duo CPU T6570 at 2.10GH$_z$ with 3.00 GB of RAM, and 32 bit operating system.

It can be observed that the computational time of ESDIRK is three times higher than the computational time for Newmark$_\beta$. On the other hand the accuracy of ESDIRK is higher at that cost.

5.4 Fluid-Structure Interaction

As the ESDIRK schemes have shown a better performance for structural dynamics than the Newmark$_\beta$ scheme, our concern is to test it for the fluid-structure problem, as a structure solver on a staggered approach with a structural predictor.

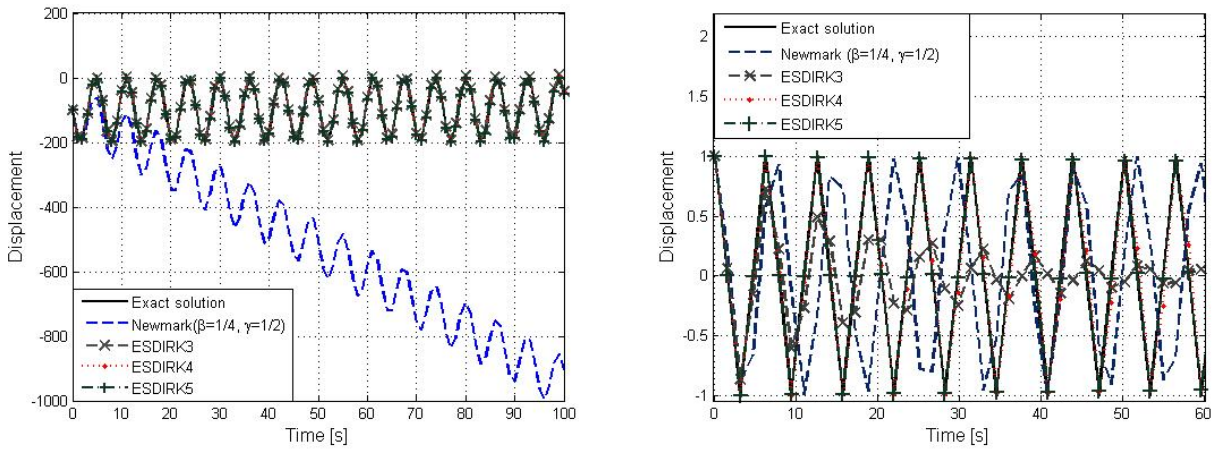

Figure 5.1: Integration of the free mass equation for sinusoidal acceleration $\ddot{q} = 100sin(t)$, $\Delta t = 1$, subject to $q_0 = -100$ and $\dot{q}_0 = -100$ (left-side), and integration of the harmonic oscillator $\ddot{q} + \omega^2 q = 0$, $\Delta t = \frac{2\pi}{4}$, subject to $q_0 = 0$ and $\dot{q}_0 = 1$ (right-side).

5.5 Fluid and structure models

Again, we consider non-linear Euler equations to model the fluid, and the harmonic oscillator (3.22) to model the structure. The fluid equations are reformulated in an ALE framework to ensure moving meshes. To discretize the fluid, we again apply the high order finite volume WENO method, as in Chapter 4.

Table 5.2: Drift error affecting various integration schemes for the data of Figure 5.1.

Scheme	$\|d_2\|$, $\Delta t = 1$	$\|d_2\|$,$\Delta t = 0.1$	Order of temporal accuracy p	$t_{CPU}[sec.]$
Newmark$_\beta$	8.56×10^{-2}	8.42×10^{-4}	3.00	88.327
ESDIRK3	6.88×10^{-4}	1.0×10^{-7}	4.5	285.417
ESDIRK4	3.92×10^{-4}	3.0×10^{-10}	5.0	285.496
ESDIRK5	1.4×10^{-7}	0.00	6.005	286.509

5.6 Structural predictor

To predict the structure, in this paper we use the first order predictor, Blom (1998):

$$\dot{q}^{n+1} = \dot{q}^n + \Delta t \ddot{q} \tag{5.6}$$

which throughout this Chapter will be denoted by $PredictorB$. We also test one of the predictors used in an FSI problem applied to the oscillating aerofoil in a inviscid flow, Piperno (1997), namely the structure predictor

$$q^{n+1} = q^n + \Delta t \dot{q}^n + \frac{1}{2}\Delta t^2 \ddot{q}^n \tag{5.7}$$

which throughout this Chapter we will denote by $PredictorP$.

Table 5.3: Parameters for the piston problem

L_0	1	m
q^0	0.2	m
L_{s0}	1.2	m
m	10	Kg
k	1×10^7	N/m
p_0	1×10^5	P_a
γ	1.4	
c_0	334	m/s

5.7 Numerical Results for FSI

The parameters for the piston problem are given in Table 5.3, and they are taken in a similar way as in Lefrançois (2010). The characteristic time-scales for fluid, structure and fluid structure interaction system are denoted by

$$T_f = \frac{L_0}{c}, \quad T_s = 2\pi\sqrt{\frac{m}{k}}, \quad T_{fs} = \frac{2\pi}{\omega_{fs}}, \tag{5.8}$$

respectively. The relation T_s/T_f determines the importance of the transient effects on the fluid behaviour, Lefrançois (2010)

Taking into account the parameters in Table 5.3, we have that $T_s \approx T_f$; therefore the coupling is considered strong, Garelli (2011).

Figure 5.2 shows the displacement and the total energy computed with a staggered approach where the Newmark$_\beta$ scheme and the ESDIRK schemes are used as structure solvers. The results show that the amplitude of the oscillations reduce in time for ESDIRK because of decreasing energy over time. The curves become more damped as the CFL number increases, as shown in Figure 5.3. An alternative to decrease the additional fictitious energy consists of introducing more accurate structural predictors. Figure 5.4 shows the structural displacement and the structural total energy computed using ESDIRK5 as a structural solver, where the coupled algorithm is supplied by the structural predictor given by (5.7). We can see that the results improved significantly, showing the better performance of predictor (5.7) compared with predictor (5.6).

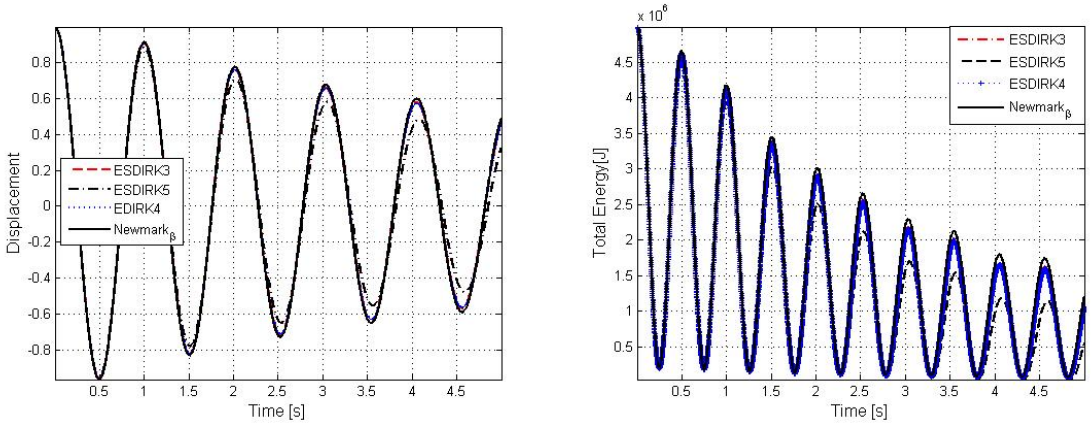

Figure 5.2: Piston displacement (right) and structure total energy (right) computed by a staggered approach. Newmark$_\beta$ method and ESDIRK schemes are used to integrate the structure.

5.8 Energy Conservation

Our concern here is to identify and to apply adequate structure predictors to reduce considerably the energy conservation errors, Piperno (1997). In this section we discuss the efficiency of the staggered scheme used with a structural predictor. This quality indicator for the efficiency of the scheme can be derived through the integration, on the domain $[0, L(t)]$, of the third conservation law from the Euler equations, such that

$$\frac{\partial}{\partial t}\int_0^{L(t)} \rho E A dx + A\Big[u(\rho E + p) - \rho E w_x\Big]_0^{L(t)} = 0. \tag{5.9}$$

Taking into account the boundary conditions

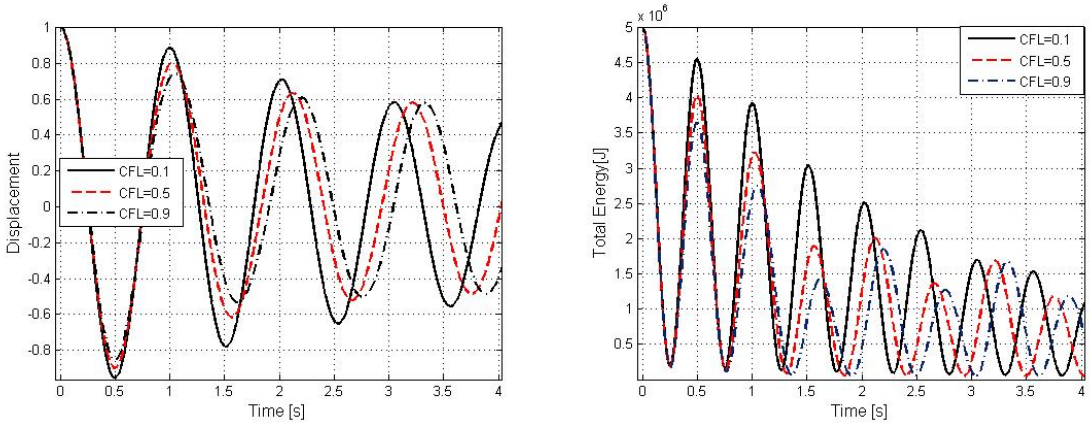

Figure 5.3: Displacement of the structure and the structure total energy computed using ESDIRK5 with predictor (5.6) for different CFL numbers

$$u(L(t),t) = w_x(L(t),t) = \dot{q}(t) \qquad \text{and} \qquad u(0,t) = w_x(0,t) = 0 \tag{5.10}$$

and integrating in time (5.9) between the initial condition and the current time t, yields

$$\int_0^{L(t)} \rho A E dx - \int_0^{L(0)} \rho A E dx = -\int_0^t A p(L,t) u(L,t) dt. \tag{5.11}$$

Equation (5.11) is called impulsion Lefrançois (2010), and here is denoted by $I(t)$. It corresponds to the total energy variation (on left-hand term) or the fluid energy required for the motion of the piston, Lefrançois (2010). On the other hand, integrating in time the mass-spring system (3.22), we can define the piston mechanical energy variation,

$$E(t) - E(0), \qquad \text{where} \qquad E(t) = \frac{1}{2} m \dot{q}^2 + \frac{k}{2}(L_{se} - q(t) + L_{s0})^2. \tag{5.12}$$

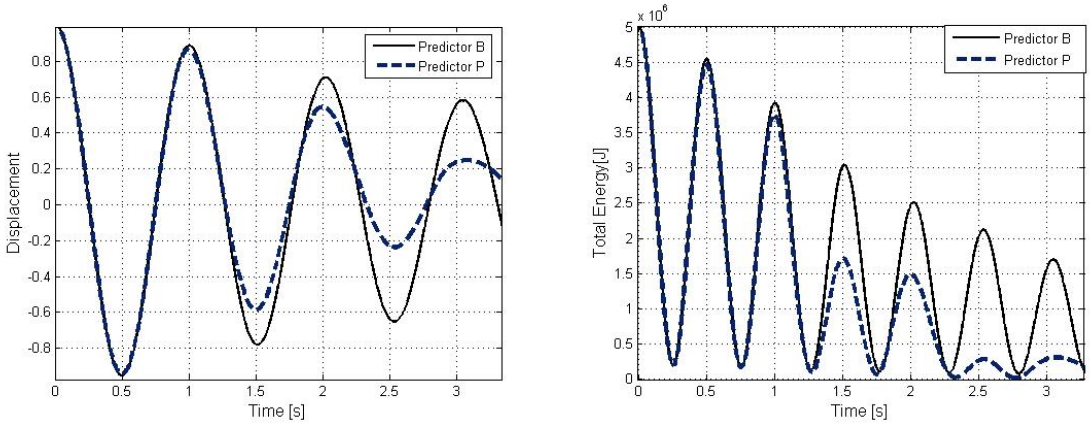

Figure 5.4: Displacement of the structure and the structure total energy computed using ESDIRK5 with structural predictors (5.6) and (5.7)

There are two components for mechanical energy: the kinetic component, denoted here by $E(t)_c$, and the potential component, denoted by $E(t)_p$.

Energy conservation is satisfied if

$$I(t) = E(t) - E(0) \qquad \text{for} \qquad t \geq 0, \tag{5.13}$$

where from the initial conditions $q(x,0) = q^0$ and $\dot{q}(x,0) = 0$

$$E_0 = \frac{1}{2}k(L_{se} - q(x,0) + L_{s0})^2 \tag{5.14}$$

Equation (5.11) is computed by the fluid solver and (5.12) is computed by the structure solver.

Figures 5.5, top, show energy conservation; by using $PredictorB$ (left-hand side) and by using $PredictorP$ (right-hand side) in both cases taking $m = 100Kg$. As it

is shown, the mechanical energy (denoted by E/E_0), and the impulsion (denoted by I/E_0), move in opposite directions, meaning that what is lost by one is taken by the other and vice-versa. Therefore the energy remains conserved. The variation in the mechanical energy indicates the transfer of the energy from the structure to the fluid. This behaviour can also be seen when $m = 10Kg$, as shown by Figure 5.5, bottom, where we can do the same analysis on the left-hand side for $PredictorB$ and on the right-hand side for $PredictorP$.

5.9 Concluding Remarks

A staggered approach with a structure predictor is considered to solve an FSI problem applied to the piston problem. The fluid is modelled by the nonlinear Euler equations written in moving mesh coordinates by the arbitrary Lagragian Euler (ALE) formulation, and the structure by the mass-spring system. The fluid domain is discretized by the arbitrary high order finite volume schemes. The structure is integrated by the Newmark$_\beta$ and ESDIRK3–5 schemes and two structure predictors are applied. ESDIRK schemes show superior results with both predictors. From the results obtained, it is believed that ESDIRK can be used as a structure solver for FSI problems instead of the usual Newmark$_\beta$ method.

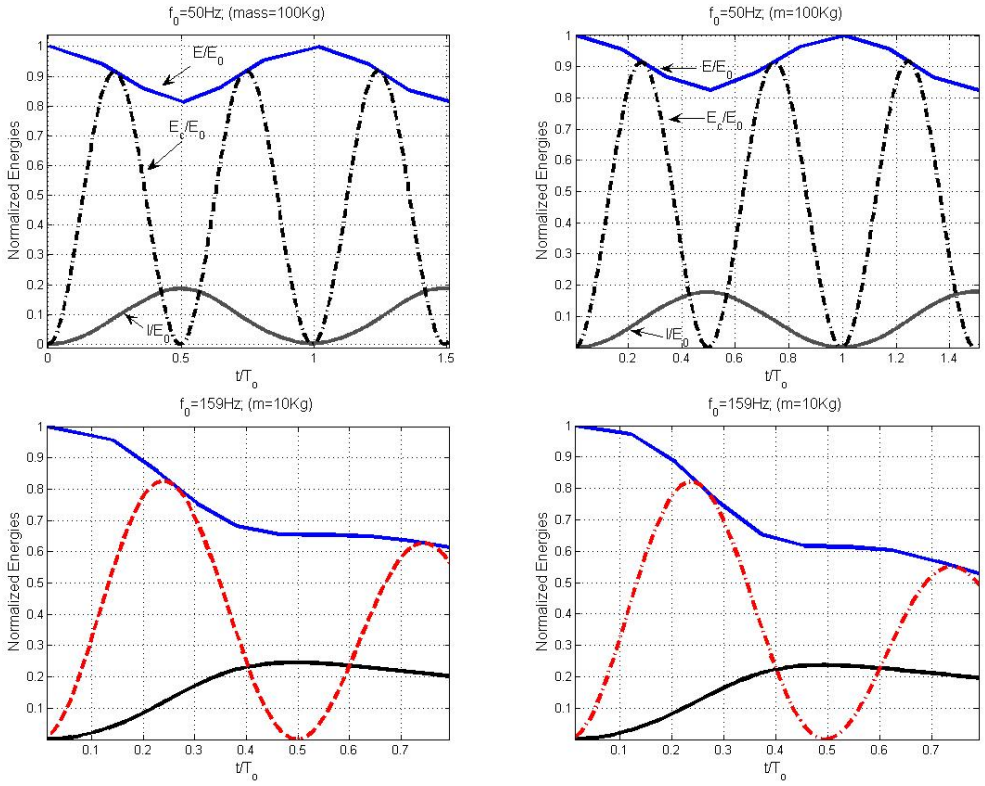

Figure 5.5: Energy conservation: The results are computed by using ESDIRK3 as both the structural solver and the structural predictors: $PredictorB$ (left-hand side) and $PredictorP$ (right-hand side.). Here $m = 100$, top, and $m = 10$, bottom.

Chapter 6

CONCLUDING REMARKS

6.1 Conclusions

A historical background that aim to introduce the reader through the main historic steps from 1960s to 2000s concerned with the fields involved in a fluid-structure interaction (FSI) problem, was presented. We found it interesting to highlight that in a historic point of view, although the concept FSI arose in 1840s it is reported that the current version of this problem is recent, and dates from 1960s. The Objectives of this study were formulated.

In this thesis, a staggered approach to an FSI problem was considered. Several fluid and structural solvers were applied to a staggered approach in a structural predictor fashion. New applications of numerical methods were realized in an attempt to establish a link between both the performance of these methods when applied to fluid or structure dynamic problems, and the methods performance when applied to FSI problems.

A high order finite volume method was applied. This method is a one-dimensional version of the arbitrary high-order non-oscillatory finite volume schemes for unstructured triangular and tetrahedral grids, in two and three dimensions, Dumbser (2007a);

Dumbser et al. (2007b). Simulations for fluid dynamics problems were carried out, and taking into account that using traditional numerical fluxes causes the high order finite volume method considerable loss of its non-oscillatory properties, a numerical flux was proposed. The numerical method resulting from this proposed numerical flux was analyzed on the basis of the general properties of finite volume methods. It was found that the proposed numerical method satisfied the properties of finite volume methods:

- it is conservative,
- it is consistent,
- it is convergent and therefore converges to a weak solution,
- it is monotone.

Several numerical tests were carried out and applied to several shock tube test problems. Comparisons with the results obtained by the local Lax-Friedrichs method, showed that the proposed method performed better with respect to the essentially non-oscillatory feature.

The physical and mathematical formulation of the FSI problem under study was presented. A theoretical overview of the FSI problem as well as some relatively

simple numerical simulations were presented in order to give an understanding in the problem.

Next, the proposed high order finite volume scheme was considered for an FSI problem, by using it to discretize the fluid in space in a staggered approach framework. The scheme was modified in an Arbitrary Lagrangian Eulerian fashion to couple with a moving mesh. For the structure, several solvers were considered. Taking into account the importance of the transient effects on the fluid behaviour both a strong and a weak coupling test case was considered. We compared the performance of this scheme with the performance of the finite element method, with both being applied to a staggered approach, using the average acceleration as the structure solver. The results showed good performance of the finite volume method, as presented in Figure 4.5.

Next, several time integration schemes for structural dynamics, such as those belonging to a family of Newmark's methods, and the trapezoidal-rule backward differentiation formulae of order 2 (TR-BDF2), were considered as fluid solvers. The aim was to relate the performance of these schemes when applied to structure-dynamic problems, and their performance when applied to a staggered approach for a FSI problem. We started by estimating the oscillation frequency of the coupled system, using parameters for weak coupling, and adding the fluid mass and stiffness to the mass-spring system. The results show that the estimated frequency compares with

the exact structural frequency, as shown in Figs.4.8 and in Table 4.5, respectively. The simulations realized by various structure solvers showed that the TR-BDF2 performed slightly better than other Newmark's structural solvers, as shown in Fig.4.13.

The study of the order of accuracy for the partitioned fluid-coupling showed that the order of accuracy of the average acceleration method and the TR-BDF2 method was practically the same; however TR-BDF2 is less CPU time consuming than the average acceleration scheme, as shown in Tables 4.3-4.4.

Finally, high order implicit Runge-Kutta schemes were applied in order to integrate structure. The fluid domain was discretized, again using the proposed high order finite volume scheme. The performance of the explicit singly diagonal implicit Runge-Kutta (ESDIRK) of the order three to five, as fluid structure solver in a staggered approach framework with structural predictor, was tested and compared with the performance of the traditionally used Newmark scheme. The superior results shown by the family of ESDIRK methods suggest that these schemes may be preferred to the traditional family of Newmark's methods.

6.2 Future work

Fluid-structure interaction is a new and a very challenging subject for mathematicians to study and/ or develop more efficient numerical schemes for. This thesis is a contribution, based mainly on the application of numerical methods for fluid and

for structure, to a staggered approach for a FSI problem. It therefore opens a way for future researchers interested in extending this field of study. Future works can involve the following:

(1) for the piston problem, the tests can be extended to the cases where the mass-spring system is governed by a more than one degree of freedom system;

(2) generalizing the tests for the case of incompressible fluid flow; and

(3) extension to the most challenging two-dimensional and three-dimensional cases.

6.3 Publications

During the work on this thesis the following articles have been published and submitted or are to be submitted,

- J. C. Pedro and P. Sibanda, An Algorithm for the Strong-Coupling of the Fluid-Structure Interaction Using a Staggered Approach. *doi* : 10.5402/2012/391974. ISRN Applied Mathematics, Volume 2012, 14 pages,

- J. C. Pedro, M. K. Banda and P. Sibanda, On one-dimensional arbitrary high-order WENO schemes of hyperbolic conservation laws. *Revised and re-submitted to Computational and Applied Mathematics.*

- J. C. Pedro and M. K. Banda, and P. Sibanda, Finite Volume WENO scheme: Application in fluid-structure interaction for gas dynamics, in preparation.

- J. C. Pedro and M. K. Banda, On High Order Implicit Runge-Kutta Schemes for Structural Dynamics and Fluid-Structure Interaction, in preparation.

REFERENCES

B. Addis, *Building: 3,000 Years of Design, Engineering and Construction,* MGMT. design,Booklyn, New York, 2007.

B. Alberto, *Hyperbolic Systems of Conservation Laws. The One-Dimensional Cauchy Problem,* Oxford University Press, 2000.

D. J. Acheson, *Elementary Fluid Dynamics,* Clarendon Press, 1990.

R. Alexander, *Diagonally implicit Runge-Kutta methods for stiff ODEs,* SIAM J. Numer. Anal., **14**, (1977)1006–1021.

H. V. Auweraer, *Structural Dynamics Modeling using Modal Analysis: Applications, Trends and Challenges,* LMS International, Budapest, Hungary 2001.

R. E. Bank, W. M. Coughran, W. Fichtner, E. H. Grosse, D. J. Rose and R. K. Smith, *Transient simulation of Silicon devices and circuits,* IEEE Transactions on computer-aided design, CAD-4:436–451, 1985.

L. Bardella and F. Genna, *Newmark's Time Integration Method From the Discretization of Extended Functionals,* Journal of Appl. Mech., **72**,(2005)527–537.

L. Bardella, A. Carini and F. Genna, *Time integration errors and some new func-*

tionals for dynamics of a free mass, Journal of Computers & Structures, **81**, (2003)2361–2372.

G. K. Batchelor, *An Introduction to Fluid Dynamics,* Cambridge University Press, 1967.

K. J. Bathe, *Conserving energy and momentum in nonlinear dynamics: a simple implicit time integration scheme,* Computers and Structures, **85**, (2007)437–445.

K. J. Bathe and M. M. I. Baig, *On a composite implicit time integration procedure for nonlinear dynamics,* Computers & Structures, **83**, (2005)2513–2524.

K. J. Bathe and G. Noh, *Insight into an implicit time integration scheme for structural dynamics,* Computers & Structures, 98–99, (2012)1–6.

K. J. Bathe and E. L. Wilson, *Numerical Methods in Finite Element Analysis,* Prentice-Hall, Englewood Cliffs, NJ, 1976.

K. J. Bathe and H. Zhang, *A mesh adaptivity procedure for CFD and fluid-structure interactions,* Computers and Structures, **87**, (2009)604–617.

A. Becchi, M. Corradi, F. Foce, and O. Pedemonte, *Essays on the History of Mechanics. In memory of Clifford Ambrose Truesdell and Edoardo Benvenuto,* Kim William Books, Italy, 2001.

O. O. Bendiksen, *A new approach to computational aeroelasticity,* AIAA Paper (1991)91–0939-CP.

H. Bijl, M. H. Carpenter and V. N. Vatsa, *Time integration Schemes for Unsteady Navier Stokes Equations*, 15th Computational Fluid Dynamics Conference, AIAA, (2001)–2612.

F. J. Blom, *A monolithical fluid-structure interaction algorithm applied to the piston problem,* Comput. Methods Appl. Mech. Engrg., **167**, (1998)369–391.

F. J. Blom and P. Leyland, *Analysis of fluid-structure interaction by means of dynamic unstructured meshes,* Païdoussis et al., eds., AD-Vol.53-1, 4th Int. on Fluid-Structure Interaction, Aeroelasticity, Flow-Induced Vibrations and Noise, Dallas, (1997)3-10.

R. Borsche, R. M. Colombo and M. Garavelo, *On the Coupling of Systems of Hyperbolic Conservation Laws with Ordinary Differential Equations,* IOP PUBLISHING Nonlinearity, **23**, (2010)2749–2770.

D. S. Burnett, *Finite Element Analysis. From Concepts to Applications,* Addison-Wesley Publishing Company, 1987.

J. C. Butcher, *The Numerical Analysis of Ordinary Differential Equations: Runge-*

Kutta and General Linear Methods, Wiley-Interscience New York, NY, USA , (1987).

J. C. Butcher, *Numerical Methods for Ordinary Differential Equations,* Second Edition, Wiley, 2003.

W. R. Cao and Z. Z. Sun, *Maximum norm errors estimates of the Crank-Nicolson scheme for solving a linear moving boundary problem,* Journal of Computational and Applied Mathematics, **234**, (2010)2578–2586.

M. H. Carpenter, S. A. Viken and E. J. Nielsen, *The Efficiency of High Order Temporal Schemes,* AIAA, **0086**, (2003)1–18.

H. Chanson, *Hydrodynamics: An Introduction to Ideal and Real Fluid Flows,* CRC Press, Taylor & Francis Group, Leiden, The Netherlands, 478 pages., 2009.

A. Chertock and A. Kurganov, *A simple Eulerian Finite-Volume Method for Compressible fluids in domains with moving boundaries,* Commun. Math. Sci., **6**, (2008)531–556.

J. Chung and G. M. Hulbert, *A Time Integration Algorithm for Structural Dynamics With Improved Numerical Dissipation: The generalized $-\alpha$ Method,* Journal of Applied Mechanics, **60**, (1993)371–375.

P. Colella and E. G. Puckett, *Modern Numerical Methods for Fluid Flow,* (1998).

M. Colombo and G. Guerra, *On general balance laws with boundary,* Journal of Differential Equations, **248**(2010)1017–1043.

R. R. Craig Jr and A. J. Kurdila, *Fundamentals of structural dynamics,* John Willey & Sons, New Jersey, (2006).

M. Dumbser, *Advanced Numerical Methods for Hyperbolic Equations and Applications. Lecture Notes,* Lecture Notes, Laboratory of Applied Mathematics, University of Trento. Via Mesiano 77, I-38040 Trento, Italy, (2011).

M. Dumbser and M. Käser, *Arbitrary high order non-oscillatory finite volume schemes on unstructured meshes for linear hyperbolic systems*, Journal of Computational Physics, **221**, (2007a)693–723.

M. Dumser, M. Käser, V. A. Titaraev and E. F. Toro, *Quadrature-free non-oscillatory finite volume schemes on unstructured meshes for nonlinear hyperbolic systems*, Journal of Computational Physics, **226**, (2007b)204–243.

C. H. Edwards and D. E. Penney, *Differential Equations And Boundary Value Problems. Computing and Modeling,* 3rd Ed., Pearson Education inc. New Jersey, 2004.

R. Eymard, T. Gallouët and R. Herbin, *Finite Volume Methods,* October 2006. This manuscript is an update of the preprint n0 97-19 du LATP, UMR 6632, Marseille,

September 1997 which appeared in Handbook of Numerical Analysis, P.G. Ciarlet, J.L. Lions eds, vol 7, pp 713-1020

C. Farhat, *High performance simulation of coupled nonlinear transient aeroelastic problems,* Cosmase Course, EPF-Lausanne, (1995).

C. Fahrat, P. Geuzaine and K. Van Der Zee, *Probably second-order time-accurate loosely-coupled solution algorithms for transient nonlinear computational aeroelasticity,* Computer Methods in Applied Mechanics and Engineering, **195**, (2006)1973–2001.

C. Farhat and T. Y. Lin, *A structure attached corotational fluid grid for transient aeroelastic computations,* AIAA J., 31(3): (1993)597—599.

C. Farhat, and M. Lesoinne, *Two efficient staggered algorithms for the serial and parallel solution of three-dimensional nonlinear transient aeroelastic problems,* Journal of Computer Methods in Applied Mechanics and Engineering, (2000), 499-515.

C. Farhat, P. Geuzaine , and C. Grandmont, *The Discrete Geometric Conservation Law and the Nonlinear Stability of ALE Schemes for the Solution of Flow Problems on Moving Grids,* Journal of Computational Physics, **174**, (2001)669-694.

C. Farhat, N. Maman and M. Lesoinne, *Mixed explicit/implicit time integration of coupled aeroelastic problems: three-field formulation, geometric conservation law*

and distributed solution, Center for Aerospace Structures 94–17, University of Colorado, (1994).

C. Farhat, K. G. van der Zee and P. Geuzaine, *Provably second-order time-accurate loosely-coupled solution algorithms for transient nonlinear computational aeroelasticity,* Computer Meth. in Appl. Mech. and Engineering, **195**, (2006)1973–2001.

R. Fazio and R. J. Leveque, *Moving-Mesh Methods for One-Dimensional Hyperbolic Problems Using CLAWPACK,* An international Journal of Computers & mathematics with applications, **45**, (2003)273–298.

C. A. Felipa and T. L. Geers, *Partitioned analysis of coupled mechanical systems,* Engrg. Comput., **5**, (1988)123–133.

C. A. Felipa and K. C. Park, *Computational aspects of time integration procedures in structural dynamics,* Part I: Implementation, J. Appl. Mech., **45**, (1978)595–602.

C. A. Felipa and K. C. Park, *Direct time integration methods in nonlinear structural dynamics,* Comp. Meths. Appl. Mech. Engrg., **17/18**, (1979)277–313.

S. H. Fernandez, *Essays in the History of the Theory of Structures: In Honour of Jacques Heyman,* Instituto Juan Herrera, Escuela Tecnica Superior de Arquitetura de Madrid, 2005.

A. F. Filipov, *Differential equations with discontinuous righthand,* Kluwer Academic Publishers Group, Dordrechet, 1988.

L. Garelli, *Fluid Structure Interaction using Arbitrary Lagrangian Eulerian Formulation, Tesis de Doctorado,* Facultad de Engeniería y Ciencias Hídricas, Universidad Nacional del Litoral, Argentina, 2011.

S. K. Godunov, *A Difference Scheme for Numerical Solution of Discontinuous Solution of Hydrodynamic Equations,* Math. Sbornik, **47**, (1959)271-306, translated US Joint Publ. Res. Service, JPRS 7226, 1969.

G. P. Guruswamy, *A review of numerical fluid/structures interface methods for computations using high-fidelity equations,* Mathematical Biosciences, **172**, (2001)55–72.

W. Haase, *Unsteady Aerodynamics Including Fluid/Structure Interaction,* Air and Space Europe, **3**, (2001)83–86.

E. Hairer, S. P. Nørsett, and G. Wanner, *Solving Ordinary Differential Equations I: Nonstiff Problems,* Springer-Verlag, Berlin, 1993.

E. Hairer, and G. Wanner, *Solving Ordinary Differential Equations II: Stiff and Differential-Algebraic Problems,* Springer-Verlag, Berlin, 1991.

A. Harten, B. Engquist, S. Osher and S. Chakravarthy, *Uniformly high order essentially non-oscillatory schemes, III,* Journal of Computational Physics, **71**, (1987)231–303.

R. Helmig, A. Mielke and B. I. Wohlmuth (Eds.) *Multifield Problems in Solid and Fluid Mechanics,* Series: Lecture Notes in Applied and Computational Mechanics, Vol. 28, Springer-Verlag Berlin Heidelberg, 2010.

J. Heyman, *Structural Analysis. A Historical Approach,* Cambridge University Press, 1998.

C. Hirsch, *Numerical Computation of Internal and External Flows: Computational Methods for Inviscid and Viscous Flows v. 2,* Wiley Series in Numerical Methods in Engineering, 1990.

K. A. Hoffmann and S. T. Chiang, *Computational Fluid Dynamics for Engineers,* 2nd edition, Engineering Education System, 1993.

M. E. Hosea and L. F. Shampine, *Analysis and Implementation of $TR - BDF2$,* Applied Numerical Mathematics, **20**, (1996)21–37.

G. Hou, J. Wang and A. Layton, *Numerical Methods for Fluid-Structure Interaction - A review,* Commun. Comput. Phys., **12** (2012)337–377.

T. Y. Hou and P. G. LeFloch, *Why nonconservative schemes converge to wrong solutions: error analysis,* Mathematics of Computation, **62**, (1994)497–530.

C. Hu and C. W. Shu, *Weighted essentially non-oscillatory schemes on triangular meshes*, Journal of Computational Physics, **150**, (1999)97–127.

T. Huges, *The Finite Element Method-Linear Static and Dynamic Finite Element Analysis,* Prentice-Hall, Inc., 1987.

V. Jean-Mark, D. V. Pascal, H. Charles and L. Benoit, *Strong coupling algorithm to solve fluid-structure interaction problems with a staggered approach,* Open Engineering SA, Report, (2009).

G. S. Jiang and, C. W. Shu, *Efficient implementation of Weighted ENO Schemes*, Journal of Computational Physics, **126**, (1996)202–228.

C. A. Kennedy and M. Carpenter, *Additive Runge-Kutta schemes for convection-diffusion-reaction equations,* Appl. Num. Math., **44**, (2003)139–181.

A. Kurganov and E. Tadmor, *New High-Resolution Central Schemes for Nonlinear Conservation Laws and Convection-Diffusion equations,* Journal of Computational Physics, **160**, (2000)241–282.

R. Löhner, *Applied Computational Fluid Dynamics Techniques: An Introduction Based on Finite Element Methods,* Second Edition. John Wiley & Sons, 2008.

E. Lefrançois and J. P. Boufflet, *An Introduction to Fluid-Structure Interaction: Application to the Piston Problem,* SIAM REVIEW, **52**, (2010)747-767.

M. Lesoinne and C. Farhat, *Geometric conservation laws for flow problems with moving boundaries and deformable meshes, and their impact on aeroelastic computations,* Comput. Methods Appl. Mech. Engrg. **134**(1996)71–90.

R. J. Leveque, *Finite Volume Methods for Hyperbolic Problems*, Cambridge University Press, (2002).

W. Li and Y. X. Ren, *High-order k-exact WENO finite schemes for solving gas dynamic Euler equations on unstructured grids,* International Journal for Numerical Methods in Fluids, (1973)JohnWiley & Sons, Ltd.

D. Liu, S. Osher and T. Chan, *Weighted essentially non-oscillatory schemes*, Journal of Computational Physics, **115**, (1994)200–212.

G. A. Maney, *Studies in Engineering,* University of Minnesota, U.S.A., 1915.

H. G. Matthies and J. Steindorf, *Strong Coupling Methods. In analysis and simulation of multifield problems,* Berlin: Springer Verlag, (2003).

C. Michler, E. H. van Brummelen, S. J. Hulshoff and R. Borst, *The relevance of conservation for stability and accuracy of numerical methods for fluid-structure inter-*

action, Computer methods in applied mechanics and engineering, **192**, (2003)4195–4215.

C. Michler, S. J. Hulshoff, E. H. van Brummelen and R. de Borst, *A monolithic Approach to Fluid-structural Interaction,* Computers & Fluids, **33**, (2004)839-848.

S. Modak and E. D. Sotelino, *The generalized method for structural dynamics applications,* Adv. In Engineering Software, **33**, (2002)565–575.

J. Mouro, *Interactions fluide structure en frands déplacements, résolution numéric et application aux composants hydrauliques automobiles*, Ph. D. Thesis, Ecole Polytechnique, France, (1996).

N. M. Newmark, *A Method of Computation for Structural Dynamics,* ASC Journal of the Engineering Mechanics Division, Vol. 85 N. EM3, (1959).

J. T. Oden (1991), *Finite elements: An Introduction in: Handbook of Numerical Analysis II,* (North-Holland,Amsterdam) 3-15.

K. C. Park, C. A. Felippa and J. A. DeRuntz, *Stabilization of staggered solution procedures for fluid-structure interaction analysis,* Comput. Methods Fluid-Structure Interaction Problems, AMD **26**, (1977)659–675.

J. C. Pedro and, P. Sibanda, *An algorithm for the strong-coupling of the fluid-structure*

interaction using a staggered approach, ISRN Applied Mathematics, **2012**, Article ID 391974, 14 pages. doi:10.5402/2012/391974.

S. Piperno, *Staggered time integration methods for a one-dimensional Euler aeroelastic problem,* Raport de Recherche CERMICS, (1994)94–33.

S. Piperno, *Simulation numéric de phénomènes d'interaction fluid-structure, Ph.D. Thesis,* Ecole Nationale Des Ponts et Chaussés, (1995).

S. Piperno, *Two-dimensional Euler aeroelastic simulations with interface matching relaxation,* Proc. Second ECCOMAS Conference on Numerical Methods in Engineering, (1996)898-904.

S. Piperno, *Explicit/Implicit Fluid/ Structure Staggered Procedures With a Substructural Predictor and Fluid Subcycling For 2D Inviscid Aeroelastic Simulations,* International Journal For Numerical Methods in Fluids, **25**, (1997)1207-1226.

S. Piperno, *Partitioned procedures for the transient solution of coupled aeroelastic problems–Part II: energy transfer analysis and three-dimensional applications,* Comp. Methods Appl. Mech. Engrg., **190**, (2001)3147–3170.

S. Piperno and C. Farhat, *Design and evaluation of staggered partioned procedures for fluid-structure interaction simulations,* Fourth US National Congress on Computational Mechanics. San Francisco, (1997).

S. Piperno, C. Farhat and B. Larrouturou, *Partitioned procedures for the transient solution of coupled aeroelastic problems. Part I: Model problem, theory and two–dimensional application,* Journal of Comput. Methods Appl. Mech. Engrg., **124**, (1995)79-112.

B. B. Prananta, M. H. L. Hounjet and R. J. Zwaan, *Thin Layer Navier-Stokes Solver and its Application for Aeroelastic Analysis of an Airfoil in Transonic Flow,* International Forum on Aeroelasticity and Structural Dynamics (1995), June 1995, pp 1...1-1.9

B. B. Prananta and M. H. L. Hounjet, *Aeroelastic simulation with advanced CFD methods in 2D and 3D transonic flow,* Proc. Unsteady Aerodynamics Conference Royal Aeronautical Socuiety, London, (1996).

B. B. Prananta and M. H. L. Hounjet, *Large time step aero-structural coupling procedures for aeroelastic simulation,* Proc. 1997 International Forum on Aeroelasticity and structural Dynamics, Vol II, AIDAA, Rome, (1997)63-70.

B. B. Prananta, M. H. L. Hounjet and R. J. Zwaan, *Thin layer Navier Stokes and its application for aeroelastic analysis of an airfoil in transonic flow,* International Forum on Aeroelasticity and Structural Dynamics, Manchester, (1996).

J. Qiu and C. W. Shu, *On the construction, comparison, and local characteristic*

decomposition for high-order central WENO schemes, Journal of Computational Physics, **183**, (2002)187–209.

R. D. Rausch, J. T. Batina and H. T. Y. Yang, *Euler flutter analysis of airfoils using unstructured dynamic meshes,* AIAA J., **31(3)**, (1993)597-599.

J. Shi, C. Hu and C. W. Shu, *A technique of treating negative weights in WENO schemes*, Journal of Computational Physics, **175**, (2002)108–127.

C. W. Shu, *Essentially Non-Oscillatory and Weighted Essentially Non-Oscillatory Scheme for Hyperbolic Conervation Laws*, NASA/CR-97-206253 ICASE Report N., (1997)97–65.

C. W. Shu and S. Osher, *Efficient implementation of essentially non-oscillatory shock-capturing schemes,* J. Comput. Phys., **77**, 439(1988).

A. Soulaïmani, Z. Feng and A. B. H. Ali, *Solution techniques for multi-physics problems with application to computational nonlinear aeroelasticity,* Nonlinear Analysis, Theory, Methods and Applications, **63**, no. 5–7, (2005)1585–1595.

M. Souli and D. J. Benson, *Arbitrary Lagrangian-Eulerian and Fluid-Structure Interaction,* ISTE and John Wiley & Sons, Inc., USA, (2010).

M. Souli, A. Ouashine and L. Lewin, *ALE formulation for fluid-structure interaction problems,* Comput. Methods Appl. Mech., **190**, (2000).

M. Spiegel, *Schaum's Outline of Calculus of Finite Differences and Difference Equations,* McGraw-Hill, New York, 1999.

E. Stein, R. Borst and T. J. R. Hughes, *Encyclopedia of Computational Mechanics,* John Wiley & Sons inc., 2004.

J. M. Stockie, J. A. Mackenzie and R. D. Russel, R.D. (2001) *A moving mesh method for one-dimensional hyperbolic conservation laws,* SIAM Journal on Scientific Computing, 22 (5). pp. 1791-1813. ISSN 1064-8275

G. G. Stokes, *On the effect of the internal friction of fluids on the motion of pendulums,* Transactions of the Cambridge Philosophical Society, **9**, (1851)8–106.

S. R. Subia and M. L. Wang, *Nonlinear hysteresis curve derived by direct numerical investigation of acceleration data,* Soil Dynamics and Earthquake Engineering, **14**, (1995)321–330.

K. V. Subramanian, W. Nian and Y. Andreopoulos, *Blast response simulation of an elastic structure: Evaluation of the fluid-structure interaction effect,* International Journal of Impact Engineering, **36**, (2009)956–974.

J. Sundnes, G. T. Lines and A. Tveito, *Efficient solution of ordinary differential equations modeling electrical activity in cardiac cells,* Computers and Structures, **80**, (2001)31–41.

H. Thomas, *The Finite Element Method- Linear Static and Dynamic Finite Element Analysis,* Prentice Hall, Inc., 1987.

V. A. Titarev and E. F. Toro, *Solution of the generalized Riemann Problem for advection-reaction equations*, Proceedings of Royal Society of London, (2002)271–281.

V. A. Titarev and E. F. Toro, *ADER schemes for scalar hyperbolic conservation laws with source terms in three space dimensions*, Journal of Computational Physics, **202**, (2005(a))196–215.

V. A. Titarev and E. F.Toro, *ADER schemes for three-dimensional nonlinear hyperbolic systems*, Journal of Computational Physics, **204**, (2005(b))715–736.

V. A. Titarev and E. F. Toro, *MUSTA schemes for multi-dimensional hyperbolic systems: analysis and improvements,* Int. J. Numer. Meth. Fluids, **49**, (2005(c))117–147.

E. F. Toro, *Rieman Solvers and Numerical Methods for Fluid Dynamics,* second Edition, Springer-Verlag, 1999.

E. F. Toro and S. J. Billet, *Centered TVD schemes for hyperbolic conservation laws*, IMA Journal of Numerical Analysis, **20**, (2000)44–79.

E. F. Toro, R. C. Millington and L. A. M. Nejad, *Towards very high order*

Gudonov schemes, E. F. Toro (Ed.), Gudonov Methods, Theory and Applications, Kluwer/Plenum Academic Publishers, (2001)905–938.

B. van Leer, *Towards the Ultimate Conservative Difference Scheme, V. A Second Order Sequel to Godunov's Method,* J. Comput. Phys., **32**, (1979)101136.

A. H. van Zuijlen and H. Bijl, *Implicit and explicit higher order time integration schemes for structural dynamics and fluid-structure interaction computations,* Journal of Computers & Structures, **83**, (2004)93–105.

M. W. Wambsganss, S. S. Chen, and J. A. Jendrzejczyk (Components Technology Division), *Added Mass And Damping of a Vibrating Rod in Confined Viscous Fluids,* TECHNICAL MEMORANDUM, ANL-CT-75-08 LMFBR COMPONENTS (UC-79k), 1974.

G. Weymouth, *Physics and Learning Based Computational Models for Breaking Bow Waves Based on New Boundary Immersion Approaches,* Ph.D. Dissertation, MIT, 2008.

G. Weymouth, D. G. Dommermuth, K. Hendrickson, and D. K. -P. Yue, *Advances in Cartesian-grid Methods for Computational Ship Hydrodynamics,* 26th Symposium on Naval Hydrodynamics, Rome, Italy, 17-22 September 2006.

E. L. Wilson, *Dynamic Response by Step-By-Step Matrix Analysis,* Proceedings, Sym-

posium On The Use of Computers in Civil Engineering, Laboratorio Nacional de Engenharia Civil, Lisbon, Portugal, Octuber 1–5, 1962.

E. L. Wilson, I. Farhoomand and K. J. Bathe, *Nonlinear Dynamic Analysis of Complex Structures,* Earthquake Engineering and Structural Dynamics, **1**, (1973)241–252.

Y. H. Zahran, *A central WENO-TVD schemes for hyperbolic conservation law*, Novi Sad J. Math, **36**, (2006), 25–42.

Y. T. Zhang and C. W. Shu, *Third order WENO schemes on three dimensional tetrahedral meshes*, Communications in Computational Physics, **5**,(2009)836–848.

W. Zhang, Y. Jiang and Z. Ye, *Two better loosely coupled solution algorithms of CFD based aeroelastic simulation,* Engineering Applications of Computational Fluid Mechanics, **1**, (2007)253–262.

D. G. Zill and M. R. Cullen, *Differential Equations with Boundary Value Problems,* PWS Publishing Company, Vol. 1 (1989).

APPENDIX

Appendix A

GENERAL NOTATION

ξ	:reference space
i	:index
$n-1$, n, and $n+1$	:indices for time steps $t-\Delta t$, t, and $t+\Delta t$

Appendix B

FLUID NOTATION

ρ	:density
p	:pressure
u	:fluid velocity
c	:speed of sound
E	:energy
L_0	:chamber length
v_x	:nodal grid velocity
γ	:specific ratio of the air
T_f	:characteristic time scale for the fluid subsystem

Appendix C

STRUCTURE NOTATION

f_d	:damping forces
f_e	:restoring forces
$\ddot{q}(t)$	:structure acceleration
$\dot{q}(t)$	:structure velocity
$q(t)$	:structure displacement
M, and m	:strcuture mass matrix, and strcuture mass
C, and c	:structure damping matrix, and structure damping
K, and k	:structure stiffness matrix, and structure stiffness
Δt	:time step
T_s	:characteristic time scale for the mass-spring system